

# Fano resonances in nanoscale structures

Andrey E. Miroshnichenko,<sup>1,\*</sup> Sergej Flach,<sup>2</sup> and Yuri S. Kivshar<sup>1</sup>

<sup>1</sup>*Nonlinear Physics Centre and Centre for Ultra-high bandwidth Devices for Optical Systems (CUDOS), Research School of Physics and Engineering, Australian National University, Canberra ACT 0200, Australia*

<sup>2</sup>*Max-Planck-Institut für Physik komplexer Systeme, Nöthnitzer Str. 38, D-01187 Dresden, Germany*

Modern nanotechnology allows to scale down various important devices (sensors, chips, fibres, etc), and, thus, opens up new horizons for their applications. The efficiency of most of them is based on fundamental physical phenomena, such as transport of wave excitations and resonances. Short propagation distances make phase coherent processes of waves important. Often the scattering of waves involves propagation along different paths, and, as a consequence, results in interference phenomena, where constructive interference corresponds to resonant enhancement and destructive interference to resonant suppression of the transmission. Recently, a variety of experimental and theoretical work has revealed such patterns in different physical settings. The purpose of this Review is to relate resonant scattering to Fano resonances, known from atomic physics. One of the main features of the Fano resonance is its asymmetric line profile. The asymmetry originates from a close coexistence of resonant transmission and resonant reflection, and can be reduced to the interaction of a discrete (localized) state with a continuum of propagation modes. We will introduce the basic concepts of Fano resonances, explain their geometrical and/or dynamical origin, and review theoretical and experimental studies for light propagation in photonic devices, charge transport through quantum dots, plasmon scattering in Josephson junction networks, and matter wave scattering in ultracold atom systems, among others.

## Contents

<b>I. Historical remarks</b>	1	A. From a single electron transistor to quantum interference	26
<b>II. The Fano resonance</b>	3	B. From Coulomb blockade to Fano resonances	28
A. Two oscillators with a driving force	3	C. From Fano to Aharonov-Bohm interferometers	28
B. Light and atoms	3	D. Correlations	29
C. Light and structured matter	5	E. Interference	30
D. Atoms and atoms	6	F. Spin filters	31
<b>III. Modeling: complex geometries</b>	7	G. Perspectives	32
A. Fano-Anderson model	7	<b>VII. Conclusions</b>	33
B. Tuning the asymmetry parameter	8	<b>Acknowledgments</b>	33
C. Many resonances	8	<b>References</b>	33
D. Nonlinear Fano resonance	9		
E. Resonant reflection of pulses and solitons	9		
F. Quadratic nonlinearities	10		
<b>IV. Modeling: complex dynamics</b>	10		
A. Scattering by discrete breathers	11		
B. Light scattering by optical solitons	12		
C. Plasmon scattering in Josephson junction ladders	13		
D. Matter wave scattering in Bose-Einstein condensates	14		
<b>V. Light propagation in photonic devices</b>	14		
A. Green's function formalism	15		
B. Defects in the waveguide	16		
C. Sharp bends	17		
D. Add-drop filters	17		
E. All-optical switching and bistability	17		
F. Overlapping resonances	19		
G. Guided resonances in photonic crystal slabs	20		
H. Light scattering by spherical nanoparticles	21		
I. Plasmonic nanocavities and tunable Fano resonance	22		
J. Extraordinary transmission of light through metallic gratings	23		
K. Resonant four-wave mixing induced autoionization	24		
<b>VI. Charge transport through quantum dots</b>	25		

## I. HISTORICAL REMARKS

One of the important diagnostic tools in physics is scattering of radiation (waves) by matter. It allows to investigate properties of matter and to control the radiation. For example, Rydberg spectral lines (1888) of the hydrogen atom allowed Niels Bohr to deduce his model of an atom (1913), which laid the basis of quantum mechanics. Later, Beutler (1935) observed that some of the Rydberg spectral atomic lines exhibit sharp asymmetric profiles in the absorption. It was Ugo Fano (1935) who suggested the first theoretical explanation of this effect and suggested a formula (also known as the Beutler-Fano formula) which predicts the shape of spectral lines based on a superposition principle from quantum mechanics. The complexity of the physical phenomena was encapsulated in a few key parameters, which made this formula a workhorse in many fields of physics, including nuclear, atomic, molecular, and condensed matter physics. According to Fano: "*the Beutler spectra showed unusual intensity profiles which struck me as reflecting interference between alternative mechanisms of excitation*" (Fano, 1977). The interpretation provided by Fano

\*Electronic address: aem124@rsphysse.anu.edu.au



FIG. 1 Ugo Fano (1912-2001) - "outstanding interpreter of how radiation interacts with atoms and cells" (Clark, 2001), and much more (this Review).

of these "strange looking shapes" of spectral absorption lines is based on the interaction of a discrete excited state of an atom with a continuum sharing the same energy level, which results in interference phenomena. The first paper with the derivation of the line-shape formula (Fano, 1935), was published in 1935, when Ugo Fano was a young postdoctoral fellow in the group of Enrico Fermi. Fano has acknowledged the influence of his teacher on the derivation of this key result. The second much more elaborated paper (Fano, 1961) became one of the most important publications in the physics of the XX century, rated between the first three most relevant works published in *The Physical Review* (Redner, 2004), with over 5300 citations by now (October 2008). *"The paper appears to owe its success to accidental circumstances, such as the timing of its publication and some successful features of its formulation. The timing coincided with a rapid expansion of atomic and condensed matter spectroscopy, both optical and collisional. The formulation drew attention to the generality of the ingredients of the phenomena under consideration. In fact, however, the paper was a rehash of work done 25 years earlier ..."* (Fano, 1977; Vittorini-Orgeas and Bianconi, 2009). In his pioneering papers, Ugo Fano introduced an important new ingredient of matter-radiation interaction in atomic physics, making him a key player in XX century physics. This was also acknowledged by the Fermi Award in 1995 for "his seemingly formal use of fundamental theory" leading to "the underpinning of a vast variety of practical results which developed naturally from this understanding".

Remarkably, the first observation of the asymmetric line-shapes can be traced back to the discovery made

by Wood in 1902, namely, the presence of unexpected narrow bright and dark bands in the spectrum of an optical reflection grating illuminated by a slowly varying light source (Wood, 1902). Wood was astounded to see that under special illumination conditions the grating efficiency in a given order dropped from maximum to minimum illumination, within a wavelength range not greater than the distance between the sodium lines. These rapid variations of intensities of the various diffracted spectral orders in certain narrow frequency bands were termed *anomalies*, since the effects could not be explained by the conventional grating theory (Wood, 1935). The first theoretical treatment of these anomalies is due to Lord Rayleigh (1907). His "dynamical theory of the grating" was based on an expansion of the scattered electromagnetic field in terms of outgoing waves only. This theory correctly predicted the wavelength (Rayleigh wavelengths) at which anomalies occurred. However, one of the limitations of Rayleigh's approach was that it yields a singularity at the Rayleigh wavelength, and, therefore, does not give the shape of the bands associated with the anomaly. Fano tried to overcome this difficulty in a series of papers (Fano, 1936, 1937, 1938, 1941) by assuming a grating consisting of lossy dielectric material, and suggesting that anomalies could be associated with the excitation of a surface wave along the grating. The resonant excitation of leaky surface waves near the grating, which occurs when a suitable phase matching between the incident plane wave and the guided wave is satisfied, leads to a strong enhancement of the field near the grating surface (de Abajo, 2007; Hessel and Oliner, 1965; Sarrazin *et al.*, 2003). As it was pointed out by Sarrazin *et al.* (2003), the observed asymmetric profiles can be fitted by the Fano formula with very good accuracy. Thus, the interaction of excited leaky modes with an incoming radiation leads to similar interference phenomena as in absorption by Rydberg atoms, where a leaky mode can be associated with a discrete state, and the incoming radiation with a continuum. These examples reveal the universality of Fano's approach in describing the origin of asymmetric line-shapes in terms of interference phenomena, regardless of the nature of the constituting waves, as well as in predicting both the position and the width of the resonance.

Similar asymmetric profiles were observed in various other systems and settings. But sometimes it is not obvious to determine the origin of the interference. In the present survey paper, we provide a very general explanation of appearance of the Fano resonances in various physical systems based on a simple model, which sheds light on the origin of the interference phenomena, which is well along the lines of Steven Weinberg: "our job in physics is to see things simply, to understand many complicated phenomena in a unified way, in terms of a few simple principles." (1979 Nobel Prize Lecture).

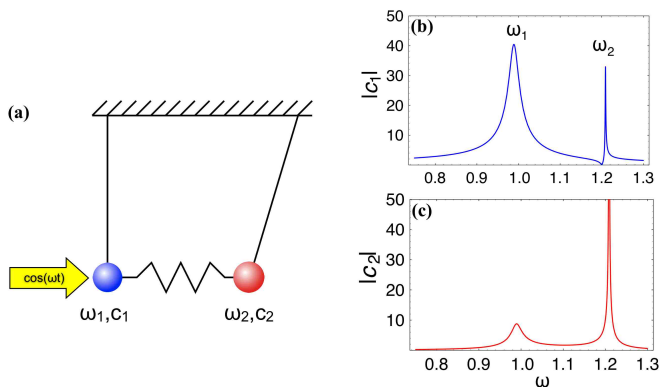


FIG. 2 (Color online) Resonances of parametrically driven coupled oscillators. (a) Schematic view of two coupled damped oscillators with a driving force applied to one of them; (b) the resonant dependence of the amplitude of the forced oscillator  $|c_1|$ , and (c) the coupled one  $|c_2|$ . There are two resonances in the system. The forced oscillator exhibits resonances with symmetric and asymmetric profiles near the eigenfrequencies  $\omega_1 = 1$  and  $\omega_2 = 1.2$  (b), respectively. The second coupled oscillator responds only with symmetric resonant profiles (c). Adapted from Joe *et al.* (2006).

## II. THE FANO RESONANCE

### A. Two oscillators with a driving force

Usually, a resonance is thought to be an enhancement of the response of a system to an external excitation at a particular frequency. It is referred to as the resonant frequency, or natural frequency of the system. One of the simplest examples is a harmonic oscillator with periodic forcing. When the frequency of the driving force is close to the eigenfrequency of the oscillator, the amplitude of the latter is growing towards its maximal value. Often many physical systems may also exhibit the opposite phenomenon, when their response is suppressed if some resonance condition is met (which lead even to the term *antiresonance*). This can be illustrated by using two weakly coupled underdamped harmonic oscillators, where one of them is driven by a periodic force [see Fig. 2(a)]. In such a system, in general, there are two resonances located close to eigenfrequencies  $\omega_1$  and  $\omega_2$  of the oscillators (Joe *et al.*, 2006). One of the resonances of the forced oscillator demonstrates the standard enhancement of the amplitude near its eigenfrequency  $\omega_1$ , while the other resonance exhibits an unusual sharp suppression of the amplitude near the eigenfrequency of the second oscillator  $\omega_2$  [see Fig. 2(b,c)]. The first resonance is characterized by a symmetric profile, described by Lorentzian function, and known as a Breit-Wigner resonance (Breit and Wigner, 1936). The second resonance is characterized by an asymmetric profile.

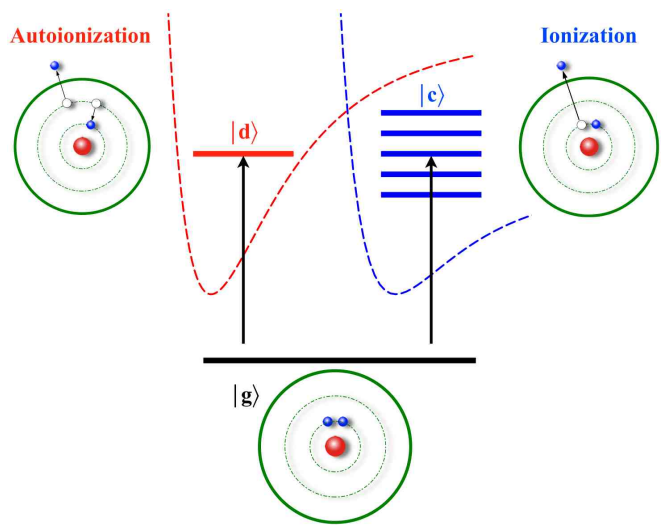


FIG. 3 (Color online) Fano resonance as a quantum interference of two processes - direct ionization of a deep inner-shell electron and autoionization of two excited electrons followed by the Auger effect. This process can be represented as a transition from the ground state of an atom  $|g\rangle$  either to a discrete excited autoionizing state  $|d\rangle$  or to a continuum  $|c\rangle$ . Dashed lines indicate double excitations and ionization potentials.

### B. Light and atoms

The second resonance was described for the first time by Fano (1935, 1961), when being attracted by unusual sharp peaks in the absorption spectra of noble gases observed by Beutler (1935). The nature of the asymmetry was established with the theory of configuration by Fano (1961). The photoionization of an atom can go along various ways. The first, straightforward one, is the excitation of the inner-shell electron above the ionization threshold  $A + \hbar\nu \rightarrow A^+ + e$ . Another possibility is to excite the atom into some quasi-discrete level, which can spontaneously ionize by ejecting an electron into the continuum  $A + \hbar\nu \rightarrow A^* \rightarrow A^+ + e$ . Such levels were named autoionizing ones after Shenstone (1938). In other words, the autoionized state is a bound state of an atom with the energy above the first ionizing threshold. Autoionization is one of the most fundamental electron-electron correlation phenomena, and it is forbidden in the noninteracting particle approximation (Connerade, 1998). One of the possible autoionized states is the excitation of two electrons by one photon, when the excitation energies of each electron are of the same order of magnitude, and the total excitation energy exceeds the atom ionization threshold. The interaction between electrons leads to the decay of this state when one electron transfers into a lower state, and the second electron is ejected into the continuum, using the energy of the relaxed electron. In spectroscopy this process is known as the Auger effect (Auger, 1925a,b, 1926). Different types of other autoionizing states are described in Smirnov (2003). In general, autoionization can be considered as a mechanism which couples bound

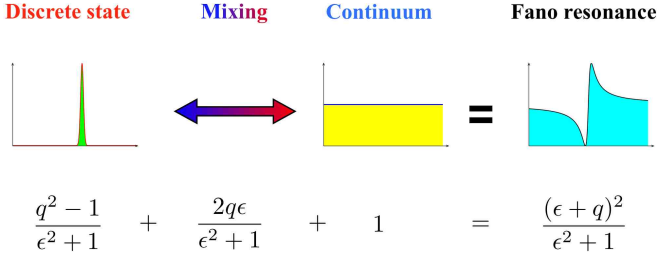


FIG. 4 (Color online) Illustration of the Fano formula (1) as a superposition of the Lorentzian lineshape of the discrete level with a flat continuous background.

states of one channel with continuum states of another. Due to the superposition principle of quantum mechanics, whenever two states are coupled by different paths, interference may occur.

Fano used a perturbation approach to explain the appearance of asymmetric resonances. He considered a so-called prediagonalized state by putting the coupling between a discrete bound state, which is degenerate in energy with a continuum of states, to zero. Such a prediagonalized state may or may not have a clear physical analogy, but serves in any case as a convenient mathematical construction, which allows to solve the problem. As a result Fano obtained the formula for the shape of the resonance profile (Fano, 1935, 1961) of a scattering cross-section

$$\sigma = \frac{(\epsilon + q)^2}{\epsilon^2 + 1} \quad (1)$$

using a phenomenological shape parameter  $q$  and a reduced energy  $\epsilon$  defined by  $2(E - E_F)/\Gamma$ .  $E_F$  is a resonant energy, and  $\Gamma$  is the width of the auto-ionized state. Formula (1) suggests that there are exactly one maximum and one minimum in the Fano profile

$$\begin{aligned} \sigma_{\min} &= 0, & \text{at } \epsilon &= -q \\ \sigma_{\max} &= 1 + q^2, & \text{at } \epsilon &= 1/q. \end{aligned} \quad (2)$$

In his original paper Fano (1961) has introduced the asymmetry parameter  $q$  as a ratio of transition probabilities to the mixed state and to the continuum. In the limit  $|q| \rightarrow \infty$  the transition to the continuum is very weak, and the lineshape is entirely determined by the transition through the discrete state only with the standard Lorentzian profile of a Breit-Wigner resonance. When the asymmetry parameter  $q$  is order of unity both the continuum and discrete transition are of the same strength resulting in the asymmetric profile (1), with the maximum value at  $E_{\max} = E_F + \Gamma/(2q)$  and minimum value at  $E_{\min} = E_F - \Gamma q/2$ . The case of zero asymmetry parameter  $q = 0$  is very unique to the Fano resonance and describes a symmetrical dip, sometimes called an anti-resonance (see Fig. 5). The main feature of the Fano resonance is the possibility of destructive interference, leading to asymmetric line shapes (Bandopadhyay *et al.*, 2004;

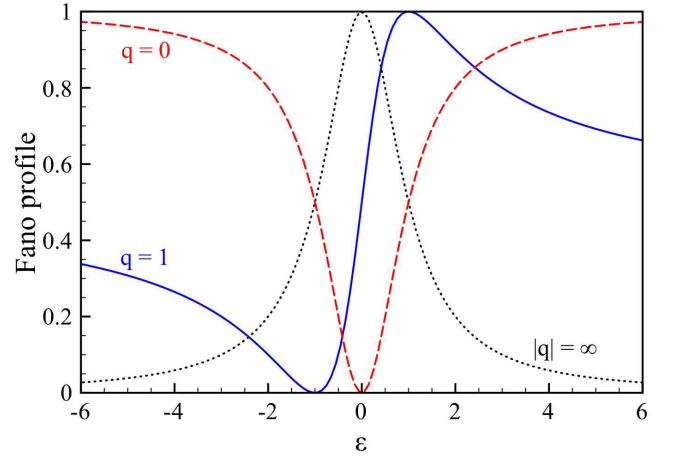


FIG. 5 (Color online) Normalized Fano profiles (1) with the prefactor  $1/(1 + q^2)$  (2) for various values of the asymmetry parameter  $q$ .

Bianconi, 2003; Lee and Kim, 2000a; Nockel and Stone, 1994; Piao *et al.*, 1990; Rau, 2004). The actual resonant frequency of the discrete level  $E_F$  may lie somewhere between the maximum and the minimum of the asymmetric profile, and the parameter  $q$  defines the relative deviation. In the situation  $|q| \rightarrow \infty$  the resonant frequency coincides to the maximum of the profile, while in the case  $q = 0$  the resonant frequency coincides to the minimum. For  $q = 1$  it is located exactly at half distance between the minimum and maximum (see Fig. 5).

Due to recent advances in the generation of ultrashort attosecond pulses Wickenhauser *et al.* (2005) theoretically investigated the possibility to observe the buildup of Fano resonances in time by using attosecond streaking techniques. Excitation by an ultrashort pump pulse opens two interfering paths from the ground state to the continuum, which are then studied by a weak probe pulse. After the characteristic time of the autoionizing level, the transient coupling to the resonant state starts to "burn a hole" in the energy distribution of the initial Gaussian. This method may become very useful in determining both coherent and incoherent pathways to ionization.

The Fano formula (1) was successfully used to fit and explain various experimental data (Aoki *et al.*, 1996; Armstrong *et al.*, 1978; Bandopadhyay *et al.*, 2004; Bandrauk and Laplante, 1976; Bar-Ad *et al.*, 1997; Becker *et al.*, 1986; Bortchagovsky and Fischer, 2003; Chergui *et al.*, 1991; Davis and Feldkamp, 1977; dell'Orto *et al.*, 1995; Dixit and Lambropoulos, 1979; Druger, 1977; Eichmann *et al.*, 2003; Fano, 1964, 1965; Fano and Cooper, 1965, 1968; Fano and Lee, 1973; Feneuille *et al.*, 1979; Fransson and Balatsky, 2007; Ganz *et al.*, 1984; Glutsch, 2002; Harmin, 1985; Hase *et al.*, 2006a; Heinzmann *et al.*, 1970; Heller and Mukamel, 1979; Janzen *et al.*, 1985; Kessler and Lorenz, 1970; Kleinpoppen and McDowell, 1976; Kokoouline *et al.*, 2002; Kolorenc *et al.*, 2005; Lee, 1998; Ley *et al.*, 1984; Maeda *et al.*,

1992; Margulis and Pyataev, 2004; Marinho *et al.*, 2001; Mehlhorn, 1998; Meijerink and Blasse, 1989; Nockel and Stone, 1994; Nussenzweig *et al.*, 1990; Oliveira and Wilkins, 1985; Patthey *et al.*, 1999; Pichl *et al.*, 2000; Ramaker and Schrader, 1974; Roney, 1994a,b, 1995; S. J. Xu and Zheng, 2006; Sanchez and Martin, 1994; Siegner *et al.*, 1995; Simonian *et al.*, 1995; Simpson and Fano, 1963; Smith *et al.*, 1973; Sturm *et al.*, 1992; Syage and Wessel, 1987; Taylor and Johnson, 1993; Ueda, 1987; Waligorski *et al.*, 1997; Wickenhauser *et al.*, 2005; Winstead and Langhoff, 1991; Yafet, 1981), thus, revealing the underlying mechanism of the observed resonances in terms of quantum-mechanical interaction between discrete and continuous states. In nuclear and atomic physics, interferences are often originating from the interaction of open (continuum) and closed (discrete levels) channels (Feshbach, 1958, 1962). Bhatia and Temkin (1984) unified the approaches of Fano and Feshbach with *ab initio* calculations and derived a rigorous expression of the asymmetry parameter  $q$  (Bhatia and Temkin, 1984).

There are limitations to the applicability of the Fano formula (1) (Connerade, 1998). First, it can be applied to describe single, isolated resonances. The appearance of more than two propagation pathes will change the profiles. Second, the width of the discrete level should be narrow enough compared to other resonant structures in the scattering profile.

In general, the Coulomb interaction between an outgoing electron  $e^-$  and a charged ion core  $A^+$  during auto-ionization leads to a renormalization of the energy levels of the many-electron system. Such a renormalization is known as the quantum defect of Rydberg series. To precisely describe the positions and width of the resonances, a multichannel quantum defect theory was developed by Seaton (1966) and Fano (1970), which provides a rigorous description of the process. It allows to derive all asymptotic quantities such as phase shifts or amplitudes of the auto-ionized levels. Eq. (1) was derived by Fano by neglecting effects due to long-range Coulomb interaction. Still it provides a physical insight into the auto-ionization process in terms of quantum-mechanical interference of discrete and continuum states.

At the resonance the phase of the scattering wave changes sharply by  $\pi$ . Thus, the interaction of scattering waves will result in constructive and destructive interference phenomena located very close to each other, corresponding to a maximum  $E_{\max}$  and a minimum  $E_{\min}$  of the transmission (absorption), respectively. The width of the resonance is proportional to the distance between them  $\Gamma \sim |E_{\max} - E_{\min}|$ . In principle, they may be located very close to each other  $E_{\max} \approx E_{\min}$ , resulting in a very narrow resonance  $\Gamma \approx 0$ , corresponding to a very long-lived quasi-bound state (Stillinger and Herrick, 1975). using artificial one-dimensional potentials one can even achieve  $\Gamma = 0$  (von Neumann and Wigner, 1929), as a proof of con-

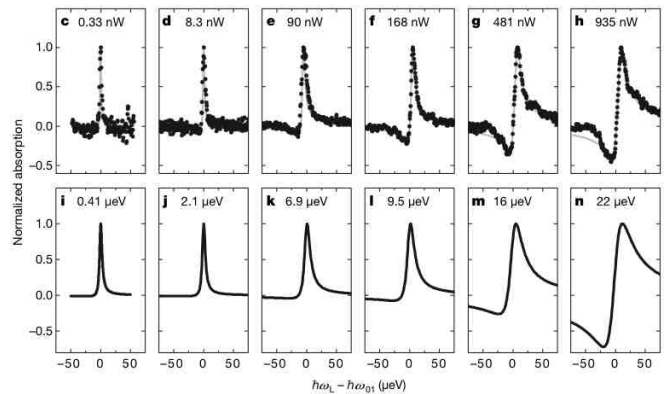


FIG. 6 Measured (upper row) and calculated (bottom row) absorption spectra of a single quantum dot for various laser powers. The absorption profile varies from a symmetrical to an asymmetrical one with increase of the laser power, indicating the enhancement of the continuum transition. From Kroner *et al.* (2008).

cept. By applying Feshbach's theory of resonances to two overlapping Fano resonances, Friedrich and Wintgen (1985a,b) demonstrated that the interference of several auto-ionizing levels of a Rydberg atom may lead to the formation of bound states in the continuum with anomalously narrow resonances.

### C. Light and structured matter

Experiments on the absorption cross-section of a single quantum dot, which is often considered as an artificial atom, have revealed that the asymmetry parameter  $q$  can be continuously tuned with the power of the laser (Kroner *et al.*, 2008). In this system, the transition rate to the discrete level saturates at high power, while the rate of the continuum transition does not (Zhang *et al.*, 2006). Eventually, the initially weak continuum transition rate will match the saturated transition rate to the discrete level with increasing laser power. As a result, a symmetric Lorentzian profile at low power will transform to an asymmetric Fano profile at sufficiently large power (see Fig. 6).

In biased semiconductor superlattices the Fano coupling parameter  $\Gamma$  between the discrete state and the continuum can be continuously tuned by varying the applied electric field (Holfeld *et al.*, 1998). The external bias gives rise to Wannier-Stark states, which interact with excitons, and result in asymmetric absorption spectra of Wannier-Stark transitions (Hino and Toshima, 2005; S. J. Xu and Zheng, 2006). The external bias determines the energy spacing of a Wannier-Stark subband, and, thus, controls the effective coupling between the discrete states and the continua. It allows to study the dephasing dynamics of the Fano resonance.

In general, the asymmetry parameter  $q$  is not restricted to be only real. In systems with broken time reversal

symmetry transition amplitudes to the discrete level and to the continuum may become complex, and so does the asymmetry parameter. The Fano resonance in such systems can be studied by analyzing the dynamical response. In particular, Misochko *et al.* (2005) found that the time-dependent reflection of light a bismuth single crystal after the excitation by an ultrashort laser pulse exhibits Fano asymmetric profiles in the Fourier transform of a time-periodic signal. They demonstrated that the asymmetric parameter varies periodically with the time delay between pump and probe pulses. The breaking of time reversal symmetry is indicated by the change of the sign of the asymmetry parameter.

Asymmetric lineshapes were also observed in Raman spectra of heavily doped semiconductors (Bechstedt and Peuker, 1975; Bell *et al.*, 1973; Cerdeira *et al.*, 1973a; Chandrasekhar *et al.*, 1978; Hopfield *et al.*, 1967; Magidson and Beserman, 2002) and high- $T_c$  superconductors (Friedl *et al.*, 1990; Limonov *et al.*, 1998, 2000; Misochko *et al.*, 2000). Although, almost any asymmetric profile of these spectra can be fitted by the Fano formula (Aleshkin *et al.*, 2007; Belitsky *et al.*, 1997; Cardona, 1983; Cardona *et al.*, 1974; Cerdeira *et al.*, 1973b; Hase *et al.*, 2006b; Jin and Xu, 2007; Jin *et al.*, 2001; Lee *et al.*, 2006; Menéndez and Cardona, 1985), a suitable theory for a quantitative description of these cases is still lacking. The general qualitative understanding is that the absorbed photon can initiate two kinds of processes. The first one is the inter- or intra-band electronic transition from the ground state to the continuum. The second process is the transition to an intermediate state followed by a one-phonon Raman emission and electron transition to either the initial ground state or to the excited donor state. Thus, the interference of two processes may in principle result in the Fano resonance.

#### D. Atoms and atoms

When two atoms collide with each other a quasi-bound state can be formed, which is characterized by a complex energy  $E = E_F + i\Gamma$ . In scattering theory this quasi-bound state is called a resonance since it possesses a finite life-time  $\hbar/\Gamma$ . The quasi-bound state is formed due to the excitation and sharing of electrons, and can be interpreted as an interaction between discrete and continuous states [see Fig. 3(b)]. In a similar manner, the observed asymmetric resonances in pre-dissociation (Bandrauk and Laplante, 1976; Cotting *et al.*, 1994; Lebech *et al.*, 2006; Lewis *et al.*, 2001; Palfy *et al.*, 2007) (or fragmentation) of molecules were explained by Rice (1933) in terms of auto-ionization. The concept was introduced by Feshbach (1958) in the context of reactions forming a compound nucleus. A Feshbach resonance in a two-particle collision appears whenever a bound state in a closed channel is coupled resonantly with a scattering continuum of an

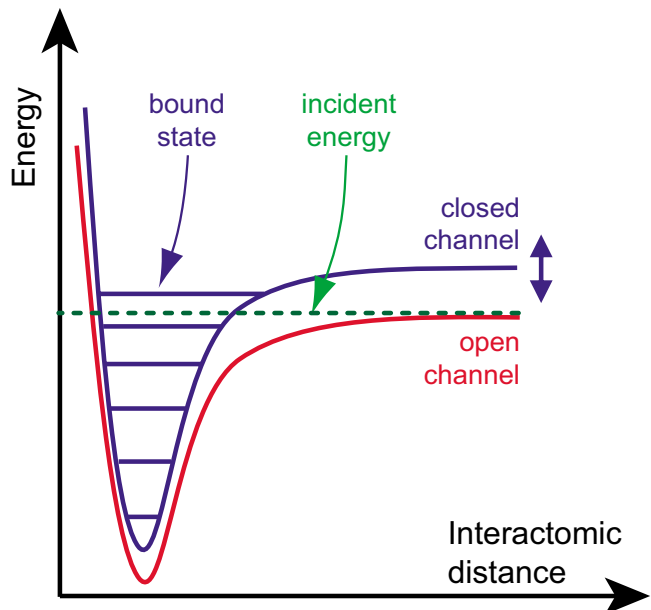


FIG. 7 (Color online) The two-channel model for a Feshbach resonance. Atoms which are prepared in the open channel, undergo a collision at low incident energy. In the course of the collision, the open channel is coupled to the closed channel. When a bound state of the closed channel has an energy close to zero, a scattering resonance occurs. From Bloch *et al.* (2008).

open channel (Bloch *et al.*, 2008). The scattered particles are temporarily captured in the quasibound state, and the associated long time delay gives rise to a Breit-Wigner-type resonance in the scattering cross section (see Fig.7).

A series of recent studies was devoted to the explicit calculation of scattering states for one-dimensional chains with two interacting bosons or fermions (Grupp *et al.*, 2007; Nygaard *et al.*, 2008a,b; Valiente and Petrosyan, 2009). These systems allow for two-particle continuum states, but also for bound states of two particles. Tuning the Bloch wave number, the bound state dissolves with the two-particle continuum. However, its trace inside the continuum remains, leads to a  $\pi$  phase shift of the scattering phase, and to corresponding Fano or Feshbach resonances in the scattering length. Notably in these problems a clear notion of resonant transport is absent, since there is no difference between a probe beam and a target due to indistinguishability of the two particles.

Efimov predicted that a three-body quantum system can support weakly bound states (trimer) under conditions when none of the three constituting pairs are bound (Efimov, 1970, 1971). Efimov trimer states appear in the limit where the two-body interaction is too weak to support a two-body bound state (dimer). Such trimer states should exist regardless of the nature of the two-body interaction, and, thus, are generic in few-body systems. Recently, the first experimental obser-

vation of Efimov states has been reported in ultracold cesium trimers (Kraemer *et al.*, 2006), by measuring the three-body recombination process  $\text{Cs} + \text{Cs} + \text{Cs} \rightarrow \text{Cs}_2 + \text{Cs}$ . The fingerprint of Efimov trimers in this system appears as a resonant enhancement and suppression of three-body collisions as a function of the two-atom interaction strength (Esry and Greene, 2006; Kraemer *et al.*, 2006), with typical asymmetric profiles. Mazumdar *et al.* (2006) explained this asymmetric response in terms of a Fano resonance, suggesting that the asymmetry can be used as a diagnostic tool for the Efimov effect.

### III. MODELING: COMPLEX GEOMETRIES

One possibility to model a Fano resonance is to choose the geometry of a given system in such a way, that (at least) two scattering pathes are available. In this Section we will consider the basic geometries which will do the job, and discuss several extensions.

#### A. Fano-Anderson model

One of the simplest models which describes the physics and the main features of the Fano resonance is the Fano-Anderson model (Mahan, 1993), which mimics the energy level structures [see Fig. 3(a)] of the model proposed by Fano (1961). In a simplified version (Miroshnichenko *et al.*, 2005b) it can be described by the following Hamiltonian

$$H = C \sum_n (\phi_n \phi_{n-1}^* + c.c.) + E_F |\psi|^2 + V_F (\psi^* \phi_0 + c.c.), \quad (3)$$

where the asterisk denotes complex conjugation. This model describes the interaction of two subsystems. One is a linear discrete chain with the complex field amplitude  $\phi_n$  at site  $n$  and nearest-neighbor coupling with strength  $C$ . This system supports propagation of plane waves with dispersion  $\omega_k = 2C \cos k$ . The second subsystem consists of a single Fano state  $\psi$  with the energy  $E_F$ . The interaction between these two subsystems is given by the coupling coefficient  $V_F$  between the state  $\psi$  and one site of the discrete chain  $\phi_0$ . A propagating wave may directly pass through the chain, or instead visit the Fano state, return back and continue with propagation. These two pathes are the ingredients of the Fano resonance.

The lattice Hamiltonian (3) generates the following differential equations:

$$\begin{aligned} i\dot{\phi}_n &= C(\phi_{n-1} + \phi_{n+1}) + V_F \psi \delta_{n0}, \\ i\dot{\psi} &= E_F \psi + V_F \phi_0. \end{aligned} \quad (4)$$

With the ansatz

$$\phi_n(\tau) = A_n e^{-i\omega\tau}, \quad \psi(\tau) = B e^{-i\omega\tau}, \quad (5)$$

we obtain a set of algebraic equations for the amplitudes:

$$\begin{aligned} \omega A_n &= C(A_{n-1} + A_{n+1}) + V_F B \delta_{n0}, \\ \omega B &= E_F B + V_F A_0. \end{aligned} \quad (6)$$

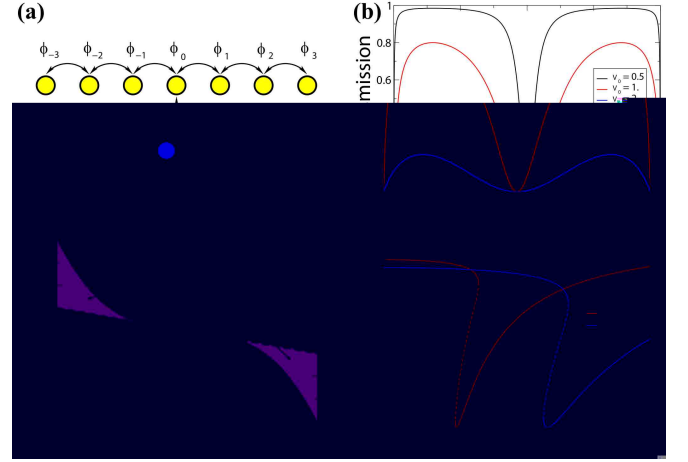


FIG. 8 (Color online) Fano-Anderson model as a discrete one-dimensional system with a single side-coupled Fano state defect. (a) The array of yellow circles corresponds to a linear chain, and the isolated blue circle is the Fano state. Arrows indicate the coupling between different states; (b) Transmission coefficient (10) for various values of the coupling coefficient  $V_F$ . Other parameters are  $C = 1$ , and  $E_F = 0$ ; (c) Areas of bistability of the nonlinear Fano resonance (dashed line) in the parameter space  $(\alpha_k, \gamma_k)$ ; (d) Nonlinear transmission coefficient versus input intensity for various frequencies  $\omega_k$  for  $C = 1$ ,  $V_F = 0.8$ ,  $E_F = 0$  and  $\lambda = 1$ . Regions of bistability are indicated by dashed lines, corresponding to unstable solutions. Adapted from Miroshnichenko *et al.* (2005b).

For a scattering problem, the system (6) should be solved for frequencies chosen from the propagation band  $\omega = \omega_k$  with the following boundary conditions

$$A_n = \begin{cases} I e^{ikn} + \rho e^{-ikn}, & n < 0, \\ \tau e^{ikn}, & n > 0, \end{cases} \quad (7)$$

where  $I$ ,  $r$ , and  $t$  have the meaning of the incoming, reflected and transmitted wave amplitudes, respectively.

From (6) it follows

$$B = \frac{V_F A_0}{\omega_k - E_F}, \quad (8)$$

and finally

$$\omega_k A_n = C(A_{n-1} + A_{n+1}) + \frac{V_F^2}{\omega_k - E_F} A_0 \delta_{n0}. \quad (9)$$

The main resulting action of the Fano state is that the strength of the effective scattering potential  $V_F^2/(\omega_k - E_F)$  resonantly depends on the frequency of the incoming wave  $\omega_k$ . If  $E_F$  lies inside the propagation band of the linear chain  $|E_F| < 2C$ , the scattering potential will become infinitely large for  $\omega_k = E_F$ , completely blocking propagation. Therefore meeting the resonance condition leads to a resonant suppression of the transmission, which is the main feature of the Fano resonance.

The transmission coefficient  $T = |\tau/I|^2$  can be computed by using the transfer matrix approach (Tong *et al.*, 1999), and expressed in the following

form (Miroshnichenko *et al.*, 2005b)

$$T = \frac{\alpha_k^2}{\alpha_k^2 + 1}, \quad (10)$$

where

$$\alpha_k = c_k(E_F - \omega_k)/V_F^2, \quad c_k = 2C \sin k. \quad (11)$$

Transmission vanishes at  $\omega_k = E_F$ . The expression of the transmission coefficient (10) corresponds to the Fano formula (1) with  $q = 0$ , where  $\alpha_k$  corresponds to the dimensionless energy, and  $E_F$  is the resonant frequency. The Fano state is an additional degree of freedom which allows waves propagating in the chain to interfere with those propagating through the discrete state.

The width of the resonance is defined as

$$\Gamma = \frac{V_F^2}{C \sin k_F}, \quad (12)$$

where  $k_F$  is the wavenumber at the resonance,  $E_F = \omega_{k_F}$ . The width of the resonance is proportional to the square of the coupling strength  $V_F^2$ .

The Fano-Anderson model (3) is perhaps the simplest one-dimensional model, which shows up with a Fano resonance. Since its asymmetry parameter  $q = 0$ , the location of the maximum in the Fano profile is tuned to infinity. The essence of the Fano resonance - destructive interference - is therefore not encapsulated in an asymmetric scattering profile with both a maximum and a minimum. It is the minimum which is generated by interference along several propagation paths. Due to its analytical simplicity the model may serve as a guideline for the analysis of more complicated physical models. There are many variations of this model (Burioni *et al.*, 2005, 2006; Chakrabarti, 2006; Miroshnichenko and Kivshar, 2005a) studied recently.

## B. Tuning the asymmetry parameter

The Fano-Anderson model (3) describes the resonant suppression of the transmission with a symmetric line-shape ( $q = 0$ ), emphasizing the main property of the Fano resonance which is destructive interference (resonant reflection). It can be easily extended in order to obtain a nonzero asymmetry parameter  $q$  with asymmetric lineshapes, such that both resonant suppression and resonant enhancement of the transmission will be located close to each other. Introducing a defect  $E_L \phi_L \delta_{nL}$  in the main array (4) [see Fig. 9(a)], both paths for scattering waves will yield phase shifts. As a result, both constructive and destructive interference phenomena may coexist, generating asymmetric transmission profiles [see Fig. 9(b)]. As observed in Fig. 9(b) the sign of the asymmetry parameter  $q$  alternates with the distance between the side-coupled defect and the defect in the main array (which is known as  $q$ -reversal (Kim and Yoshihara, 1993))

$$\text{sign}(\omega_{T_{\max}} - \omega_{T_{\min}}) = (-1)^L. \quad (13)$$

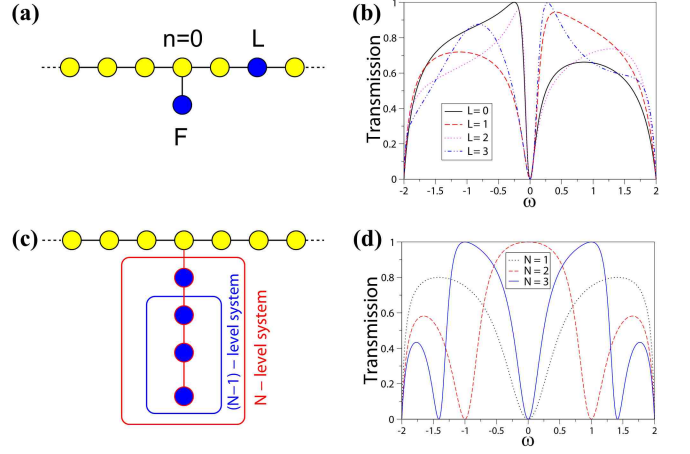


FIG. 9 (Color online) Variations of the Fano-Anderson model. (a) Schematic view of the Fano-Anderson model with an additional defect in the chain. (b) Transmission coefficient for different distances between the Fano site and the additional defect for parameters  $C = 1$ ,  $V_F = 0.5$ ,  $E_F = 0$ , and  $E_L = 1$ . (c) Schematic view of the Fano-Anderson model with a locally coupled  $N$ -defect chainlet. (d) Transmission coefficient of the  $N$ -site chainlet model. All sites in the chainlet are identical and with zero eigenfrequencies  $E_m = 0$ , and the couplings are  $C = V_m = 1$ . Adapted from Miroshnichenko and Kivshar (2005a).

Note that the maximum of the transmission does not need to reach the value  $T = 1$ . This incomplete constructive interference is due to additional phase accumulation along the propagation distance between two defects. It does not affect the destructive interference, at which strictly  $T = 0$ , confirming that  $T = 0$  is the only necessary and sufficient result of destructive interference and the Fano resonance.

## C. Many resonances

Consider now a replacement of the Fano site in the Fano-Anderson model by a finite chainlet, consisting of  $N$  coupled sites (Burioni *et al.*, 2005; Miroshnichenko and Kivshar, 2005a) [see Fig. 9(c)]. If the chainlet is decoupled from the linear discrete chain, the standing waves of the chainlet will give rise to  $N$  eigenfrequencies. Once the chainlet is coupled back to the linear discrete chain, each of the standing waves will provide with an additional path for a propagating wave, leading to a variety of interference phenomena. The finite chainlet could be considered as an approximation of a complex  $N$ -level system, such as a quantum dot, for example. Miroshnichenko and Kivshar (2005a) showed that, in general, there are exactly  $N$  total reflection ( $T = 0$ ) and  $N - 1$  total transmission ( $T = 1$ ) resonances [see Fig. 9(d)]. Each frequency of the total reflection corresponds to an eigenfrequency of the chainlet standing wave, and each total transmission corresponds to an eigenfrequency of the chainlet with  $(N - 1)$  sites,

indicated in Fig. 9(c). The resonances of some particular eigenstates of the side-coupled chainlet are excited.

Many other inhomogeneous networks were considered to design various topological filters (Burioni *et al.*, 2005, 2006). One can even plant Cayley trees into a discrete array and gather very well pronounced Fano resonances [see Fig. 10(a)].

#### D. Nonlinear Fano resonance

The Fano state amplitude becomes largest

$$|B_{\max}|^2 = 4V_F^2|I|^2/\Gamma^2, \quad (14)$$

exactly at the resonant value of the wave number  $k_F$ , and it diverges (and is therefore much larger than the amplitudes in the chain which are bounded by  $I$ ) in the limit of small coupling strength  $V_F$ .

Whatever the physical origin of the waves whose scattering is studied, large amplitudes call for corrections - either many-body interactions in a quantum setting, or nonlinear response corrections in a classical setting. Notably these corrections apply in first order only for the Fano state. Taking the classical setting, nonlinear Fano resonances (Miroshnichenko *et al.*, 2005b) were studied by introducing nonlinear corrections to the evolution equation for the Fano state only (6)

$$\omega B = E_F B + \lambda |B|^2 B + V_F A_0. \quad (15)$$

The nonlinear transmission coefficient can be expressed in the following form (Miroshnichenko *et al.*, 2005b)

$$T = \frac{x^2}{x^2 + 1}, \quad (16)$$

where  $x = -\cot \delta(k)$  is a function of the scattering phase  $\delta(k)$ , and satisfies the cubic equation

$$(x^2 + 1)(x - \alpha_k) - \gamma_k = 0, \quad (17)$$

with the parameter  $\gamma_k = \lambda c_k^3 |I|^2 / V_F^4$ . The nonlinear Fano resonance condition corresponds to  $x = 0$  in Eq.(17), which needs the condition  $\gamma_k = -\alpha_k$  to be satisfied [see Fig. 8(c)]. The transmission coefficient depends not only on the frequency of the incoming wave  $\omega_k$ , but on its intensity  $|I|^2$  as well. The presence of nonlinearity leads to a renormalization of the self-energy of the Fano state, and consequently to an intensity-dependent shift of the resonance. Miroshnichenko *et al.* (2005b) have shown that the nonlinear Fano resonance exists for any value of the input intensity  $|I|^2$  [see Fig. 8(c)]. Therefore, nonlinearity allows to tune the location of the Fano resonance by changing the intensity of the input waves. In general, there exist up to three solutions of the cubic Eq.(17), which will result in bistable transmission [see Fig. 8(d)].

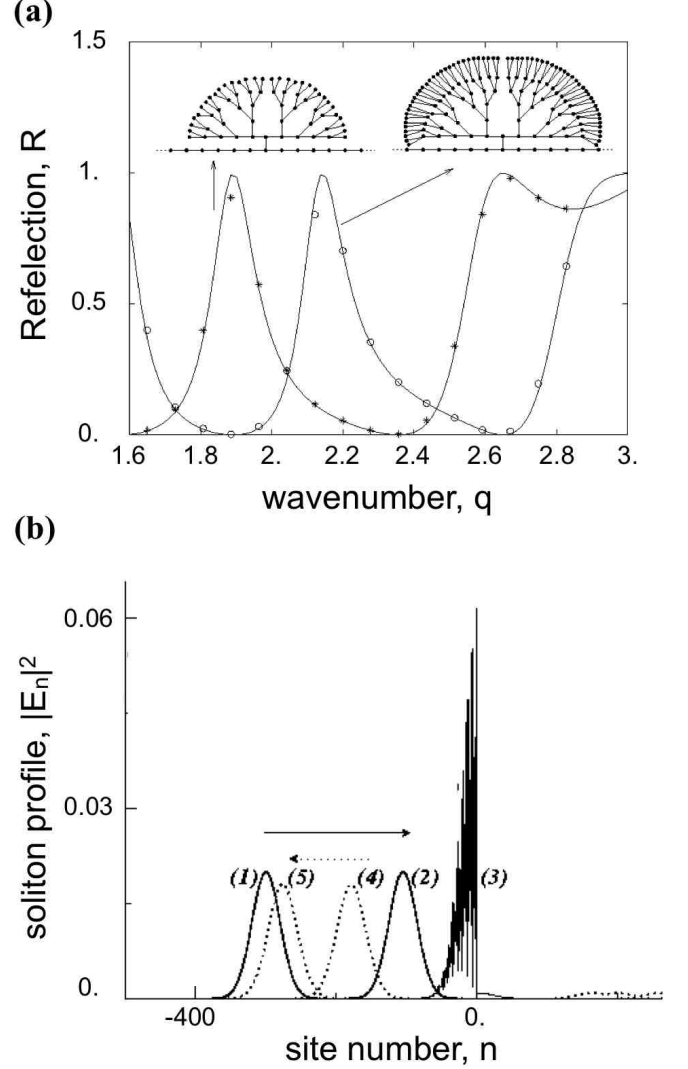


FIG. 10 Resonant reflection of a soliton in topological networks (a) The reflection coefficient versus wavenumber  $k$  for two Cayley trees of length  $M = 5$  (line) and  $M = 6$  (line) attached to the discrete array. Empty circles and stars correspond to direct numerical simulations of the soliton propagation. (b) Example of the soliton reflection by a Fano-like defect. From Burioni *et al.* (2005).

#### E. Resonant reflection of pulses and solitons

So far we discussed the scattering of monochromatic plane waves. Consider a pulse instead which is launched towards the scattering region. The more narrow the pulse is in real space, the broader is its spectral decomposition in Fourier (plane wave) space  $k$ , which is characterized by the maximum frequency  $\omega_m$  and the spectral width  $\Delta\omega$ . Each pulse component in Fourier space  $k$  will scatter as discussed above. The spectral width  $\Delta\omega$  has to be compared with the width of a Fano resonance  $\Gamma$ . If  $\Delta\omega \ll \Gamma$ , tuning  $\omega_m$  into resonance with a Fano resonance will lead to a practically complete reflection of the pulse. If on the contrary  $\Delta\omega \gg \Gamma$ , only a narrow part of the spectral

component of the pulse will be reflected, while the rest will be transmitted with a spectral hole 'burned' into it.

If nonlinearities are added into the propagation channel, they lead to an interaction between the various plane waves constituting the pulse and may ultimately yield nondispersing solitons. Their scattering by Fano defects was studied as well (Burioni *et al.*, 2005, 2006; Miroschnichenko *et al.*, 2003; Wulf and Skaložub, 2005). There are two characteristic time scales important for the scattering of solitons. One of them is the time the soliton resides in the vicinity of the defect  $\tau_{rs}$ , which is inversely proportional to its spectral width  $\Delta\omega$  and the soliton velocity  $v$ . The second one is set by the nonlinearity. It is the time scale on which the plane wave which constitute the soliton interact with each other  $\tau_{int}$  (Miroschnichenko *et al.*, 2003). For fast propagating solitons the residence time is much smaller than the interaction time  $\tau_{rs} \ll \tau_{int}$ . Then, during the scattering process the soliton can be considered as a set of noninteracting plane waves, and the results of the above pulse scattering apply (Burioni *et al.*, 2005, 2006; Miroschnichenko *et al.*, 2003) [see Fig. 10(b)]. In the opposite case, when the residence time is much larger than the interaction time  $\tau_{rs} \gg \tau_{int}$ , the nonlinearity-induced mode-mode interaction becomes crucial during the scattering process. In general a nonlinear interaction between many degrees of freedom (modes or plane waves) will lead to chaotic dynamics, and consequently to a dephasing of individual plane waves. Therefore phase coherence will not be maintained during the scattering, and interference effects will vanish. Therefore the Fano resonance should quickly deteriorate as the soliton parameters are tuned into the region of validity of the second case. This was numerically confirmed by Miroschnichenko *et al.* (2003).

## F. Quadratic nonlinearities

Consider the wave scattering in an array of channel waveguides with quadratic nonlinearity generated by periodic poling of several waveguides (Miroschnichenko *et al.*, 2005a). When the matching conditions are satisfied, the fundamental-frequency (FF) mode with frequency  $\omega$  can parametrically generate a second-harmonic (SH) wave with the frequency  $2\omega$  [see Fig. 11(a)], such that a structure with several poled waveguides may behave as a nonlinear defect with spatially confined quadratic nonlinearity (Iwanow *et al.*, 2004). The waveguide array can be described by a discrete model of weakly coupled linear waveguides with several waveguides having a quadratic nonlinear response (Iwanow *et al.*, 2004; Miroschnichenko *et al.*, 2005a), which is very similar to the Fano-Anderson model (4). The fundamental mode in this case can be considered as a continuum of propagating states, while the generated second harmonic can be either extended or effectively localized depending on the phase matching condition (Miroschnichenko *et al.*, 2005a). In the latter

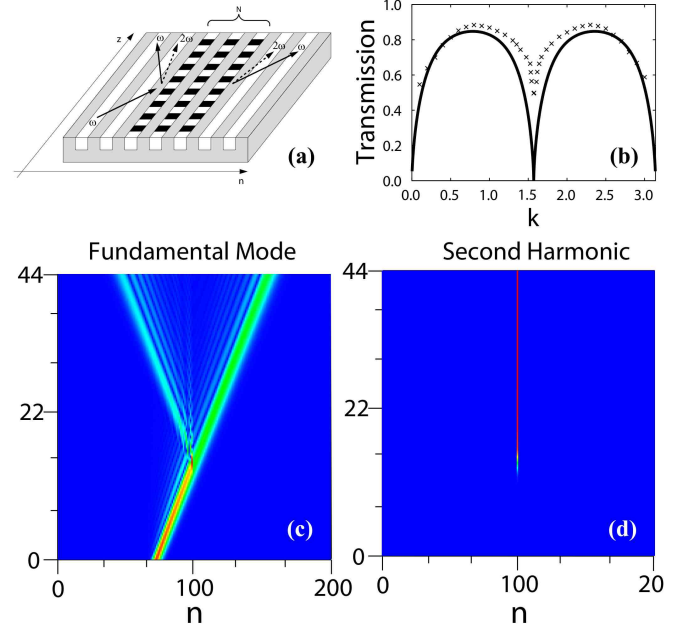


FIG. 11 (Color online) Light scattering in an array of channel waveguides with quadratic nonlinearity. (a) Schematic view of a one-dimensional array of channel waveguides with nonlinear defects, created by periodic poling. Arrows indicate the scattering process. (b) Comparison of the transmission coefficients of plane waves (solid line) and a Gaussian beam (crosses). Bottom: Example of the Gaussian beam scattering by a single nonlinear defect showing the resonant reflection part of the beam at the fundamental frequency (c), and resonant excitation of the second harmonic (d). Adapted from Miroschnichenko *et al.* (2005a).

case the excited second harmonic will act as a discrete state in the continuum, leading to the appearance of a Fano resonance in the transmission [see Fig. 11(b)]. Results of the direct numerical simulations of the Gaussian beam scattering are in a good agreement with the plane wave analysis [see Fig. 11(b)]. Figures 11(c,d) show the evolution of the fundamental and second harmonic of the Gaussian beam scattering at resonance. A part of the fundamental harmonic of the Gaussian beam is resonantly reflected by a single nonlinear defect [see Fig. 11(c)]. Since the spectral width of the Gaussian beam is larger than the width of the resonance some part of the beam still propagates through the defect. During the scattering the second harmonic is resonantly excited [see Fig. 11(d)]. After the scattered beam parts leave the defect region, the second harmonic persists in a self-sustained form.

## IV. MODELING: COMPLEX DYNAMICS

Several propagation pathes and interference phenomena can be generated not only by imprinting complex geometries, but also by using complex dynamics. Nonlinear wave excitations, e.g. discrete solitons, when scat-

tering small amplitude waves, generate several propagation paths purely dynamically. The reason is that the scattering potentials are time-dependent (in fact usually time-periodic). The amplitude and the temporal period can be tuned by controlling the characteristics of the nonlinear excitations (Emmanouilidou and Reichl, 2002; Li and Reichl, 1999; Martinez and Reichl, 2001). Total resonant reflection was also observed (Bagwell and Lake, 1992). This is because the time-periodic scattering potential generates several harmonics. In general, these harmonics will correspond to open and closed propagation channels, respectively. The presence of such dynamically generated channels is equivalent to a local increase of the spatial dimensionality, discussed in the previous Section. In other words, each new channel generates an alternative pathway for the scattering wave to propagate. The spectrum of excitations in each additional closed channel may contain discrete (localized) states, which happen to resonate with the continuum of the original open channel. As a result, Fano resonances can be expected, where the Fano state is the discrete state from a dynamically generated closed channel.

### A. Scattering by discrete breathers

Discrete breathers (DBs) are known as time-periodic and spatially localized solutions of nonlinear wave equations on lattices (Aubry, 1997; Flach and Gorbach, 2008; Flach and Willis, 1998; MacKay and Aubry, 1994). They originate from a constructive interplay between nonlinearity and discreteness. DBs exist independent of the lattice dimension, and are not relying on integrability properties. In return, these excitations can not freely move through lattices. Therefore, they act as scattering centers for small amplitude plane waves. Tuning the amplitude of the DB excitation, one tunes its temporal period, and all other characteristics of the resulting time-periodic scattering potential. DBs were detected and studied experimentally in interacting Josephson junction networks (Binder *et al.*, 2000; Trías *et al.*, 2000), coupled nonlinear optical waveguides (Eisenberg *et al.*, 1998), lattice vibrations in crystals (Swanson *et al.*, 1999), anti-ferromagnetic structures (Schwarz *et al.*, 1999), micro-mechanical cantilever arrays (Sato *et al.*, 2003), Bose-Einstein condensates loaded on optical lattices (Eiermann *et al.*, 2004), and many others (Flach and Gorbach, 2008).

Resonant scattering of plane waves by DBs was studied and showed Fano resonances with zero transmission  $T = 0$  (Flach *et al.*, 2003a,b; Kim and Kim, 2000, 2001; Lee and Kim, 2000b; Miroshnichenko *et al.*, 2005c). Below we will demonstrate the concept using a particular example of wave scattering by DBs in the discrete nonlinear Schrödinger model (DNLS) (Flach *et al.*, 2003b).

The equations of motion for the DNLS are given by

$$i\dot{\Psi}_n = C(\Psi_{n+1} + \Psi_{n-1}) + |\Psi_n|^2\Psi_n, \quad (18)$$

where  $n$  is an integer labeling the lattice sites,  $\Psi_n$  is a complex scalar variable and  $C$  describes the nearest neighbor interaction (hopping) on the lattice. The last term in (18) is a cubic nonlinearity. For small amplitude waves  $\Psi_n(t) = \epsilon e^{i(\omega_k t - kn)}$  the dispersion relation

$$\omega_k = -2C \cos k \quad (19)$$

follows from Eq.(18).

The DNLS model supports DB solutions with a single harmonic

$$\hat{\Psi}_n(t) = \hat{A}_n e^{-i\Omega_b t}, \quad \hat{A}_{|n| \rightarrow \infty} \rightarrow 0, \quad (20)$$

where the time-independent amplitude  $\hat{A}_n$  can be taken real valued, and the breather frequency  $\Omega_b \neq \omega_k$  is some function of the maximum amplitude  $\hat{A}_0$ . The spatial localization is given by an exponential law  $\hat{A}_n \sim e^{-\lambda|n|}$  where  $\cosh \lambda = |\Omega_b|/2C$ . Thus the DB can be approximated by a single-site excitation if  $|\Omega_b| \gg C$ . In this case the relation between the single-site amplitude  $\hat{A}_0$  and  $\Omega_b$  becomes  $\Omega_b = \hat{A}_0^2$ . In the following, the DB amplitudes for  $n \neq 0$  will be neglected, i.e.  $\hat{A}_{n \neq 0} \approx 0$ , since  $\hat{A}_{\pm 1} \approx (C/\Omega_b)\hat{A}_0 \ll \hat{A}_0$ .

Let us perturb the breather solution with small fluctuations  $\phi_n(t)$

$$\Psi_n(t) = \hat{\Psi}_n(t) + \phi_n(t) \quad (21)$$

and substitute this ansatz into (18). Linearization in the small fluctuating perturbation leads to the following set of equations:

$$i\dot{\phi}_n = C(\phi_{n+1} + \phi_{n-1}) + \Omega_b \delta_{n,0}(2\phi_0 + e^{-2i\Omega_b t} \phi_0^*) \quad (22)$$

with  $\delta_{n,m}$  being the Kronecker symbol. The DB generates a scattering potential that consists of two parts: a static (dc) one, which depends on the breather intensity only  $\sim \Omega_b = \hat{A}_0^2$ , and a dynamical (ac) one, which depends periodically on time  $\sim \Omega_b e^{-2i\Omega_b t}$ . With the two channel ansatz

$$\phi_n(t) = X_n e^{i\omega t} + Y_n^* e^{-i(2\Omega_b + \omega)t}, \quad (23)$$

Eq. (22) is reduced to a set of algebraic equations for the complex channel amplitudes  $X_n$  and  $Y_n$

$$-\omega X_n = C(X_{n+1} + X_{n-1}) + \Omega_b \delta_{n,0}(2X_0 + Y_0), \quad (24)$$

$$(2\Omega_b + \omega)Y_n = C(Y_{n+1} + Y_{n-1}) + \Omega_b \delta_{n,0}(2Y_0 + X_0). \quad (25)$$

For propagating the frequency  $\omega$  should be chosen from the propagation band  $\omega_k$ . As a result, the channel  $X_n$  supports extended waves, while for  $Y_n$  channel does not, since the frequency  $-(2\Omega_b + \omega_q)$  is outside the propagation band  $\omega_k$  (Flach *et al.*, 2003b) [see Fig. 12(a)]. Therefore the scattering takes place with an open channel  $X_n$  which interacts with a closed channel  $Y_n$ .

Let us consider the more general set of equations

$$-\omega_k X_n = C(X_{n+1} + X_{n-1}) - \delta_{n,0}(V_x X_0 + V_a Y_0), \quad (26)$$

$$(\Omega + \omega_k)Y_n = C(Y_{n+1} + Y_{n-1}) - \delta_{n,0}(V_y Y_0 + V_a X_0). \quad (27)$$

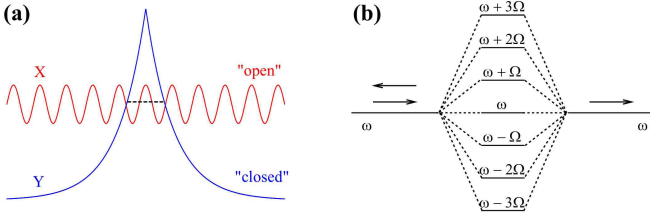


FIG. 12 (Color online) Time-periodic scattering potentials. (a) Schematic view of the open channel  $X$  and closed channel  $Y$  from the Eqs. (24-26). The dashed line indicates the localized state of the closed channel  $Y$  inside the open channel  $X$ ; (b) Schematic view of the virtual states, generated by a possibly infinite number of harmonics of the time-periodic scattering potential.

which can be reduced to Eq. (24) with the following parameters  $\Omega = 2\Omega_b$  and  $V_x = V_y = 2V_a = -2\Omega_b$ . For  $V_a = 0$  the closed channel  $Y_n$  possesses exactly one localized eigenstate

$$Y_n = Y e^{-\lambda|n|}. \quad (28)$$

with eigenfrequency

$$\omega_L^{(y)} = -\Omega + \sqrt{V_y^2 + 4C^2}. \quad (29)$$

The transmission coefficient for the general case  $V_a \neq 0$  (Flach *et al.*, 2003b)

$$T = \frac{4 \sin^2 k}{\left(2 \cos k - a - \frac{d^2 \eta}{2 - b\eta}\right)^2 + 4 \sin^2 k}, \quad (30)$$

$$a = \frac{-\omega_k + V_x}{C}, \quad b = \frac{\Omega + \omega_k + V_y}{C}, \quad d = \frac{V_a}{C}.$$

From Eq. (30) it follows that the transmission coefficient vanishes, when the condition

$$2 - b\eta = 0 \quad (31)$$

is satisfied, which is equivalent to requesting the resonance condition

$$\omega_k = \omega_L^{(y)}. \quad (32)$$

The conclusion is, that total reflection takes place when a local mode, originating from the closed  $Y$ -channel, resonates with the plane wave spectrum  $\omega_k$  of the open  $X$ -channel. The resonance condition is not renormalized by the actual value of  $V_a$ . The existence of local modes which originate from the  $X$ -channel for nonzero  $V_x$  and possibly resonate with the closed  $Y$ -channel is evidently not of any relevance. The resonant total reflection is a Fano resonance, as it is unambiguously related to a local state resonating and interacting with a continuum of extended states. The fact that the resonance is independent of  $V_a$  is due to the local coupling between the Fano state (originating from the  $Y$ -channel) and the open

channel, and originates from the approximative DB solution in the limit  $|\Omega_b| \gg C$ . Corrections to the DB solution will increase the range of coupling between the Fano state and the continuum, and correspondingly lead to a renormalization of the resonance location (Flach *et al.*, 2003b). Therefore we conclude, that the resonance location is not significantly renormalized, if the wavelength of the propagating wave is large compared to the extension of the space region where the coupling between a Fano state and a continuum occurs (Flach *et al.*, 2003a).

If the closed channel is reduced to the localized discrete Fano state  $Y$  only, the equations for the amplitudes take the form

$$\begin{aligned} -\omega X_n &= C(X_{n-1} + X_{n+1}) + V_a Y \delta_{n0}, \\ -\omega Y &= E_F Y - V_a X_0. \end{aligned} \quad (33)$$

The different signs in front of the coupling between the chain and the Fano state are due to the fact, that time-periodic scattering potentials correspond to eigenvalue problems with a symplectic propagator. At variance, complex geometries (6) do not leave the grounds of unitary propagators. Remarkably, these differences in the symmetries of the underlying dynamical processes do not alter the final result of destructive interference and Fano resonances.

The above analysis leads to a recipe of finding the position of resonances. One first calculates the localized states of closed channels decoupled from the open one (Flach *et al.*, 2003a,b). Switching on the coupling again, Fano resonances will take place exactly at the eigenfrequencies of the localized states for weak coupling. For stronger coupling the positions of the resonances will renormalize. In general, there is an infinite number of harmonics of the DB, which generate an infinite number of closed channels (Flach *et al.*, 2003a,b). The approach described above is rather generic and can be applied to the scattering through many types of oscillating barriers, self-induced (like DBs) or parametrically driven (by external forces) (Bagwell and Lake, 1992; Boese *et al.*, 2000; Emmanouilidou and Reichl, 2002; Kim, 2002; Li and Reichl, 1999; Longhi, 2006; Martinez and Reichl, 2001). All of them produce similar scattering potentials with an open and a number of closed channels for small amplitude scattering waves.

## B. Light scattering by optical solitons

The above concept of scattering by solitary excitations was applied to predict resonant light scattering by optical solitons in a slab waveguide with an inhomogeneous refractive index core (Flach *et al.*, 2006, 2005). The soliton is generated in a nonlinear planar waveguide by a laser beam injected into the slab along the  $z$ -direction [see Fig. 13(a)]. The soliton beam is confined in the  $y$ -direction by total internal reflection. The localization in the  $x$ -direction is achieved by a balance between linear diffraction and an instantaneous Kerr-type nonlinearity.

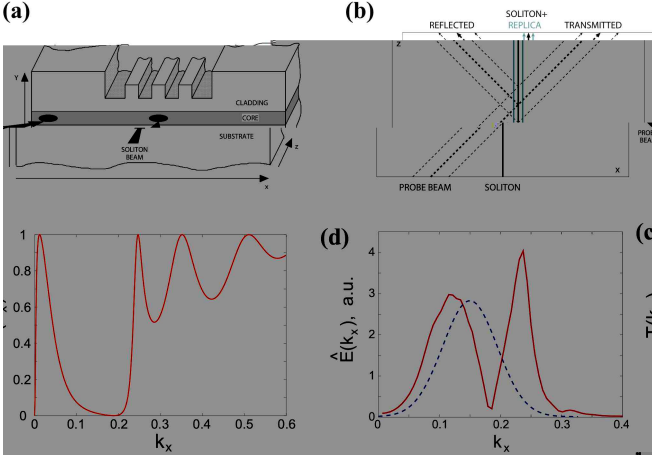


FIG. 13 (Color online) Light scattering by optical solitons. (a) Sketch of the scattering setup by an optical soliton in a one-dimensional waveguide array. The soliton beam is sent along the  $z$ -axis, while the probe beam propagates in the  $xz$ -plane at some angle to the soliton; (b) top view of the scattering process; (c) transmission coefficient vs  $k_x$  for plane waves under oblique incidence. There is total suppression of the transmission near  $k_x \approx 0.181$ ; (d) Fourier spectrum of the incident (dashed line) and transmitted (solid line) beams. The suppression of the resonant frequency [see plot (c)] in the spectrum is observed. Adapted from Flach *et al.* (2005).

The analogy with the discussed above scattering problem by time-periodic potentials comes from the possibility to interpret the spatial propagation along the  $z$ -direction as an artificial time (Agrawal, 1995). Thus, the propagation constant of the soliton can be considered as the frequency of the breather. The evolution of the soliton envelope function satisfies the nonlinear Schrödinger equation (NLS), the continuum analog of Eq. (18) (Flach *et al.*, 2005). The analysis of the scattering problem is similar to the above discussed one. Figure 13(c) shows the dependence of the transmission coefficient for oblique incident light for various  $k_x$  wavenumbers. It results in a Fano resonance for plane waves at  $k_x \approx 0.181$ , where the transmission coefficient vanishes. This result has been confirmed by direct numerical simulations of a propagating small-amplitude wavepacket scattered by the optical soliton (Flach *et al.*, 2006) [see Fig. 13(b)]. The Fourier spectrum of the transmitted wavepacket reveals that the resonant wavenumber  $k_x \approx 0.181$  was filtered out from the initial wavepacket [see Fig. 13(d)]. Such a spectral hole burning effect can be used as a characteristic feature for the detection of the Fano resonance in an experimental setup.

### C. Plasmon scattering in Josephson junction ladders

Another theoretical prediction concerns the plasmon wave scattering by DBs in Josephson junction ladders (JJs). JJs are formed by an array of small Josephson junctions that are arranged along the spars and rungs

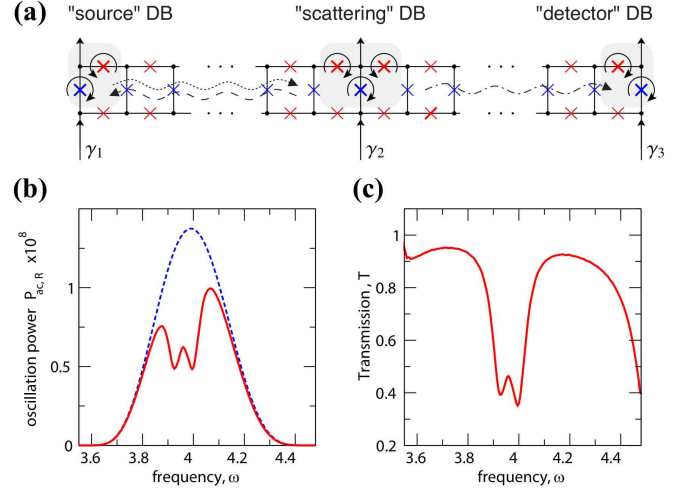


FIG. 14 (Color online) Plasmon scattering by discrete breathers in Josephson junction ladders. (a) Schematic setup for the measurement of plasmon scattering with the use of controlled bias currents  $\gamma_i$ ; (b) Oscillating power  $P_{ac,R}$  at the right end with (red solid line) and without (blue dashed line) the DB; (c) Transmission coefficient  $T$ , derived from (b) by using Eq. (34). Adapted from Miroshnichenko *et al.* (2005c).

of a ladder [see Fig. 14(a)]. Each junction consists of two small weakly coupled superconducting islands. The dynamical state of a junction is described by the phase difference  $\phi(t)$  (Josephson phase) of the superconducting order parameters of two neighbouring islands. When the difference does not vary in time  $\phi(t) = \text{const}$ , the junction is traversed by a superconducting current only, with zero voltage drop. Otherwise, the junction is traversed in addition by a resistive current component with a nonzero voltage drop  $V \propto \dot{\phi}(t)$ . It was observed experimentally that JJs support dynamic localized states (DBs) (Binder *et al.*, 2000; Trías *et al.*, 2000). A discrete breather is characterized by a few junctions being in the resistive state  $\langle \dot{\phi} \rangle \neq 0$  while the others reside in the superconducting state  $\langle \dot{\phi} \rangle = 0$ . The frequency of a DB is proportional to the average voltage drop across the resistive junctions  $\Omega_b \propto \langle \dot{\phi} \rangle$ . Miroshnichenko *et al.* (2005c) have recently proposed an experimental setup to measure Fano resonances in that transmission line. Small amplitude waves are generated in a JJL with open ends by applying locally a time-periodic current  $\gamma_1(t) = \gamma_{ac} \cos(\omega t)$ . The local current acts as a local parametric drive. It excites edge junctions at a frequency  $\omega$ . This tail extends into the ladder. To monitor the linear wave propagation in the system, the time-averaged oscillation power  $P_{ac,n} = \langle \dot{\phi}_n^2 \rangle$  is measured. The transmission coefficient can be obtained by relating the oscillation power at the right boundary with and without an excited DB in the system

$$T = \frac{P_{ac,R}(\text{with DB})}{P_{ac,R}(\text{without DB})}. \quad (34)$$

Figures 14(b,c) show the presence of resonant suppression of the transmission coefficient for particular frequencies  $\omega$ . The analysis in Ref. (Miroschnichenko *et al.*, 2005c) reveals that they correspond to Fano resonances, which originate from localized states of closed channels of the time-periodic scattering potential which is generated by the DB.

#### D. Matter wave scattering in Bose-Einstein condensates

Over the last couple of years, it has been shown that optical lattices, generated by counter-propagating laser beams and providing a periodic potential modulation for the atoms, introduce many interesting and potentially useful effects by modifying single atom properties and enhancing correlations between atoms (Morsch and Oberthaler, 2006). Using about 1000  $^{87}\text{Rb}$  atoms in a quasi one-dimensional optical lattice, Eiermann *et al.* (2004) obtained a spatially localized Bose-Einstein condensate (BEC) which is an experimental manifestation of a gap soliton, or a discrete breather. The solitary state exists due to the atom-atom interaction, which can be tuned in various ways experimentally.

Vicencio *et al.* (2007) considered a BEC on a lattice, where interactions between atoms are present only in a very localized region (see Fig. 15). Such a situation could be realized experimentally by combining optical lattices with atom-chip technology (Hänsel *et al.*, 2001; Ott *et al.*, 2001) or in optical micro-lens arrays (Dumke *et al.*, 2002). The system is described by the discrete nonlinear Schrödinger (DNLS) equation, a classical variant of the Bose-Hubbard model appropriate for a BEC in a periodic potential in the tight binding limit (Morsch and Oberthaler, 2006). With interactions being present only on site number  $n_c$ , it follows

$$i\frac{d\Psi_n}{dt} = -(\Psi_{n+1} + \Psi_{n-1}) - \gamma|\Psi_{n_c}|^2\Psi_{n_c}\delta_{n,n_c}, \quad (35)$$

where  $\Psi_n$  is the complex amplitude of the condensate field at site  $n$  and  $-\gamma = U/J$  is the interaction strength on site  $n_c$ , where  $J$  is the tunneling energy between the lattice sites and  $U$  is on-site interaction energy per atom.

Equations (35) support a localized state  $\Psi_n(t) = bx^{|n-n_c|} \exp(-iE_b t)$ , where  $x = -\frac{1}{2}(E_b + g)$  with  $g = \gamma b^2$ ,  $b$  is the condensate amplitude and  $E_b = -(4 + g^2)^{1/2}$  is the chemical potential.

The scattering of propagating atomic matter waves with the energy  $E_k = -2\cos k$  by this localized BEC were calculated analytically within the framework of the Bogolyubov-DeGennes equations (Vicencio *et al.*, 2007). The transmission  $T(k)$  is shown in Fig. 16 for three values of  $g$  (solid curves). As  $g$  increases, the width and the position of the resonance increase. Furthermore, the more localized the BEC becomes, the stronger it reflects the atom beam off resonance. By tuning the nonlinear parameter  $g$ , we can thus choose the amount of the beam which passes through the BEC. Off resonance (for larger

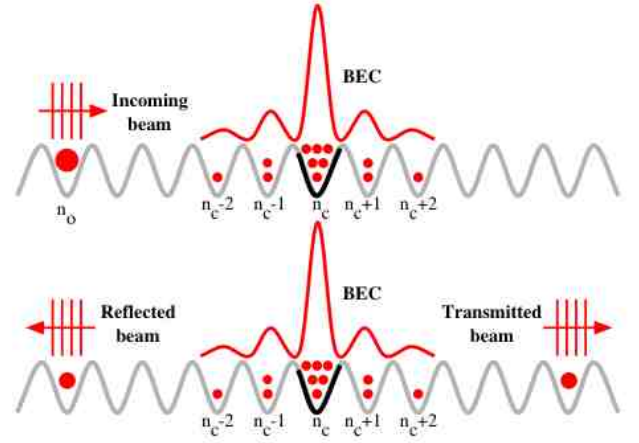


FIG. 15 (Color online) Scattering scheme in an optical lattice. The incoming, reflected, and transmitted beams of atoms are represented as plane waves. The atoms interact only around  $n = n_c$ , where the BEC is centered. From Vicencio *et al.* (2007).

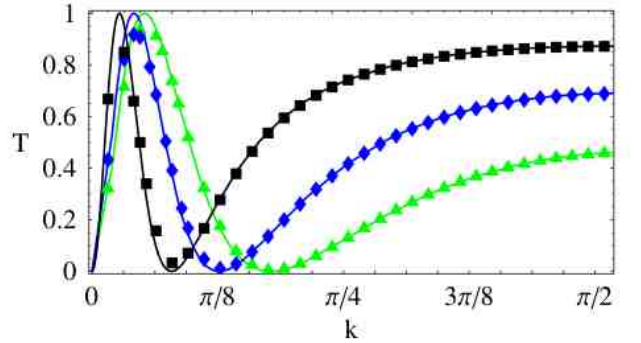


FIG. 16 (Color online). Transmission  $T$  versus momentum  $k$ . Lines: analytic solution, symbols: real time numerical simulations of Eq. (35) using wave packets for  $g = 0.36$  (line and boxes),  $g = 0.6$  (line and diamonds), and  $g = 0.9$  (line and triangles). From Vicencio *et al.* (2007).

values of  $k$ ), we can select the percentage of the incoming beam that is transmitted for a defined quasi-momentum. Therefore, the actual setup can be used as a 100% blockade or as a selective filter.

The analytical results have been confirmed by numerical simulation of Eq. (35) with a Gaussian atom beam profile. The results are shown in Fig. 16 by the symbols for three different values of the parameter  $g$ . The agreement between theory and simulations is very good.

#### V. LIGHT PROPAGATION IN PHOTONIC DEVICES

Optical microcavity structures are of great interest for device applications, and many of these structures

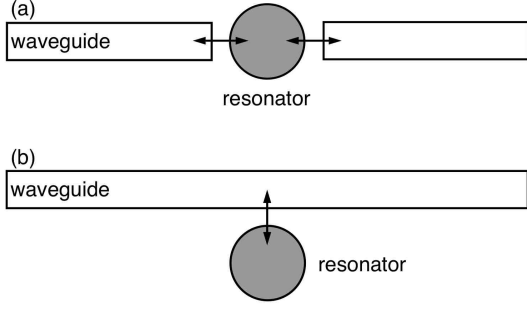


FIG. 17 Schematic setup for (a) a waveguide directly coupled to a cavity and (b) a waveguide side-coupled to a cavity.

involve coupling of one or several cavities to a waveguide. Such waveguide-cavity systems can naturally exhibit Fano resonances with high quality factors, and they can be used for optical modulations and switching. The on/off switching functionality can be realized by shifting the resonant frequency either toward or away from the signal frequency.

The basic geometry of a waveguide-cavity system which demonstrates a sharp Fano resonance has been introduced and analyzed in Refs. (Haus and Lai, 1991; Xu *et al.*, 2000). It consists of a waveguide coupled to a cavity (or resonator). In general, two-port photonic devices based upon waveguide-resonator interaction can be presented in two geometries, as shown in Figs. 17(a,b). The first configuration is based on a direct-coupling geometry (Marin Soljačić and Joannopoulos, 2002), and the second geometry is a waveguide side coupled with a single-mode cavity (Xu *et al.*, 2000; Yanik *et al.*, 2003a). Such structures are tunable by adding cavities with nonlinear response or by employing an external control. Below, we review the basic properties of the simplest waveguide-cavity systems, and discuss several generalizations including all-optical switching structures based on the concepts of Fano resonances.

### A. Green's function formalism

The Green's function approach (Mingaleev and Kivshar, 2002a,b) allows to obtain very accurate results in comparison to the time-consuming direct numerical finite-difference time-domain (FDTD) simulations, even for rather complex geometries of the waveguide-cavity systems. To derive the corresponding equations, one takes the explicit temporal dependencies into account which allow one to study the pulse propagation and scattering.

We consider a photonic crystal created by a periodic square lattice of infinite cylindrical rods parallel to the  $z$  axis. We neglect the material dispersion and assume the

dielectric constant  $\epsilon(\vec{r})$  to be periodic in two transverse directions,  $\vec{r} = (x, y)$ . The evolution of the  $E$ -polarized electric field propagating in the  $(x, y)$  plane is governed by the scalar wave equation

$$\nabla^2 E_z(\vec{r}, \tau) - \frac{1}{c^2} \partial_\tau^2 [\epsilon(\vec{r}) E_z(\vec{r}, \tau)] = 0, \quad (36)$$

where  $\nabla^2 = \partial_x^2 + \partial_y^2$ . We assume that the light field propagating in such structures can be separated into fast and slow components,  $E_z(\vec{r}, \tau) = e^{-i\omega\tau} E(\vec{r}, \tau|\omega)$ , where  $E(\vec{r}, \tau|\omega)$  is a slowly varying envelope of the electric field, i.e.  $\partial_\tau^2 E(\vec{r}, \tau|\omega) \ll \omega \partial_\tau E(\vec{r}, \tau|\omega)$ . This allows to simplify Eq. (36) to the following form

$$\left[ \nabla^2 + \epsilon(\vec{r}) \left( \frac{\omega}{c} \right)^2 \right] E(\vec{r}, \tau|\omega) \simeq -2i\epsilon(\vec{r}) \frac{\omega}{c^2} \frac{\partial E(\vec{r}, \tau|\omega)}{\partial \tau} \quad (37)$$

Both the straight waveguide and the side-coupled cavity are created by introducing defect rods into a perfect two-dimensional periodic structure. Therefore, the dielectric constant can be represented as a sum of two components, describing the periodic and defect structures  $\epsilon(\vec{r}) = \epsilon_{pc} + \delta\epsilon$ . We employ the Green's function of the two-dimensional periodic structure without defects, and rewrite Eq. (37) in the integral form

$$E(\mathbf{x}, \tau|\omega) = \int d^2\mathbf{y} G(\mathbf{x}, \mathbf{y}|\omega) \hat{L} E(\mathbf{y}, \tau, \omega), \quad (38)$$

where we introduce the linear operator

$$\hat{L} = \left( \frac{\omega}{c} \right)^2 \delta\epsilon(\vec{r}) + 2i\epsilon(\vec{r}) \frac{\omega}{c^2} \frac{\partial}{\partial \tau}, \quad (39)$$

and consider the time evolution of the slowly varying envelope as a perturbation to the steady state.

The defect rods introduced into the periodic structure can formally be described as follows:

$$\delta\epsilon(\vec{r}) = \sum_{n,m} \left[ \delta\epsilon_{m,n}^{(0)} + \chi^{(3)} |E(\mathbf{x}, \tau|\omega)|^2 \right] \theta(\mathbf{x} - \mathbf{x}_{n,m}), \quad (40)$$

where we use the  $\theta$ -function to describe the position of a defect rod at site  $n, m$ , with  $\theta(\mathbf{x}) = 1$  for  $\mathbf{x}$  inside the defect rods, and  $\theta(\mathbf{x}) = 0$  otherwise.  $\delta\epsilon_{m,n}^{(0)}$  is the variation of the dielectric constant of the defect rod  $(m, n)$ . Importantly, this approach allows us to incorporate a nonlinear response in a straightforward manner, which is assumed to be of the Kerr type being described by the term  $\chi^{(3)} |E|^2$ .

Substituting Eq. (40) into the integral equation (38) and assuming that the electric field does not change inside the dielectric rods, we can evaluate the integral at the right hand side of Eq. (38) and derive a set of *discrete nonlinear equations*

$$i\sigma \frac{\partial}{\partial \tau} E_{n,m} - E_{n,m} + \sum_{k,l} J_{n-k,m-l}(\omega) (\delta\epsilon_{k,l}^{(0)} + \chi^{(3)} |E_{k,l}|^2) E_{k,l} = 0, \quad (41)$$

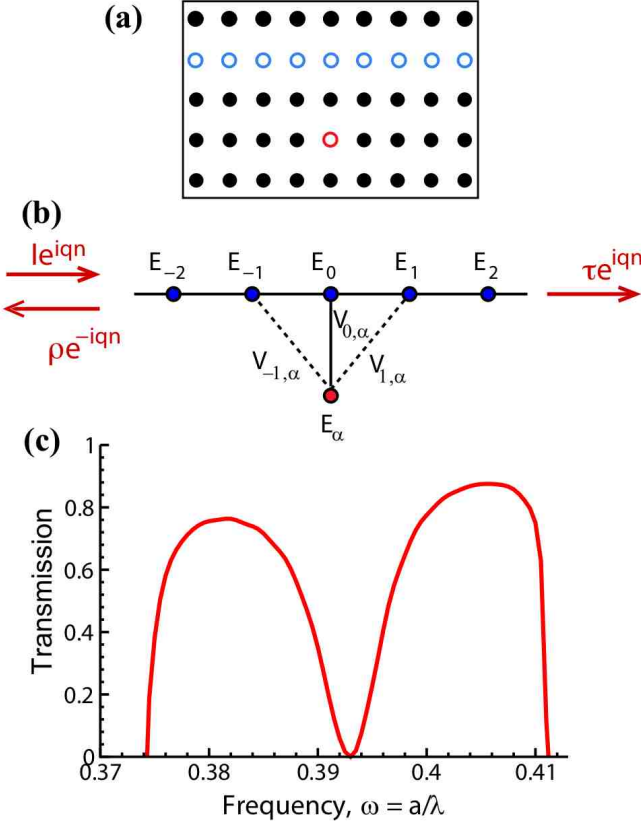


FIG. 18 Schematic view of (a) photonic crystal waveguide with an isolated side-coupled cavity, and (b) effective discrete system. (c) Typical profile of the Fano resonance.

for the amplitudes of the electric field  $E_{n,m}(\tau|\omega) = E(\mathbf{x}_{n,m}, \tau|\omega)$  calculated at the defect rods. The parameters  $\sigma$  and  $J_{k,l}(\omega)$  are determined by using the corresponding integrals of the Green's function, where the whole information about the photonic crystal dispersion is now hidden in their specific frequency dependencies, which can be found in Refs. (Mingaleev and Kivshar, 2001; Mingaleev *et al.*, 2006). In this way, the Green's function needs to be calculated only once for a given photonic structure, e.g. by employing the approach outlined in Ref. (Ward and Pendry, 1998), and then it can be used to study any photonic circuit in that structure.

For the simple system when the photonic crystal has a waveguide side coupled to a single defect see Fig. 18(a)], the problem describes a discrete system studied earlier [see Fig. 18(b)], and the transmission shows a Fano resonance [see Fig. 18(c)], analyzed in details in Refs. (Mingaleev *et al.*, 2006; Miroshnichenko *et al.*,

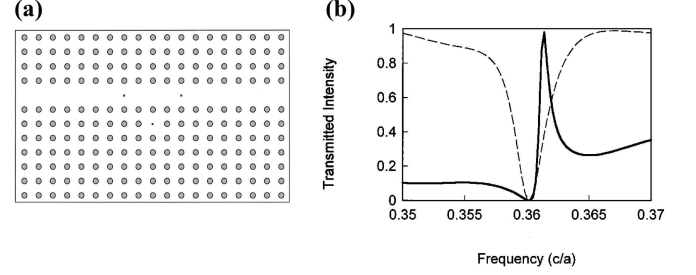


FIG. 19 Light propagation in a photonic crystal waveguide with a side-coupled cavity. (a) Photonic crystal waveguide formed by removing a single row of rods. Within the line defect there are two smaller rods. A point defect, created by reducing the radius of a single rod, is placed away from the waveguide. (b) Transmission spectra through the structure (a) with (solid) and without (dashed) the two defects in the waveguide. From Fan (2002).

2005b).

In a general case, the effective interaction between defect rods is of long-range nature (Mingaleev and Kivshar, 2002b; Mingaleev *et al.*, 2000). However, the coupling strength decays exponentially with the distance and, as a result, for coupled-resonators optical waveguides the specific discrete arrays with nearest-neighbor interactions (at  $L = 1$ ) give already an excellent agreement with direct FDTD simulations (Mingaleev and Kivshar, 2002b).

## B. Defects in the waveguide

The two basic geometries shown in Figs. 17(a,b) can be further improved by placing partially reflecting elements into the waveguides (Fan, 2002; Khelif *et al.*, 2003). These elements allow creating sharp and asymmetric response line shapes. In such systems, the transmission coefficient can vary from 0% to 100% in a frequency range narrower than the full width of the resonance itself.

To illustrate the effect of defects, Fan (Fan, 2002) simulated the response of the structure shown in Fig. 19(a) using a FDTD scheme with perfectly matched layer boundary conditions. A pulse is excited by a monopole source at one end of the waveguide. The transmission coefficient is then calculated by Fourier transforming the amplitude of the fields at the other end, and is shown as a solid line in Fig. 19(b). In comparison, the transmission spectra for the same structure, but without the two small cylinders in the waveguide, is shown by a dashed line.

Importantly, no detailed tuning of either the resonant

frequency or the coupling between the cavity and the waveguide is required to achieve asymmetric line shapes. Also, since the reflectivity of the partially reflecting elements need not to be large, the underlying physics here differs from typical coupled-cavity systems, and resembles Fano resonances involving interference between a continuum and a discrete level.

### C. Sharp bends

One of the most fascinating properties of photonic crystals is their ability to guide electromagnetic waves in narrow waveguides created by a sequence of line defects, including light propagation through extremely sharp waveguide bends with nearly perfect power transmission (Lin *et al.*, 1998; Mekis *et al.*, 1996). It is believed that the low-loss transmission through sharp waveguide bends in photonic crystals is one of the most promising approaches to combine several devices inside a compact nanoscale optical chip.

Interestingly, the transmission through sharp bends in photonic crystal waveguides can be reduced to a simple model with Fano resonances, where the waveguide bend hosts a specific localized defect. Miroshnichenko and Kivshar (2005b) derived effective discrete equations for two types of the waveguide bends in two-dimensional photonic crystals and obtained exact analytical solutions for the resonant transmission and reflection.

### D. Add-drop filters

Fano resonances can be employed for a variety of photonic devices based on resonant tunneling. In particular, if two waveguides interact through a coupling element which supports a localized mode, a channel add-drop filter can be realized via the resonant tunneling between the waveguides (Fan *et al.*, 1998, 1999; Soljačić *et al.*, 2003). The schematic diagram of a generic coupled system of this kind is shown in Fig. 20(a). At Fano resonance, the propagating state excites the resonant modes, which in turn decay into both waveguides. The transmitted signal in the first waveguide is made up of the directly propagating signal and the signal which originates from the second path which visits the coupling region. In order to achieve complete transfer from one waveguide to the other one, these two signal components must interfere destructively. The reflected amplitude, on the other hand, originates entirely from the second path into the coupling region. Hence, at least two states in the coupling region are needed to achieve also destructive interference of backscattered waves in the first waveguide. With these conditions satisfied, one may resonantly transfer the excitation from the first into the second waveguide.

This concept was developed by Fan *et al.* (1998) for the propagation of electromagnetic waves in a two-

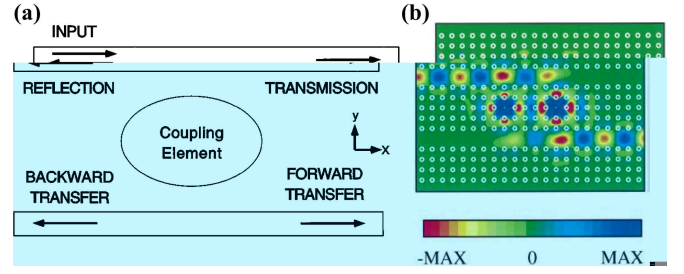


FIG. 20 (Color online) Add-drop filter. (a) Schematic diagram of two waveguides coupled through an element which supports a localized resonant state. (b) Electric field pattern of the photonic crystal at the resonant frequency. The white circles indicate the position of the rods. From Fan *et al.* (1998).

dimensional photonic crystal. To realize this concept, they used two photonic crystal waveguides and two coupled single-mode high- $Q$  cavities, as shown in Figure 20(b). The photonic crystal is made of a square lattice of high-index dielectric rods, and the waveguides are formed by removing two rows of dielectric rods. The cavities are introduced between the waveguides by reducing the radius of two rods. The resonant states have different symmetry. An accidental degeneracy, caused by an exact cancellation between the two coupling mechanisms, is enforced by reducing the dielectric constant of four specific rods in the photonic crystal. The cancellation could equally have been accomplished by reducing the size of the rods instead of their dielectric constant.

Figure 20(b) shows the field pattern at resonance. The quality factor is larger than  $10^3$ . The backward transferred signal is almost completely absent over the entire frequency range.

This type of four-port photonic crystal systems can be employed for optical bistability, being particularly suitable for integration with other active devices on a chip (Soljačić *et al.*, 2003). A similar concept can be employed for the realization of all-optical switching action in a nonlinear photonic crystal cross-waveguide geometry with instantaneous Kerr nonlinearity. There the transmission of a signal can be reversibly switched on and off by a control input (Yanik *et al.*, 2003b).

### E. All-optical switching and bistability

A powerful principle that could be explored to implement all-optical transistors, switches, and logical gates is based on the concept of optical bistability. The use of photonic crystals enables the system to be of a size of the order of the wavelength of light, consume only a few milliwatts of power, and have a recovery and response time smaller than 1 ps. Several theoretical and experimental studies explored nonlinear Fano resonances for designing optimal bistable switching in nonlinear photonic crystals (Cowan and Young, 2003;

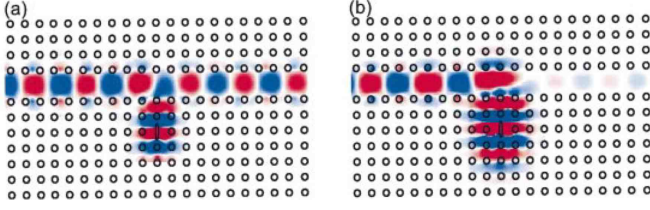


FIG. 21 (Color online) Electric field distributions in a photonic crystal for (a) high and (b) low transmission states. Red and blue colors represent large positive or negative electric fields, respectively. The same color scale is used for both panels. The black circles indicate the positions of the dielectric rods. From Yanik *et al.* (2003a).

Maes *et al.*, 2008; Marin Soljačić and Joannopoulos, 2002; Mingaleev and Kivshar, 2002b; Mingaleev *et al.*, 2007, 2006; Yanik *et al.*, 2003a). A photonic crystal provides an optimal control over the input and output and facilitates further large-scale optical integration.

The main idea of using the Fano resonance for all-optical switching and bistability is quite simple: One should introduce an element with nonlinear response and achieve nonlinearity-induced shifts of the resonant frequency, as was discussed above for discrete models. Thus, by employing *nonlinear Fano resonances* we can achieve bistability in many of the device structures suggested on the photonic-crystal platform. For example, for the side-coupled geometry shown in Fig. 17(b), one could take advantage of the interference between the propagating wave inside the waveguide and the decaying wave from the cavity, to greatly enhance achievable contrast ratio in the transmission between the two bistable states. This approach was realized by Yanik *et al.* (2003a) who demonstrated that such a configuration can generate extremely high contrast between the bistable states in its transmission with low input power.

One of the great advantages in using nonlinear photonic-crystal cavities is the enhancement of nonlinear optical processes, including nonlinear Fano resonance (Bravo-Abad *et al.*, 2007; Soljačić and Joannopoulos, 2004). Such an enhancement can be very efficient in the regime of the slow-light propagation, that was demonstrated experimentally with the smallest achieved group velocity  $c/1000$  (Gersen *et al.*, 2005; Jacobsen *et al.*, 2005; Notomi *et al.*, 2001; Vlasov *et al.*, 2005). Because of this success, the interest in slow-light applications based on photonic-crystal waveguides is rapidly growing, and posing problems of a design of different types of functional optical devices which would efficiently operate in the slow-light regime.

Recently, Mingaleev *et al.* (2007) have studied the resonant transmission of light through a photonic-crystal waveguide coupled to a nonlinear cavity, and demonstrated how to modify the structure geometry for achieving bistability and all-optical switching at ultra-low powers in the slow-light regime. This can be achieved by

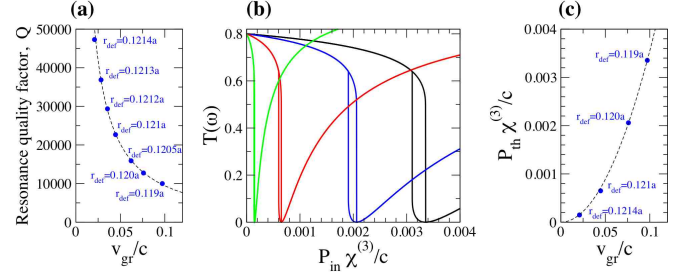


FIG. 22 (Color online) Ultra-low all-optical switching in the slow-light regime. (a) Quality factor  $Q$  vs. group velocity  $v_g$  at resonance for the waveguide-cavity structure. (b) Nonlinear bistable transmission at the frequencies with 80% of linear light transmission vs. the incoming light power for different values of the rod radius; (c) Switch-off bistability threshold vs. the group velocity at resonance. From Mingaleev *et al.* (2007).

placing a side-coupled cavity between two defects of a photonic-crystal waveguide assuming that all the defect modes and the cavity mode have the same symmetry. In this structure the quality factor grows inversely proportional to the group velocity of light at the resonant frequency and, accordingly, the power threshold required for all-optical switching vanishes as a square of the group velocity (see Fig. 22).

The numerically obtained dependence  $Q(v_{gr}) \sim 1/v_{gr}$  is shown in Fig. 22(a), and it is in an excellent agreement with the theoretical predictions. Since the bistability threshold power of the incoming light in waveguide-cavity structures scales as  $P_{th} \sim 1/Q^2$  (Mingaleev *et al.*, 2006), one observes a rapid diminishing of  $P_{th} \sim v_g^2$  when the resonance frequency approaches the band edge, as shown in numerical calculations summarized in Figs. 22(b,c).

By now, several experimental observations of optical bistability enhanced through Fano interferences have been reported (Weidner *et al.*, 2007; Yang *et al.*, 2007). In particular, Yang *et al.* (2007) employed a high- $Q$  cavity mode ( $Q = 30000$ ) in a silicon photonic crystal and demonstrated Fano resonance based bistable states and switching with thresholds of  $185\mu\text{W}$  and  $4.5\text{ fJ}$  internally stored cavity energy that might be useful for scalable optical buffering and logic.

It is important to note, that the nonlinear Fano resonance shows dynamical instabilities with plane wave excitations (Miroshnichenko *et al.*, 2009). Near the resonance the intensity of the scattered wave starts to grow in time, leading to modulational instability, while far from resonance it converges to a steady-state solution (see Fig. 23). However, as it was demonstrated by Miroshnichenko *et al.* (2009) this instability can be suppressed for temporal Gaussian pulses excitations, providing with an effective method of recovering the bistable transmission.

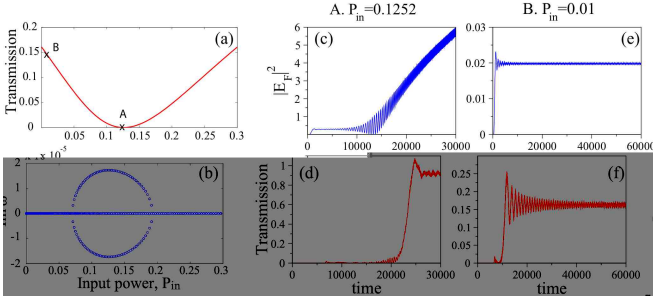


FIG. 23 (Color online) Dynamical instability of the nonlinear Fano resonance. (a) Nonlinear transmission coefficient, and (b) imaginary part of eigenvalues of the stability problem vs input power. In the vicinity of the nonlinear Fano resonance the plane wave excitation becomes dynamically unstable. Temporal evolution of (c,e) the field inside the side-coupled cavity, and (d,f) the transmission coefficient for two different values of the input power values, indicated in plot (a). Near the resonance the dynamics of the field inside the nonlinear cavity yields a buildup of a modulation instability in time. Adapted from Miroshnichenko *et al.* (2009).

## F. Overlapping resonances

A very important effect associated with the Fano resonances in double-resonator photonic structures can be linked to the electromagnetically-induced transparency (EIT) (Fleischhauer *et al.*, 2005). Coupled-resonator-induced transparency (CRIT) structures have been introduced in 2004 (Maleki *et al.*, 2004; Smith *et al.*, 2004; Suh *et al.*, 2004), although the early work (Opatrny and Welsch, 2001) suggested already an idea of macroscopic double-resonator optical system exhibiting the EIT-like effect. Recently, the CRIT effect has been observed experimentally in the system of two interacting microresonators (glass spheres of about 400  $\mu\text{m}$  in diameter) with whispering-gallery modes (Naweed *et al.*, 2005), in a cavity with at least two resonant modes (Franson and Hendrickson, 2006), and in integrated photonic chips with two microring resonators (Tomita *et al.*, 2009; Xu *et al.*, 2006). Providing an efficiently tunable transparency on an optical chip, such CRIT devices are considered as a crucial step towards the development of integrated all-optical chips (Boyd and Gauthier, 2006).

To explain the origin of CRIT resonances, we characterize the light transmission by the transmission and reflection coefficients which can be presented in the form

$$T(\omega) = \frac{\sigma^2(\omega)}{\sigma^2(\omega) + 1}, \quad R(\omega) = \frac{1}{\sigma^2(\omega) + 1}, \quad (42)$$

where the detuning function  $\sigma(\omega)$  may have quite different type of frequency dependence for different types of waveguide-cavity structures. Zero transmission (total reflection) corresponds to the condition  $\sigma(\omega) = 0$ , while perfect transmission (zero reflection) corresponds to the condition  $\sigma(\omega) = \pm\infty$ .

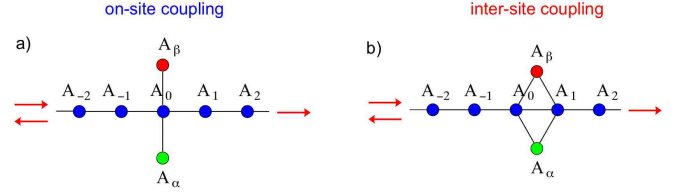


FIG. 24 (Color online) Two types of the geometries of a photonic-crystal waveguide side coupled to two nonlinear optical resonators. Light transmission and bistability are qualitatively different for (a) on-site and (b) inter-site locations of the resonator along the waveguide. Adapted from Mingaleev *et al.* (2008).

For the waveguide-cavity structure shown in Fig. 17(b), we obtain (Mingaleev *et al.*, 2006)

$$\sigma(\omega) \simeq \frac{(\omega_{\alpha} - \omega)}{\gamma_{\alpha}}, \quad (43)$$

where  $\omega_{\alpha}$  is the eigenfrequency of the localized cavity mode of an isolated cavity  $\alpha$ . The spectral width  $\gamma_{\alpha}$  of the resonance is determined by the overlap integral between the cavity mode and the guided mode at the resonant frequency.

To find  $\sigma(\omega)$  for the two-cavity structure, one can apply a variety of methods but the simplest approach is based on the transfer-matrix technique (Fan, 2002). When two cavities are separated by the distance  $d = 2\pi m/k(\omega_t)$ , where  $k(\omega)$  is the waveguide's dispersion relation,  $m$  is any integer number, and the frequency  $\omega_t$  is defined below, and there is no direct coupling between the cavities, we obtain

$$\sigma(\omega) \simeq \frac{(\omega_{\alpha} - \omega)(\omega_{\beta} - \omega)}{\Gamma(\omega_t - \omega)}, \quad (44)$$

with the total resonance width  $\Gamma = \gamma_{\alpha} + \gamma_{\beta}$  and the frequency of perfect transmission  $\omega_t = (\gamma_{\alpha}\omega_{\beta} + \gamma_{\beta}\omega_{\alpha})/(\gamma_{\alpha} + \gamma_{\beta})$ , lying in between the two cavity frequencies,  $\omega_{\alpha}$  and  $\omega_{\beta}$ , of zero transmission.

In the case when the cavities  $\alpha$  and  $\beta$  are identical, we obtain a single-cavity resonance and the only effect of using two cavities is the doubling of the spectral width,  $\Gamma = 2\gamma_{\alpha}$ , of the resonant reflection line, as it is illustrated in Fig. 25(a). However, introducing even the smallest difference between two cavities leads to the opening of an extremely narrow resonant transmission line on the background of this broader reflection line, as it is illustrated in Fig. 25(c). Indeed, for slightly different cavities we may rewrite Eq. (44) in the vicinity of the resonant transmission frequency,  $\omega_t = \omega_{\alpha} + \delta\omega/2$ , as  $\sigma(\omega) \approx \Gamma_t/(\omega - \omega_t)$ , with the line width  $\Gamma_t = \delta\omega^2/8\gamma_{\alpha}$ , which can easily be controlled by tuning the frequency difference  $\delta\omega$ . The quality factor of this transmission line,  $Q_t = \omega_t/2\Gamma_t \approx 4\gamma_{\alpha}\omega_{\alpha}/\delta\omega^2$ , grows indefinitely when  $\delta\omega$  vanishes. As mentioned above, this effect is the all-optical analogue of the electromagnetically-induced

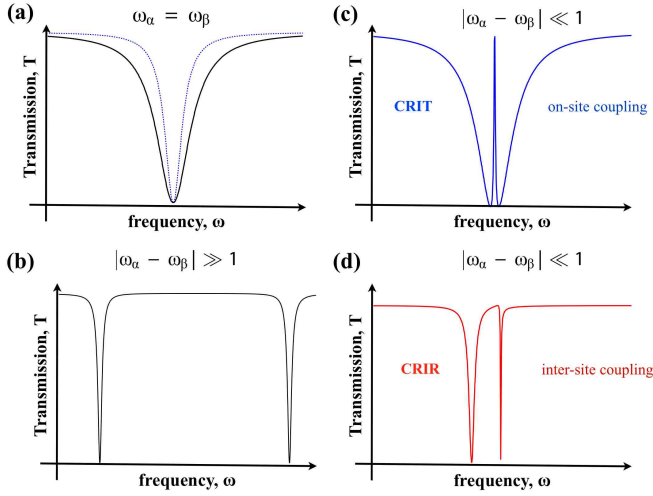


FIG. 25 (Color online) Typical transmission curves for four different cases (a) two identical side-coupled defects  $\omega_\alpha = \omega_\beta$  (solid). Transmission for a single side-coupled cavity is shown by a dashed line; (b) two side-coupled cavities with strongly detuned eigenfrequencies  $|\omega_\alpha - \omega_\beta| \gg 1$ ; (c,d) two side-coupled cavities with slightly detuned eigenfrequencies  $|\omega_\alpha - \omega_\beta| \ll 1$  for (c) on-site coupling and (d) inter-site coupling. From Mingaleev *et al.* (2008).

transparency and is now often referred to as the effect of coupled-resonator-induced transparency (Smith *et al.*, 2004).

In contrast, the inter-coupling between two cavities, as shown in Fig. 24(b) manifests itself as a qualitatively new effect of coupled-resonator-induced reflection (CRIR): for small detuning  $\delta\omega = \omega_\beta - \omega_\alpha$ , one of the resonant reflection frequencies shifts very close to the perfect transmission frequency,  $\omega_t$ , producing a narrow resonant reflection line, as is illustrated in Fig. 25(d). The frequency of this line is always close to the frequency  $\omega_\alpha$  of the cavity mode, while its spectral width is determined by the frequency difference  $\delta\omega$ , growing indefinitely as  $\delta\omega$  vanishes (Landobasa Y. Mario and Chin, 2006; Mingaleev *et al.*, 2008).

It should be emphasized that despite such a qualitative difference in their spectral manifestations, both CRIT and CRIR effects have the same physical origin which can be attributed to the Fano-Feshbach resonances (Feshbach, 1958, 1962; Mies, 1968) which are known to originate from the interaction of two or more resonances (e.g., two Fano resonances) in the overlapping regime, where the spectral widths of resonances are comparable to or larger than the frequency separation between them. In a general situation it leads to a drastic deformation of the transmission spectrum and the formation of additional resonances with sharp peaks. The Fano-Feshbach resonances are associated with a collective response of multiple interacting resonant degrees of freedom, and they have numerous evidences in quantum mechanical systems (Magunov *et al.*, 2003; Raoult and Mies, 2004).

Finally, we discuss the interaction between two Fano resonances (Hino, 2001; Miroschnichenko, 2009) which can be employed to stop and store light coherently, with an all-optical adiabatic and reversible pulse bandwidth compression process (Yanik and Fan, 2004; Yanik *et al.*, 2004). Such a process overcomes the fundamental bandwidth delay constraint in optics and can generate arbitrarily small group velocities for any light pulse with a given bandwidth, without any coherent or resonant light-matter interaction. The mechanism can be realized in a system consisting of a waveguide side coupled to tunable resonators, which generates a photonic band structure that represents a classical EIT analogue (Maes *et al.*, 2005; Yanik *et al.*, 2004).

### G. Guided resonances in photonic crystal slabs

Scattering of light by photonic crystal slabs leads to another class of Fano resonances associated with the presence of guided resonances in periodic structures. A photonic crystal slab consists of a two-dimensional periodic index contrast introduced into a high-index guiding layer Fig. 26(a). Such modulated structures support in-plane guided modes that are completely confined by the slab without any coupling to external radiations (Magnusson and Wang, 1992). In addition to in-plane waveguiding, the slabs can also interact with external radiations in a complex and interesting way (Fan and Joannopoulos, 2002; Fan *et al.*, 2003; Koshino, 2003). Of particular importance is the presence of guided resonances in the structures. Guided resonances can provide an efficient way to channel light from within the slab to the external environment. In addition, guided resonances can significantly affect the transmission and reflection of external incident light, resulting in complex resonant line shapes which can be linked to Fano resonances.

Fan and Joannopoulos (2002) calculated the transmission and reflection coefficients at various  $k$  points for the structure shown in Fig. 26(a). The calculated spectra for s-polarized incident waves are shown in Figs. 26(b,c). The spectra consist of sharp resonant features superimposed upon a smoothly varying background. The background resembles Fabry-Perot oscillations when light interacts with a uniform dielectric slab. To clearly see this, the background is fitted to the spectra of a uniform slab, which are shown as dashed lines in Figs. 26(b,c). The uniform slab has the same thickness as the photonic crystal. Resonances can be described by employing the Fano-type formulas, with the effective dielectric constant as the only fitting parameter. The fitting agrees very well with the numerical simulations [see also (Koshino, 2003)].

By introducing a nonlinear layer into the slab with a periodic lateral structure, we can generate a bistable transmission for significant intensity ranges due to Fano resonances, and achieve a strong frequency-dependent transparency variation related to the transfer via guided

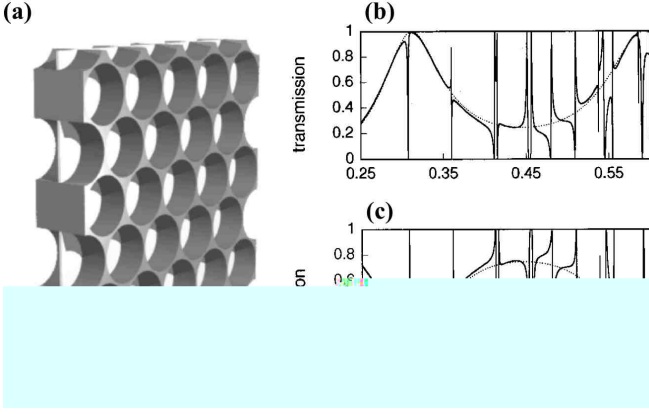


FIG. 26 Light scattering by photonic crystal slabs. (a) Geometry of the photonic-crystal film. (b) Transmission and (c) reflection spectra. The solid lines are for the photonic crystal structure, and the dashed lines are for a uniform dielectric slab with a frequency-dependent dielectric constant. Adapted from Fan and Joannopoulos (2002).

modes. A self-consistent simulation tool which allows for the computation of multivalued transmission has been developed by Lousse and Vigneron (2004). It explained the peculiar shape of the hysteresis loops associated with nonlinear Fano resonances.

Complex resonant line shapes due to Fano resonances were observed experimentally in several settings (Chen *et al.*, 2009; Grillet *et al.*, 2006; Harbers *et al.*, 2007; Qiang *et al.*, 2008; Yang *et al.*, 2008). In particular, Grillet *et al.* (2006) observed Fano resonances in the optical transmission spectrum of a chalcogenide glass photonic crystal membrane and demonstrated, for the first time, the suppression of optical transmission by over 40 dB, the strongest reported so far, and a remarkable result for a dielectric structure with a thickness of only 330 nm. These results will allow further progress towards the engineering of very sharp resonances and, combined with the large intrinsic nonlinearity of the chalcogenide glasses, should allow for the observation of optical bistability in a photonic-crystal mirror.

Recently, it was experimentally demonstrated that the shape of the Fano resonance in the light scattering by a high-Q planar photonic crystal nanocavity can be controlled by varying the waste of the Gaussian beam (Galli *et al.*, 2009). For a tightly focused beam with a spot diameter  $d_1 \approx 2\mu\text{m}$  a strong asymmetric Fano resonance was observed with the asymmetry parameter  $q_1 = -0.348$  [see Fig. 27(a)]. On the other hand, for a slightly defocused Gaussian beam with the spot diameter  $d_2 \approx 10\mu\text{m}$  a symmetric Fano resonance was observed with  $q_2 = -0.016$  [see Fig. 27(b)]. In this geometry the light reflected from the nanocavity mimics the scattering through a discrete level, while the light reflected from the photonic crystal pattern, can be considered as the scattering to the continuum. The interference of these two

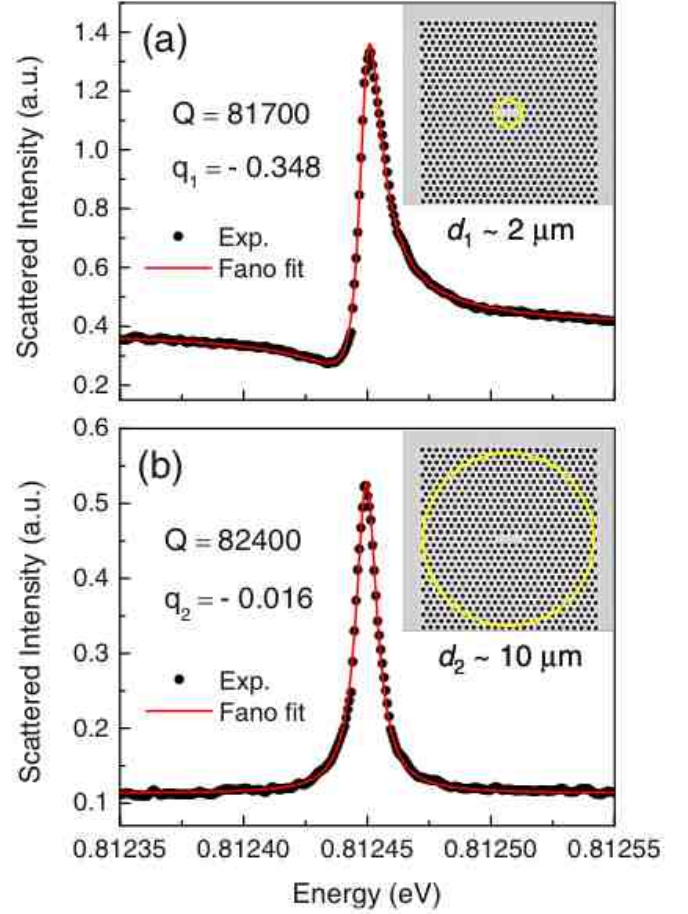


FIG. 27 (Color online) Measured scattering spectra (dots) and fitting by the Fano formula (solid lines) of a photonic crystal nanocavity for two different excitation conditions: (a) a tightly focused, and (b) a slightly defocused laser beam of diameters  $d_1$  and  $d_2$ , respectively, indicated by circles. Note here, that the actual profiles are inverted ones because of the use of crossed polarized detection. From Galli *et al.* (2009).

reflected components leads to the Fano resonance. The variation of the Fano profile with the increase of the excitation area can be understood as an enhancement of the scattering to the continuum, leading to the decrease of the asymmetry parameter  $q$ . Indeed, the variation of the asymmetry parameter  $q_1/q_2 \sim 22$  is proportional to the variation of the excitation areas  $(d_2/d_1)^2 \sim 25$ . Thus, by changing the excitation conditions it is possible to tune the Fano resonance in the scattering by photonic crystal nanocavity.

#### H. Light scattering by spherical nanoparticles

Light scattering by an obstacle is one of the fundamental problems of electrodynamics, see, e.g., monographs (Bohren and Huffman, 1998; Born and Wolf, 1999; van der Hulst, 1981). It was first described by Lord Rayleigh and is characterized by a sharp increase

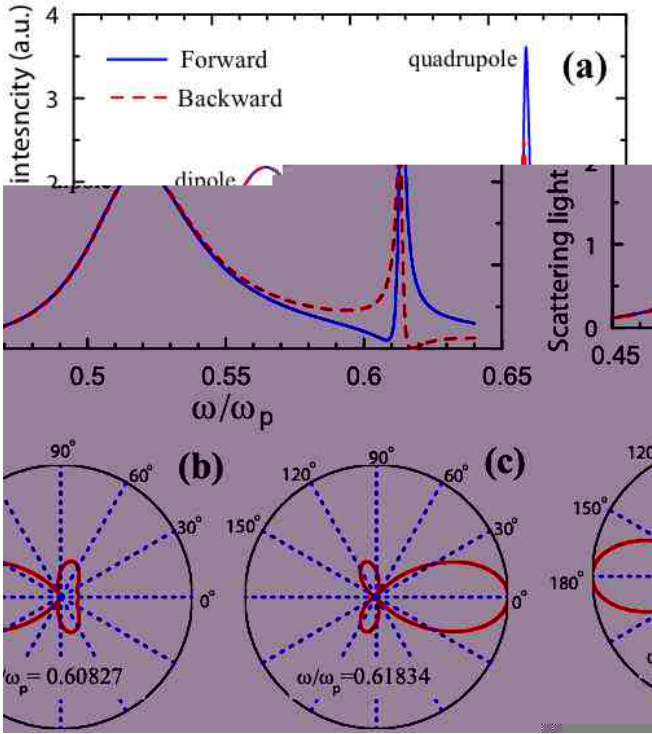


FIG. 28 (Color online) Exact Mie solution of the light scattering by a plasmonic nanoparticle. The radius of the nanoparticle is much smaller than the light wavelength  $a/\lambda = 0.083$ . (a) Frequency dependence of the scattering light intensity in the vicinity of the dipole and quadrupole resonances. In the latter case both forward (solid lines) and backward (dashed lines) scattering profiles exhibit asymmetric Fano resonances. (b,c) The angular dependence of the light scattering in the vicinity of the quadrupole resonance. The plasmonic frequency is normalized to  $\omega_p a/c = 1$ . Adapted from Luk'yanchuk *et al.* (2008).

in scattering intensity with increasing the light frequency (Rayleigh, 1871a,b,c). It is used to explain why we can enjoy the blue sky during day time (the intensely scattered blue component of the sunlight), and scarlet sunrises and sunsets at dawn and dusk (the weakly scattered red component). Lord Rayleigh's studies were generalized by Gustav Mie who obtained the complete analytical solution of Maxwell's equations for the scattering of electromagnetic radiation by a spherical particle valid for any ratio of diameter to the wavelength (Mie, 1908).

A common assumption is that the general Mie solution transforms into that of Rayleigh when particles are small. However, recent studies of resonant scattering by small particles with weak dissipation rates (Bashevoy *et al.*, 2005; Tribelsky and Luk'yanchuk, 2006) have revealed new and unexpected features, namely giant optical resonances with an inverse hierarchy (the quadrupole resonance is much stronger than the dipole one, etc.), a complicated near-field structure with vortices, unusual frequency and size dependencies, which allow to name such

a scattering anomalous. Tribelsky *et al.* (2008) revealed that the physical picture of this anomalous scattering is analogous to the physics of Fano resonances. This analogy sheds new light to the phenomenon. It allows to employ powerful methods developed in the theory of the Fano resonances (such as, e.g., the Feshbach-Fano partitioning theory) to describe the resonant light scattering. It also easily explains certain features of the anomalous scattering and related problems, namely sharp changes in the scattering diagrams upon small changes in  $\omega$  (see Fig. 28). Tribelsky *et al.* (2008) analytically obtained an asymmetric profile of the resonance lines by analyzing the exact Mie solution of the light scattering problem by a spherical nanoparticle (Miroshnichenko *et al.*, 2008).

Figure 28 demonstrates light scattering by a potassium colloidal nanoparticle immersed in a KCl crystal, calculated with a realistic dependence  $\epsilon(\omega)$  and fitting actual experimental data (Luk'yanchuk *et al.*, 2008; Tribelsky *et al.*, 2008). A slight variation of the incident light frequency in the vicinity of the quadrupole resonance drastically changes the scattering pattern (see Fig. 28), resulting in asymmetric Fano-like profiles for intensities of the forward and backward scattered light. In this case, excited localized plasmons (polaritons) are equivalent to the discrete levels in Fano's approach, while the radiative decay of these excitations is similar to the tunneling to the continuum. In general, it may lead to a significant suppression of the scattering along any given direction. Note, that in accordance with the theoretical expression obtained from the Mie formula, the points of destructive interference for the forward and backward scattering lie on different sides of the corresponding resonant peaks.

## I. Plasmonic nanocavities and tunable Fano resonance

Recent progress in the fabrication and visualization of nano-sized structures gave rise to a novel and rapidly emerging field of nanoplasmonics. The optical properties of metals are governed by coherent oscillations of conduction-band electrons, known as plasmons (Bohm and Pines, 1951). The interaction between light and metallic nanoparticles is mostly dominated by charge-density oscillations on the closed surfaces of the particles, called localized surface plasmon resonances (LSPs). The studies of LSPs in noble-metal nanoparticles, such as gold and silver, extended applications from various surface-enhanced spectroscopies (Moskovits, 1985) to novel nanometer optical devices and waveguides (Barnes *et al.*, 2003; Ozbay, 2006). One of the most important properties of LSPs is the possibility of strong spatial localization of the electron oscillations, combined with their high frequencies varying from UV to IR ranges. LSPs have the ability to strongly scatter, absorb, and squeeze light on nanometer scales, producing huge enhancement of electromagnetic field amplitudes. Such unique properties of nanomate-

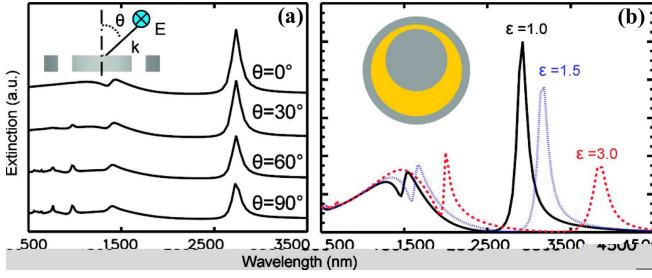


FIG. 29 (Color online) A metallic nanostructure consisting of a disk inside a thin ring supports superradiant and very narrow subradiant modes. Symmetry breaking in this structure enables a coupling between plasmon modes of differing multipolar order, resulting in a tunable Fano resonance: (a) extinction spectra as a function of incident angle  $\theta$ ; (b) the impact of filling the cavity with a dielectric material on the extinction spectrum or permittivity  $\epsilon = 1$  (solid line),  $\epsilon = 1.5$  (dashed line), and  $\epsilon = 3$  (dotted line). Adapted from Hao *et al.* (2008).

materials are essential for the development of novel material functions with potential technological and medical applications with specific optical, magnetic, and reactivity properties.

Plasmonic nanostructures can be considered as a physical realization of coupled oscillator systems at the nanoscale. The energies and linewidths of the LSPs depend mostly on the nanoparticle geometries, such as size and shape. Thus, the spectral tunability of LSPs has been widely investigated. As it was suggested by Hao *et al.* (2007), promising geometries for fine tuning are rings and disks. In such structures the dipole-like resonance can be tuned into the near-infrared region by changing the width of the metallic ring, for example. One of the important issues of nanoplasmonics is the effect of symmetry breaking, which allows to excite higher-order multipolar modes leading to larger electromagnetic field enhancements. The symmetry breaking can be easily achieved in metallic ring/disk cavity structures by displacing the disk with respect to the center of the ring. The plasmon resonances of a ring/disk cavity system can be understood in terms of the interaction or hybridization of the single ring and disk cavity plasmons. This hybridization leads to a low energy symmetric plasmon and high energy anti-symmetric plasmon (Hao *et al.*, 2007). The latter one is superradiant, i.e. it strongly radiates because disk and ring dipolar plasmons are aligned and oscillate in phase. The low energy symmetric plasmon is subradiant because of opposite alignment of dipolar moments. It turns out that in a symmetry-broken structure, the quadrupole ring resonance couples to the superradiant high energy anti-symmetric disk-ring dipole mode (Hao *et al.*, 2008). The direct coupling interferes with the dispersive coupling between the quadrupolar ring mode and the superradiant mode, resulting in a Fano resonance in the extinction spectrum (see Fig. 29). By varying the incident angle, the shape of the Fano res-

onance can be altered from asymmetric to a symmetric one.

Other examples of nanoplasmonic structures supporting the asymmetric Fano resonance are metallic nanoshells near a metallic film (Le *et al.*, 2007), and heterogeneous dimers composed of gold and silver nanoparticles (Bachelier *et al.*, 2008). Both structures show up with a highly tunable plasmonic Fano resonance, accompanied by large local electric field enhancement. Thus, the strong response of LSP resonances may be effectively used for biological and medical sensing applications.

A novel type of nonlinear Fano resonance has been found in hybrid molecules composed of semiconductor and metal nanoparticles (Zhang *et al.*, 2006). The latter ones support surface plasmons with a continuous spectrum, while the former ones support discrete interband excitations. Plasmons and excitons become strongly coupled via Förster energy transfer. At high light intensities, the absorption spectrum demonstrates a sharp asymmetric profile, which originates from the coherent interparticle Coulomb interaction, and can be understood in terms of a nonlinear Fano resonance.

## J. Extraordinary transmission of light through metallic gratings

The scattering by metallic gratings was the subject of extensive research for over a century. One of the important early achievements of the optics of metallic gratings was the discovery and understanding of Wood's anomalies (Rayleigh, 1907; Wood, 1902, 1935). One type of anomaly is due to the excitation of surface plasmon-polaritons propagating on the metallic surface. Another one is the diffractive anomaly, when a diffracted order becomes tangential to the plane of the grating. It is characterized by a rapid variation of the diffracted order intensity, corresponding to the onset or disappearance of a particular spectral order (Wood, 1935). This resonant behaviour of the Wood's anomaly can be understood in terms of the coupling of the incoming waves with the surface-bound states of periodic arrays (Fano, 1936, 1937, 1938, 1941; Hessel and Oliner, 1965). Thus, by considering a surface-bound state as a discrete level and scattered waves as a continuum, Wood's anomaly can be interpreted as a Fano resonance (Billaudeau *et al.*, 2009).

It was demonstrated that for a periodic thin-film metallic grating, formed from a two-dimensional array of holes, the transmitted fraction of the incident light can exceed the open fraction of the array for certain wavelengths (Ebbesen *et al.*, 1998; Ghaemi *et al.*, 1998). The enhancement in the transmitted zero-order beam is reported to be several orders of magnitude larger than that from pure metallic slab without holes. This phenomenon has been called extraordinary transmission through periodic arrays of subwavelength holes in metallic films.

The common understanding of the extraordinary transmission is due to a resonant excitation

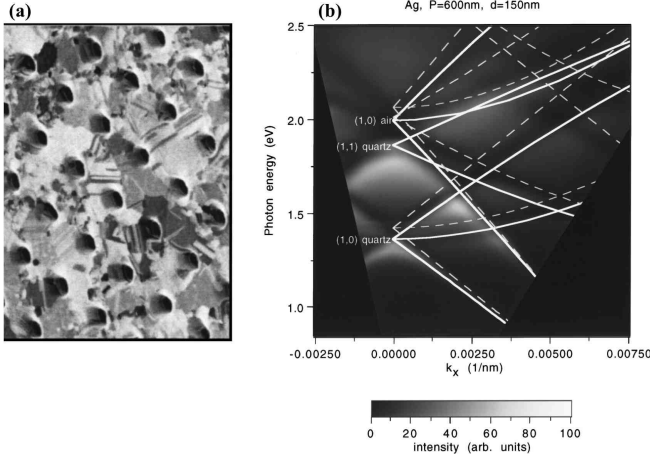


FIG. 30 Light scattering by metallic gratings. (a) Focused ion beam image of a two-dimensional hole array in a polycrystalline silver film. (b) Observed transmission intensity as a function of photon energy and  $k_x$  with predicted energy dispersion of surface plasmon-polaritons (solid) and loci of Wood's anomaly (dashed lines). From Ghaemi *et al.* (1998).

of surface plasmon-polaritons by incoming radiation (Ghaemi *et al.*, 1998; van der Molen *et al.*, 2005). In addition to the resonant enhancement of the transmission the resonant suppression was observed as well. It was demonstrated that these transmission minima correspond exactly to loci of Wood's anomaly (see Fig. 30) (Ghaemi *et al.*, 1998). According to experimental observations, each extraordinary transmission is accompanied by resonant suppression of transmission resulting in asymmetric lineshapes, which can be perfectly fitted by the Fano formula (de Abajo, 2007). Moreover, it was theoretically demonstrated by Spevak *et al.* (2009) that periodically modulated ultrathin metal films may exhibit resonant suppression of the transmittance, emphasizing the Wood's anomaly effect. Thus, the extraordinary resonant scattering of light by modulated metal film can be described in terms of the Fano resonance, revealing the interference nature of the phenomenon.

Kobyakov *et al.* (2009) suggested to use active layers to simultaneously enhance both transmittance and reflectance at the resonance in subwavelength periodic planar bimetallic grating by exciting gain-assisted surface plasmons.

### K. Resonant four-wave mixing induced autoionization

Four-wave mixing involves the interaction of three laser beams to produce a nonlinear polarization via the cubic electric susceptibility  $\chi^{(3)}$ . The induced polarization acts as the source of a fourth coherent light beam, detected as the signal. Four-wave mixing can be considered as the formation and scattering from laser-induced gratings.

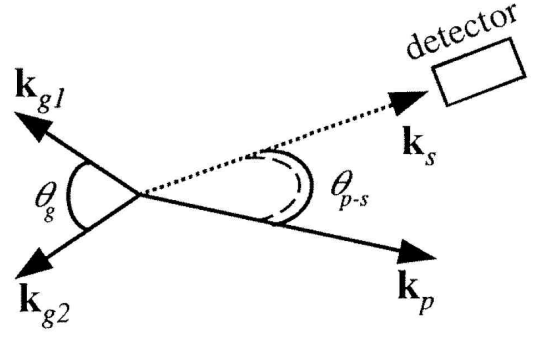


FIG. 31 Planar wavevector diagram illustrating the phase-matching condition for RFWM. From Teodoro and McCormack (1999).

The grating is formed by two laser beams, called grating beams, with wavevector  $\mathbf{k}_g$ . The third probe beam with the wavevector  $\mathbf{k}_p$  is then scattered off the laser-induced grating and produces the fourth scattered beam, which is detected as the four-wave mixing signal. Due to energy conservation, the frequency of the signal beam must be equal to the frequency of the probe beam  $\omega_s \equiv \omega_p$ . Momentum conservation results in a phase-matching condition for the signal wavevector

$$|\mathbf{k}_s| = |\mathbf{k}_{g1} - \mathbf{k}_{g2} + \mathbf{k}_p| = \omega_p/c, \quad (45)$$

and the Bragg-scattering angular condition

$$\frac{\omega_p}{\omega_g} = \frac{\sin(\theta_g/2)}{\sin(\theta_{p-s}/2)}, \quad (46)$$

where  $\theta_g$  is the angle between two grating beams, and  $\theta_{p-s}$  is the angle between the probe and signal beams (see Fig. 31).

In general, the four-wave mixing process can take place in any material. When the frequency of the incident laser beams matches the transition resonances of the medium, a drastic enhancement of the signal intensity can be observed. Such processes are called resonant four-wave mixings (RFWMs), and they are used as spectroscopic and diagnostic tools for probing stable and transient molecular species. Armstrong and Wynne (1974) studied experimentally four-wave mixing involving an autoionizing resonance in alkali-metal atomic vapor. In their experiment a two-photon transition between two bound states of the metal was excited, followed by a single-photon absorption to the autoionizing level. The detected signal demonstrated a characteristic asymmetric response. Using the Fano formalism, the authors derived an expression for the line-shape and fitted it with the Fano formula (Armstrong and Wynne, 1974), which allows to obtain the width and asymmetry parameter for the autoionizing states (Agarwal and Lakshmi, 1983; Alber and Zoller, 1983; Armstrong and Beers, 1975; Crance and Armstrong, 1982a,b; Haan and Agarwal, 1987; Meier *et al.*, 1995). Thus, this form of RFWM

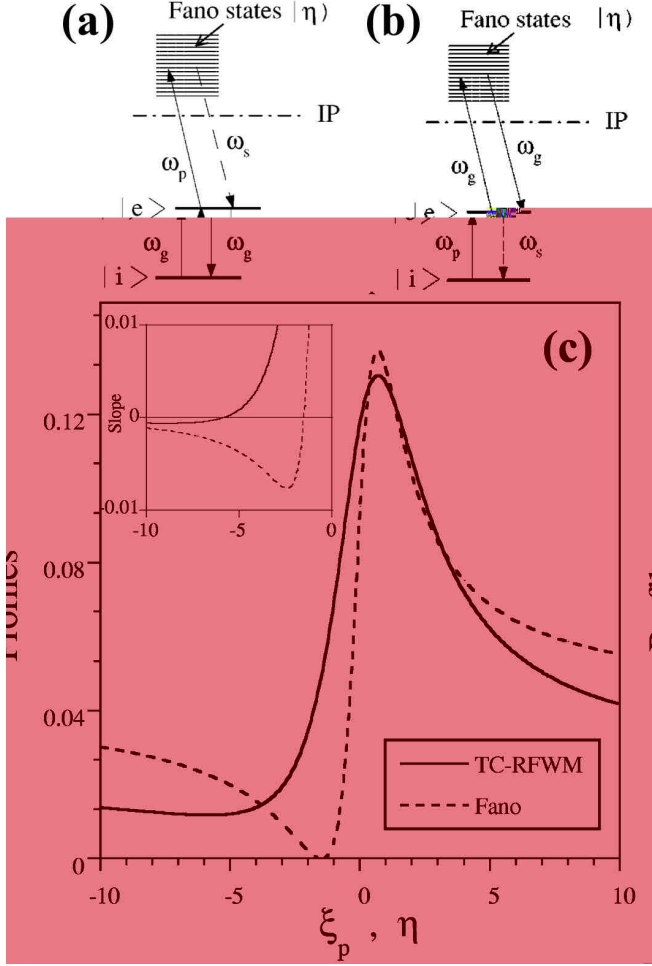


FIG. 32 Two-color resonant four-wave mixing. (a) Non-parametric and (b) parametric TC-RFWM process. The autoionizing level (Fano state) above the ionization potential is indicated by  $|\eta\rangle$ .  $|i\rangle$  and  $|e\rangle$  are ground and intermediate states, respectively. (c) TC-RFWM and Fano profiles. Inset: the slopes of two profiles. Note the separation between the slope zeros which correspond to profile minima. From Teodoro and McCormack (1998).

can be considered as one of the techniques to study autoionizing levels.

A double resonance version of RFWM is called two-color RFWM (TC-RFWM) and takes place, when two optical fields have frequencies in resonance with two different transitions. It yields a variety of excitation schemes, which are very useful for high-resolution spectroscopy. In Figure 32 possible TC-RFWM excitation schemes are shown, where the grating beams are in resonance with the lower transition and the probe is tuned to the upper transition [see Fig. 32(a)], and vice-versa [see Fig. 32(b)]. Because of the presence of autoionizing states in overall the FWM process, in both cases TC-RFWM exhibits asymmetric profiles, which can be approximated by the Fano formula [see Fig. 32(c)]. Unlike the Fano pro-

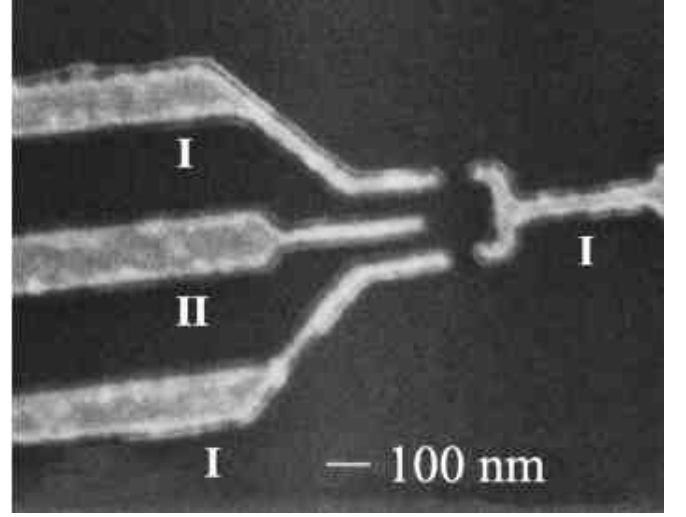


FIG. 33 Electron micrograph of a single electron transistor based on a GaAs/AlGaAs heterostructure. The split gates (I) define the tunnel barriers and the additional gate electrode (II) adjusts the potential energy on the quantum dot. From Göres *et al.* (2000).

file, the TC-RFWM spectral lines have no exact zeroes. This can be explained using the dephasing during nonlinear parametric conversions, which is a key difference to the usual Fano resonance case. Nevertheless, TC-RFWM provides with an efficient way to coherently control the signal lineshape (McCormack *et al.*, 1998).

## VI. CHARGE TRANSPORT THROUGH QUANTUM DOTS

In recent decades charge transport through quantum dots (QD) has been extensively studied both theoretically and experimentally (Altshuler *et al.*, 1991; Hanson *et al.*, 2007; Kastner, 1992; Koch and Lübbig, 1992; Reimann and Manninen, 2002). One of the reasons of that interest is the further miniaturization of electronic device components. A comprehensive picture of a big variety of underlying physical phenomena has emerged (see e.g. Aleiner *et al.* (2002); Alhassid (2000) and references therein). The finite size of the dot is responsible for a dense but discrete set of single particle levels. Confinement of electrons in small quantum dots leads to the necessity of taking into account their Coulomb repulsion. As a result, at temperatures below the charging energy the Coulomb blockade emerges (Aleiner *et al.*, 2002; Alhassid, 2000). At even lower temperatures the phase coherence of the excitations in the quantum dot is preserved during the scattering, and additional interference phenomena appear, depending on the coupling strength to the leads. In view of the enormous literature available, we will briefly introduce the main physics, and focus on results which are directly related to the finding of destructive interferences and Fano resonances.

### A. From a single electron transistor to quantum interference

A quantum dot is a small confinement region for electrons (typically almost two-dimensional) with leads coupled to it. The manufacturing of a huge variety of geometries is easily possible. In the simplest case two leads are used, and a voltage  $V$  is applied, resulting in a current of electrons which enter the dot through one lead, and eventually exit into the second lead. Various gate voltages can be additionally applied, e.g.  $V_g$  which controls the energy of the electrons in the dot relative to the leads, and others which control the strength of the coupling between the leads and the dot. Here we will consider only situations where the applied voltage  $V$  between the two leads is small so that the energy  $eV$  is smaller than all other relevant energy scales. This is also called the equilibrium case, at variance to the non-equilibrium case which is also frequently studied.

Let us consider a closed dot with linear size  $L$ , when the leads are decoupled. If one neglects the contribution from Coulomb interaction, the spectrum of many body states in a quantum dot can be obtained from the solution of the single particle problem. The single particle level spacing  $\Delta_{sp} = \pi\hbar^2/m^*L^2$  (Alhassid, 2000). The effective mass of an electron in GaAs is rather low:  $m^* = 0.067m_e$  (Alhassid, 2000). For  $L = 100\text{nm}$  one obtains  $\Delta_{sp} \approx 2\text{K}$ , while for  $L = 500\text{nm}$  the spacing is reduced to  $\Delta_{sp} \approx 90\text{mK}$ . Adding one electron to the closed dot therefore leads to an energy increase of the order of  $\Delta_{sp}$ . Now take Coulomb interaction into account. If the number of electrons in the dot is  $N$ , then the charging energy of adding one additional electron is  $E_c \sim Ne^2/L$ . Therefore, for large values of  $N$ , and not too small values of  $L$ ,  $E_c \gg \Delta_{sp}$ . Note that typical dot sizes are of the order  $100\text{nm} - 1\mu\text{m}$ .  $N$  can strongly vary, with values  $N \sim 10^2 - 10^3$ . Characteristic values of the charging energy are in the range  $E_c \sim 100 - 400\text{K}$  ( $12 - 50\text{meV}$ ). Therefore, for all practical purposes,  $E_c \gg \Delta_{sp}$ .

The number of electrons in a quantum dot is defined by minimizing the energy of the dot with respect to  $N$ . This energy is given by (Alhassid, 2000)

$$E(N) = -NeV_g + N^2e^2/2C, \quad (47)$$

where  $C$  is the total capacitance between the dot and its surroundings. Apart from special values of the gate voltage, there will be a given electron number  $N$  with smallest energy, and changing the number of electrons will cost an amount about one charging energy  $E_c$ . For particular values of the gate voltage  $V_g^{(n)}$  however degeneracies between  $E(N)$  and  $E(N+1)$  appear.

Consider an experimental geometry shown in Fig.33. If the coupling to the leads is weak enough and the temperature  $kT < E_c$  the Coulomb blockade regime sets in. As long as  $V_g \neq V_g^{(n)}$  the charging energy prevents lead electrons from entering the dot, and the conductance  $G$  is practically zero. However, when  $V_g = V_g^{(n)}$ , the degeneracy between  $N$  and  $N+1$  electron states on the

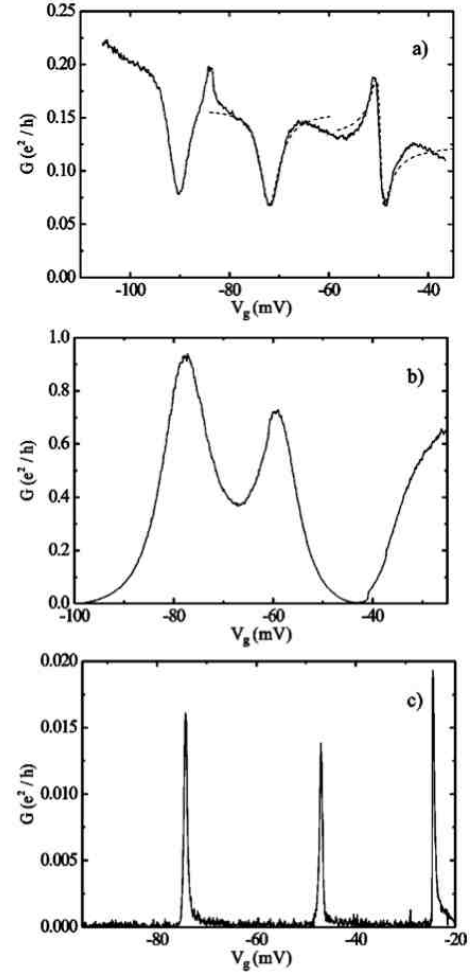


FIG. 34 Conductance versus gate voltage. Comparison of conductance measurements in the (a) Fano regime, (b) intermediate regime, and (c) Coulomb blockade regime. From (c) to (a) the lead-dot coupling increases. Fits to the Fano formula (1) are shown for the center and right resonances in (a). The respective asymmetry parameters are  $q = -0.03$  and  $q = -0.99$ . From Göres *et al.* (2000).

dot sets in. Therefore, electrons can pass through the dot one by one, and the conductance takes the universal value  $G = 2e^2/h$  (here the factor 2 accounts for spin degeneracy). Note that the Coulomb interaction is treated in a mean-field type way, therefore no phase coherence of dot electrons is required.

Lowering the temperature further, the phase coherence of the dot electrons becomes essential [see e.g. (Aikawa *et al.*, 2004; Ji *et al.*, 2000)]. Note that the typical electron mean free path can be of the order of  $10\mu\text{m}$ , one-two orders of magnitude larger than the dot size. It may also be possible to reduce *decoherence* effects within some suitable range by *increasing* the coupling of the dot to the leads, which may lead to a shorter residence time of electrons inside the dot and therefore to less scattering. With the option of having several channels which electrons can use to pass through the dot, phase coherence

will lead to interference effects, and therefore to possible Fano resonances.

If a magnetic field is added, orbital and spin effects have to be considered as well. The Zeeman energy  $E_Z = g\mu_B H$  sets another temperature scale. Depending on the Lande factor  $g$ , which can vary strongly from sample to sample, the corresponding Zeeman energy  $E_Z$  is of the order of  $100 - 200 mK$  for  $B = 1T$ . Allowing the electrons to traverse the dot along different paths, an Aharonov-Bohm phase shift  $\phi$  occurs due to a nonzero magnetic flux penetrating the area  $S$  enclosed by them (Altshuler *et al.*, 1980):  $\phi = \frac{e}{h} BS$ . With  $S = L^2$  we find for  $L = 100nm$  that  $\phi/2\pi = 0.38B/T$ , and for  $L = 1\mu m$  that  $\phi/2\pi = 38B/T$ .

Therefore, for  $L = 100nm$  and  $B = 1T$  it follows  $E_Z \ll \Delta_{sp}$ . Then at low temperatures  $kT < E_Z$  of the order of  $T \sim 50 - 100 mK$  and at a magnetic field  $B \sim 1T$  the Coulomb blockaded dot has a well defined spin: either  $|S_z| = 1/2$ , or  $S_z = 0$ . Changing the gate voltage and reaching the next degeneracy  $E(N) = E(N + 1)$ , an electron with a well-defined spin is allowed to enter the dot - either spin up or spin down. The allowed spin value alternates as one further tunes the gate voltage to the next degeneracy. If the phase coherence of electrons is preserved during the scattering, one may again expect interference phenomena - but this time, depending on the chosen value of  $V_g$ , only electrons with spin up (respectively spin down) will interfere along different channels. Increasing the coupling to the leads may cause spin-selective destructive interference for a given spin species, while the other spin species is freely passing through. The orbital effect of the magnetic field leads to an additional phase shift of the order of  $0.8\pi$ , independent of applied gate voltages.

For  $L = 1\mu m$  the single particle spacing  $\Delta_{sp} \approx 20mK$ . Therefore at  $B = 1T$  it follows  $E_Z \gg \Delta_{sp}$ . Then at temperatures  $T \sim 50 - 100mK$  the Coulomb blockaded dot is magnetized, but electrons which enter the dot can have any spin, preventing spin-selective destructive interference. The orbital effect of the magnetic field is huge with a  $2\pi$  phase shift every  $25mT$  upon changing the magnetic field.

Before proceeding, let us briefly mention related studies of the Kondo effect in transport through quantum dots. In the Coulomb blockade, the number of electrons on the dot is well defined, and either even or odd. Assuming a ground state only, the total electronic spin is either  $1/2$  (odd number of electrons) or zero (even number). In the absence of a magnetic field and for odd numbers of electrons, the whole dot could be viewed as some magnetic impurity with spin  $1/2$ , which scatters conduction electrons passing from one lead to another. That calls for an analogy with the well known Kondo effect which is observed in the low temperature properties of the conductivity of electrons in metals with magnetic impurities (Hewson, 1993). The resistivity in metals usually drops with lowering the temperature, since the number of phonons, which are responsible for electron scattering

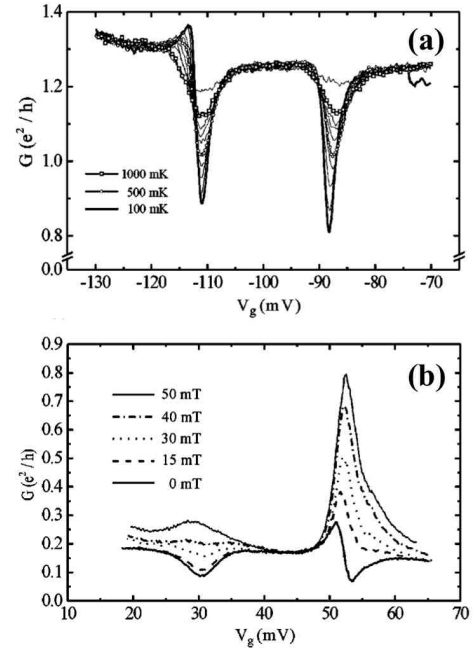


FIG. 35 Conductance versus gate voltage. (a) Temperature dependence of the conductance for two Fano resonances. (b) Conductance as a function of the gate voltage for various magnetic fields applied perpendicular to the two-dimensional electron gas. Adapted from Göres *et al.* (2000).

due to electron-phonon interaction, decreases. At around  $30K$  a minimum in the resistivity appears for some metals, and subsequently the resistivity increases again with further lowering the temperature. This increase is due to scattering of electrons by magnetic impurities, and originates from an exchange interaction of the conduction electron spin with the spin of the magnetic impurity. The exchange interaction sets an energy and temperature scale (the Kondo temperature  $T_K$ ), which is typically of the order of  $T_K \sim 100mK - 1K$ , similar to the Zeeman energy of an electronic spin  $1/2$  in a magnetic field of 1 Tesla. For temperatures  $T < T_K$  the impurity spin is screened by a cloud of renormalized conduction electrons. The Kondo temperature depends sensitively on the coupling strength (hybridization)  $\Gamma$  between the conduction electrons and the magnetic impurities. For weak coupling  $T_K$  is exponentially small in  $-1/\Gamma$ . This analogy stirred ideas to observe the Kondo effect in the conductance of electrons through quantum dots. For that low temperatures have to be used, and the coupling of the leads to the dot has to be increased (in order to increase  $T_K$ ). An enormous amount of theoretical studies was performed (Aleiner *et al.*, 2002). Experimental results showed a deviation from the Coulomb blockade regime for strong lead-dot coupling (see below). The relation to theoretical models based on Kondo mechanisms is still debated [see e.g. (Aleiner *et al.*, 2002; Ji *et al.*, 2000)].

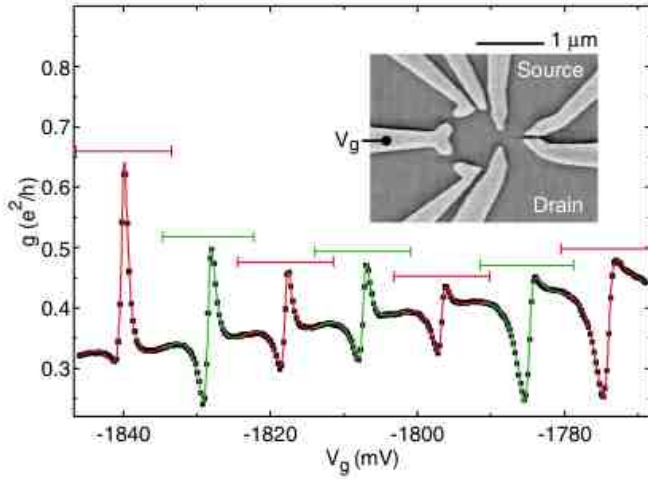


FIG. 36 Channel conductance data (squares) and fits (curves) vs gate voltage in the Fano regime. Bars show fitting ranges. Inset: SEM image of a similar sample. From Johnson *et al.* (2004).

### B. From Coulomb blockade to Fano resonances

A number of experimental studies report on the observation of Coulomb blockade in various quantum dot realizations on the basis of AlGaAs heterostructures (Cronenwett *et al.*, 1998; Goldhaber-Gordon *et al.*, 1998a, 2001, 1998b; Göres *et al.*, 2000; Kobayashi *et al.*, 2002; Schmid *et al.*, 1998). The charging energies are in the range  $E_c \sim 100 - 300 K$ . Temperatures were as low as  $30 mK$ , applied magnetic fields up to 1T, and higher. Therefore, the Zeeman energy  $E_Z$  is 2-3 orders of magnitude lower than the charging energy  $E_c$ . The Coulomb blockade is usually observed in the case of weak coupling between the leads and the dot. In Fig. 34 the results of Göres *et al.* (2000) are shown, which correspond to the setup in Fig. 33. For weak lead-dot coupling (c) the Coulomb blockade regime is nicely observed (temperatures are around  $100 mK$ , and the drain source voltage  $V_{ds} \approx 5 \mu V \ll V_g$ ). With increasing coupling the sharp peak structure is smeared out (b), which has been discussed in relation to the Kondo effect. Even further increasing the coupling, Fano resonances are observed in the strong coupling case (a). A fitting yields asymmetry parameters  $q = -0.03$  and  $q = -0.99$  for the center and right resonances, respectively. Note that also the peaks in (c) separating Coulomb blockades with different numbers of electrons on the dot, are clearly asymmetric. The same authors studied the temperature and weak magnetic field dependence of the Fano profiles in the strong coupling regime for even larger absolute values of the gate voltage, shown in Fig. 35.

The fitting of the resonances in Fig. 35(a) yields an almost linear decrease of the linewidth  $\Gamma$  with temperature, reaching values of  $2 meV$  at  $100 mK$ . The depth of the Fano resonance increases with decreasing temperature, making the Fano resonance sharper and deeper

at low temperatures. The Fano resonances show very strong dependence on the value of a weak applied magnetic field Fig. 35(b). Note that the largest applied fields are at  $50 mT$ , which corresponds to a Zeeman energy of the order of  $10 mK$  or less.

The origin of the observed Fano resonances is interferences of electrons along several channels (paths) traversing the quantum dot. When the lead-dot coupling is weak, the background conductance is very small [see Fig. 34(c)]. Still an asymmetric line shape is observed. The Fano resonance (dip) may either be hard to be detected with that background, or simply be absent, since essentially only one path is active. Another possibility is that the antiresonance is extremely narrow (weak coupling to a dot state). Since the Fano resonances are well observed at large lead-dot coupling, phase coherence of electrons passing through the dot is therefore established, and is further increased with lowering the temperature.

The dramatic change of the resonance shape at weak magnetic fields is attributed to a suppression of the coupling into the dot states (Göres *et al.*, 2000). That leads to an enhancement of the asymmetry parameter  $q$ , and respectively to a shifting of the Fano resonance (dip) out of the window of available gate voltages. The alternative explanation of loosing phase coherence of traversing electrons does not account for the extremely low-field scale at which the change occurs (Göres *et al.*, 2000). In a similar way one can exclude orbital Aharonov-Bohm effects, since the expected phase shifts are of the order of  $\phi \leq 0.12$ .

### C. From Fano to Aharonov-Bohm interferometers

In the above described experiments, the quantum dot design allowed essentially only to control the lead-dot coupling. To further advance in the tunability of Fano resonances with quantum dots, interferometer devices have been manufactured. In addition to a small quantum dot, which can be traversed by electrons, a second region (second dot, or additional channel, or additional arm) is coupled in a controlled way. Therefore, the coupling to a second channel can be tuned systematically. Of course there may be already several channels involved in the traversing of electrons through the primary dot.

Impressive results have been obtained by Johnson *et al.* (2004) in designing a tunable Fano interferometer which consists of a quantum dot and an additional tunnel-coupled channel (see Fig.36).

A sequence of several Fano resonances was observed, and well fitted with the Fano formula (1). Moreover, Johnson *et al.* (2004) performed careful fittings of various resonance shapes as shown in Fig.37. In panel (a) another set of resonances is observed. Upon variation of the gate voltage the asymmetry of the resonance shape clearly changes, as also seen in panel (e). In addition, also the line width  $\Gamma$  is changing (panel (d)). In another gate voltage window [panel (f)] these changes are even more

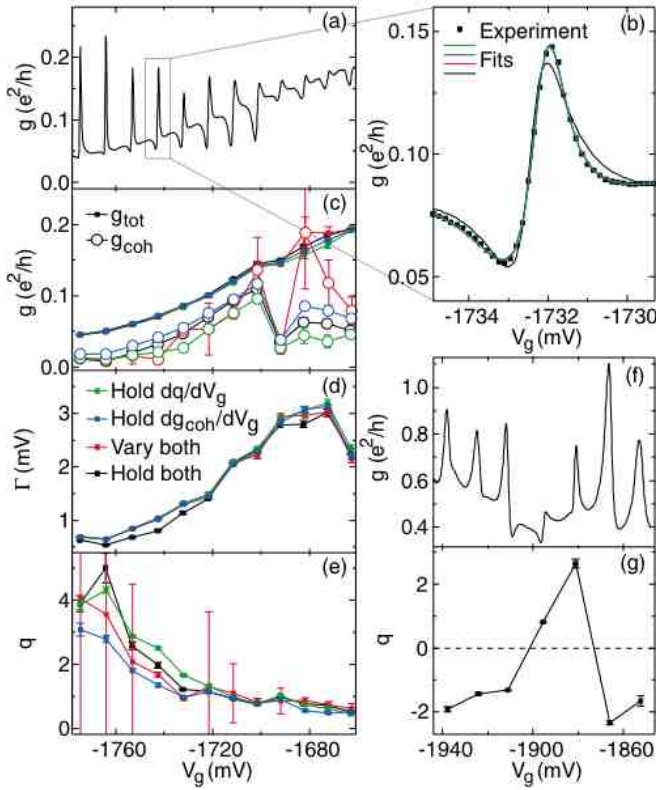


FIG. 37 Tunable Fano interferometer. (a) Experimental data with 12 Fano resonances. (b) Fits of one resonance using different fitting parameters. (c)-(e)  $g_{tot}$ ,  $g_{coh}$ ,  $\Gamma$ , and  $q$  from (a). (f) Data exhibiting reversals of  $q$ . (g) Extracted  $q$  values. From Johnson *et al.* (2004).

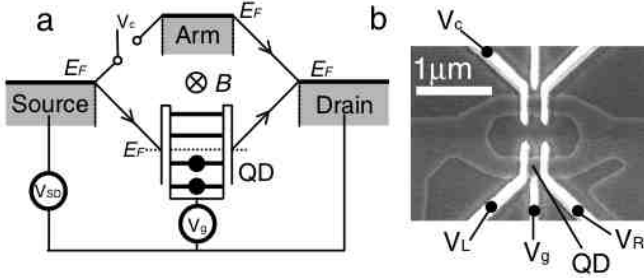


FIG. 38 An Aharonov-Bohm ring with an embedded QD in one of its arms. (a) Schematic representation of the experimental setup. (b) Scanning electron micrograph of the fabricated device. From Kobayashi *et al.* (2002).

drastic. Indeed, the fit yields a change of the sign of  $q$  with  $V_g$  (panel (g)). Note, that according to (1) at  $q = 0$  a symmetric resonant reflection, with no resonant transmission, is predicted. Indeed, around the value  $V_g \approx -1900$  mV the conductance in panel (f) shows practically a dip only.

Yet another twist was taken by Kobayashi *et al.* (2002) with a qualitatively similar geometry but an additional magnetic field penetrating the interferometer area and turning it into an Aharonov-Bohm (AB) device (see

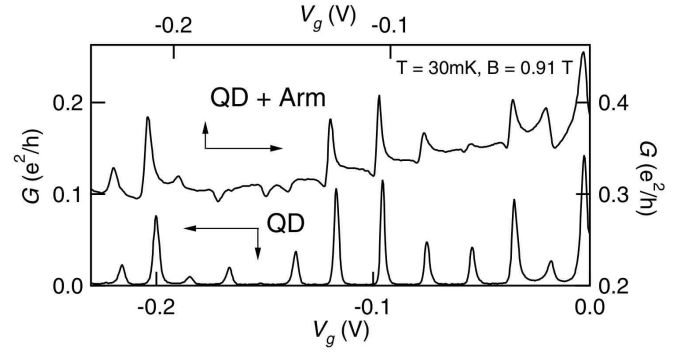


FIG. 39 Coulomb oscillation at  $V_c = -0.12$  V with the arm pinched off, and asymmetric Coulomb oscillation at  $V_c = -0.086$  V with the arm transmissible. Here  $T = 30$  mK and  $B = 0.91$  T. Adapted from Kobayashi *et al.* (2002).

Fig.38). The current through the quantum dot and the additional arm (channel) can be controlled independently. Magnetic fields were around 1 Tesla. With the arm switched off, a series of Coulomb blockade peaks is observed (see Fig.39).

When making the arm transmittable, clear interference effects are observed through asymmetric Fano lineshapes (see Fig.39). In that system, the discrete level and the continuum are spatially separated, allowing to control Fano interference via the magnetic field piercing the ring as shown in Fig.40. The line shape changes periodically with the AB period  $\sim 3.8$  mT, which agrees with the expected value using the ring dimension (Kobayashi *et al.*, 2002). As magnetic field  $B$  is swept, an asymmetric line shape with negative  $q$  continuously changes to a symmetric one and then to an asymmetric one with positive  $q$ . Kobayashi *et al.* (2002) argue, that due to the breaking of time reversal symmetry in the presence of a magnetic field, the matrix elements defining  $q$  are not real as usually assumed, but complex, therefore leading to complex  $q$  values. This confirms theoretical investigations for the noninteracting single particle AB interferometer case (Aharony *et al.*, 2002, 2003; Entin-Wohlman *et al.*, 2002a,b; Sasada and Hatano, 2005).

#### D. Correlations

An enormous bulk of theoretical literature on various facets of the conductance properties of quantum dots is available. We will discuss some of these results below. Let us remind the reader about some characteristic scales. The Coulomb energy (charging energy) of quantum dots is of the order of  $50$  meV ( $380$  K). The Kondo temperature in a typical metal with magnetic impurities is of the order of  $10$   $\mu$ eV ( $100$  mK), comparable to the Zeeman energy of a spin  $1/2$  electron in a magnetic field of around 1 Tesla. Therefore, when operating at temperatures of the order of the Zeeman energy, the charge on a typical quantum dot is extremely well fixed by the number of electrons. The next question is whether a con-

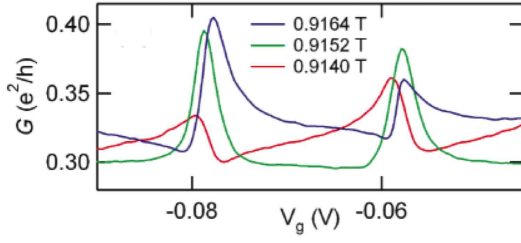


FIG. 40 Conductance of (a) two Fano peaks at 30mK and selected magnetic fields, (b) one Fano peak vs  $V_g$  and  $B$ , (c) Same as (b) but for larger windows of  $V_g$  variations. The white line represents the AB phase as a function of  $V_g$ . From Kobayashi *et al.* (2002).

ductance electron, when penetrating the quantum dot, is able to efficiently interact with an excess spin 1/2 particle for odd electron numbers, or whether it will usually follow a path which avoids strong exchange interaction. These, partly open, issues make it sometimes to hard to judge the relevance of many interesting theories.

The simplest model, which keeps the effect of Coulomb interactions and correlations, uses exactly one level from the quantum dot, adds links to leads (left and right), and takes Coulomb interaction of spin up and spin down electrons into account - but only on the dot (see Fig.41a). The resulting Hamiltonian has the following form:

$$H_s = H_D + H_W, \quad H_D = \epsilon_d \sum_{\sigma} n_{\sigma} + U n_{\uparrow} n_{\downarrow}, \quad (48)$$

$$H_W = \sum_{k\sigma r} \epsilon_{kr} c_{k\sigma r}^{\dagger} c_{k\sigma r} + (V_r c_{k\sigma r}^{\dagger} d_{\sigma} + H.c.). \quad (49)$$

Here  $n_{\sigma} = d_{\sigma}^{\dagger} d_{\sigma}$  measures the number of electrons on the quantum dot level, which interact with each other with strength  $U$ . The left and right leads are denoted by  $r = L(R)$ . The level energy  $\epsilon_d$  is measured from the Fermi energy of the leads. The lead states are chosen in the momentum representation. All fermionic creation and annihilation operators  $c, c^{\dagger}, d, d^{\dagger}$  obey the standard anticommutation relations.

### E. Interference

There are many ways to incorporate interference and multiple paths, in order to reach Fano resonances. One of the simplest ones is a T-shaped scheme, which is a small change of the above model by *side-coupling* the quantum dot to the quantum wire (leads) (see Fig.41b):

$$H_T = -t \sum_{n,\sigma} (c_{n,\sigma}^{\dagger} c_{n-1,\sigma} + c_{n,\sigma}^{\dagger} c_{n+1,\sigma}) + \sum_{\sigma} \epsilon_{d,\sigma} n_{\sigma} + \sum_{\sigma} (V d_{\sigma}^{\dagger} c_{0,\sigma} + V^* c_{0,\sigma}^{\dagger} d_{\sigma}) + U n_{\uparrow} n_{\downarrow}. \quad (50)$$

The lead states are chosen in the coordinate representation. Interference is possible because electrons can directly pass from the left to the right, but can also visit

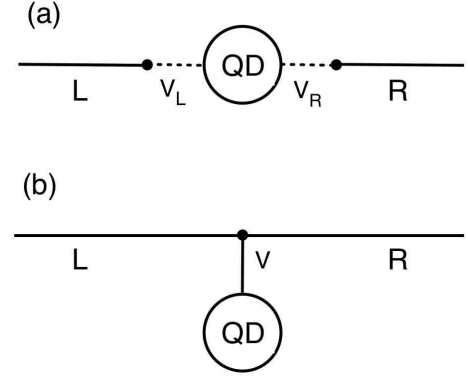


FIG. 41 Schematic representation of (a) a serial model of leads and a quantum dot (48)-(49), and (b) a T-shape model of leads and a side-coupled quantum dot (50).

the side dot and exit again. These two pathes are enough for destructive interference.

Another possibility is to extend the serial dot scheme (48)-(49) by adding a direct path (arm) for electrons to transit from the left to the right leads (Hofstetter *et al.*, 2001):

$$H_{AB} = H_s + H_a, \quad H_a = \sum_{kq\sigma} W e^{i\phi} c_{k\sigma R}^{\dagger} c_{q\sigma L} + H.c.. \quad (51)$$

The phase  $\phi$  models a magnetic flux which is encompassed by the loop of the direct path and the path via the quantum dot.

The Hamiltonians (48)-(49),(50) belong to the class of Anderson Hamiltonians (Anderson, 1961). Thus the thermodynamic properties of both models are similar, e.g. the average number of (spin up and spin down) electrons on the dot  $\langle n_{\sigma} \rangle$ . However, the transport properties depend crucially on the chosen geometry (Luo *et al.*, 2004). Note that changing the dot level  $\epsilon_d$  is qualitatively similar to varying the gate voltage of a quantum dot. The dot level is capable of accepting at most one spin up and one spin down electron.

Wiegmann and Tsvelick (1983) obtained analytical results for  $\langle n_{\sigma} \rangle$  assuming a linearized spectrum of lead electrons, which is not a crucial constraint, as long as the lead electron bands are partially filled (ideally half-filling), and as long as the temperature is much smaller than the distance from the Fermi energy to the band edges. In addition, there exist various numerical methods to compute  $\langle n_{\sigma} \rangle$  approximately.

With standard scattering matrix approaches, as well as using the Friedel sum rule (Hewson, 1993; Langreth, 1966), the conductance of the serial dot scheme (48)-(49) at zero temperature can be expressed in the following way (Glazman and Raikh, 1988; Ng and Lee, 1988):

$$g_{\sigma} = \left( \frac{2V_L V_R}{V_L^2 + V_R^2} \right)^2 \sin^2 \pi \langle n_{\sigma} \rangle. \quad (52)$$

Hofstetter *et al.* (2001) studied Fano resonances in transport through the the AB interferometer model (51)

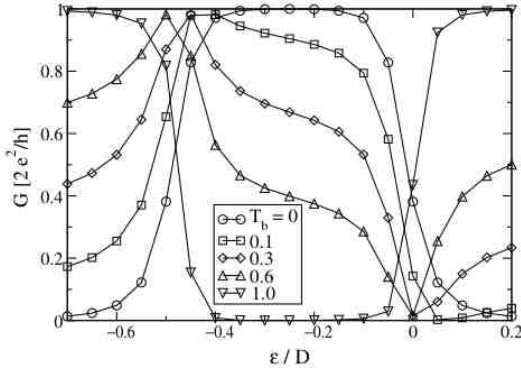


FIG. 42 Conductance as a function of  $\epsilon_d$  for different values of background transmission  $T_b$ . The AB phase  $\phi = 0$ . From Hofstetter *et al.* (2001).

at zero temperature. The schematic view of the AB interferometer is similar to Fig.38(a). For zero AB phase  $\phi = 0$ , and the direct path being switched off  $W = 0$ , there are three states of a Coulomb blockade to be expected upon variation of the gate voltage  $\epsilon_d$ : the dot contains either zero, one, or two electrons, with sharp transitions between them. We remind again, that the empty dot is almost not conducting (Coulomb energy too large), and the dot filled with two electrons as well (Pauli principle). When there is one electron on the dot, a second can enter while the first leaves. Despite of applying a magnetic field, model (51) is invariant under spin reversal (because the bare dot levels are not Zeeman splitted). This may be not easy to be achieved in an experiment. Therefore, when there is one electron on the dot, it can have either spin up or spin down, and on average  $\langle n_\sigma \rangle = 1/2$  in that case. For  $\epsilon_d > 0$  (Fermi energy is placed at zero) the dot is empty, and the conductance is zero. When  $-U < \epsilon_d < 0$ , one electron can enter the dot, but not two. Then additional electrons can tunnel through, giving maximal conductance. Finally, for  $\epsilon_d < -U$ , two electrons occupy the dot, and the conductance is zero again. This broad region of almost perfect conductance is due to spin exchange processes on the quantum dot level, and can be therefore related to the discussed above Kondo effect. Indeed, in Fig.42 this is observed for  $T_b = 0$  with  $T_b = 4x/(1+x)^2$  being the background transmission probability, where  $x = \pi^2 W^2 N_L N_R$ , and  $N_{L,R}$  is the density of states in the left (right) lead. With increasing  $T_b$  the curves change dramatically. Most importantly, a Fano resonance is appearing in the studied energy window, qualitatively similar to experimental observations (Kobayashi *et al.*, 2002). For the considered model the resonance location is shifting towards  $-U/2$ , and its width tends to  $-U$ , as  $T_b$  further increases Fig.42. A variation of the AB phase  $\phi$  in some intermediate  $T_b$  regime yields the possibility to change the sign of the asymmetry parameter  $q$ .

## F. Spin filters

When a magnetic field is applied to the AB interferometer setup in Fig.38(a), it is reasonable to consider also its action on the quantum dot region itself, which leads to a Zeeman splitting of the dot level. This is incorporated in the side dot model (50) with specifying

$$\epsilon_{d,\uparrow} = \epsilon_d + \Delta/2, \quad \epsilon_{d,\downarrow} = \epsilon_d - \Delta/2, \quad (53)$$

where  $\Delta$  is the Zeeman energy up to which the single particle level is splitted for spin down and spin up electrons. It is easy to incorporate the AB phase shift as well, we will discuss it below.

For  $U = 0$  (50) is reduced to the Fano-Anderson model (6), and the transmission is computed within the one-particle picture for an electron moving at the Fermi energy  $\epsilon_F$ :

$$-\epsilon_F \phi_i = t(\phi_{n-1} + \phi_{n+1}) + V^* \varphi \delta_{n0}, \quad (54)$$

$$-\epsilon_F \varphi = -\epsilon_{d,\sigma} \varphi + V \phi_0, \quad (55)$$

where  $\phi_n$  refers to the amplitude of a single particle at site  $n$  in the conducting channel and  $\varphi$  is the amplitude at the side dot. With the help of the Friedel sum rule (Hewson, 1993; Langreth, 1966) one arrives at (Torio *et al.*, 2004)

$$g_\sigma = \cos^2 \pi \langle n_\sigma \rangle. \quad (56)$$

This relation has a geometric origin and actually holds for arbitrary  $U$  (at zero temperatures). For a nonzero magnetic field  $\Delta \gg \Gamma$  the two Fano resonances for spin up and spin down electrons are energetically separated. Therefore, the current through the channel is completely polarized at  $\epsilon_F = \epsilon_{d,\uparrow}$  and  $\epsilon_F = \epsilon_{d,\downarrow}$ . The AB phase can be easily included into the model (50) similar to (51). Remarkably it will not change the position of the resonances (cf. also (9)), since the position of the Fano resonance is entirely determined by the matching condition between the dot level(s) and the Fermi energy.

The obtained spin filter will operate at temperatures  $kT \ll \Delta$ . For a field of a few Tesla that implies temperatures less than 100mK. While that is possible in principle, two more problems appear. First, to control such a spin filter, one would have to control the gate voltage on the scale of  $\mu\text{eV}$  (because the spin polarized Fano resonances are separated in the gate voltage by the same amount of the Zeeman energy). Second, as discussed above, Coulomb interactions have to be taken into account.

For nonzero  $U$  and  $\Delta$ , the results for the mean number of particles on the dot, and for the spin-resolved conductance, have been obtained by Torio *et al.* (2004), and are shown in Fig.43. The main outcome is, that the presence of a strong Coulomb interaction is shifting the two Fano resonances for spin up and spin down electrons further apart. Therefore, the current through the channel is completely polarized at  $\epsilon_F = \epsilon_{d,\uparrow} + U$  and  $\epsilon_F = \epsilon_{d,\downarrow}$ .

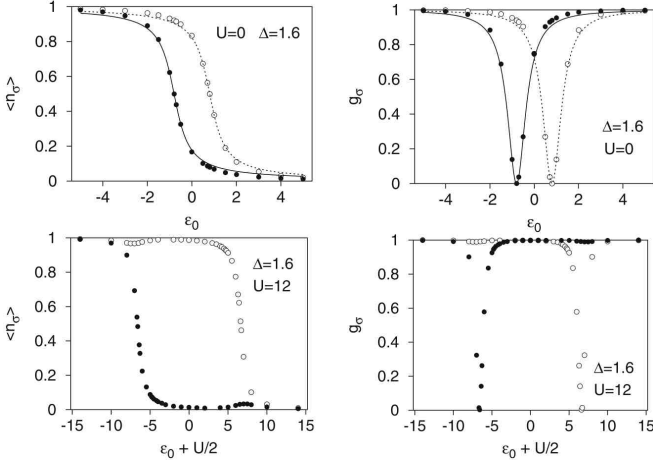


FIG. 43 Left plots:  $\langle n_\sigma \rangle$  versus  $\epsilon_d$  for a finite splitting  $\Delta = 1.6$ ,  $U = 0$  (top) and  $U = 12$  (bottom). The black (white) dots represent the numerical results for the spin up (spin down) occupation number. Right plots:  $g_\sigma$  versus  $\epsilon_d$  for finite splitting  $\Delta = 1.6$ ,  $U = 0$  (top) and  $U = 12$  (bottom). The conductance is computed numerically for spin up (black dots) and spin down (white dots) electrons. The solid and the dashed lines on the top figures represent the exact results of Eq. (56). Adapted from Torio *et al.* (2004).

For  $U \gg \Delta$  the distance between the two spin polarized Fano resonances is of the order of the charging energy (and not the Zeeman energy). At the same time, the Kondo regime is completely suppressed. For  $\epsilon_F < \epsilon_{d,\downarrow}$ , the dot level is empty, and electrons pass directly from the left to the right lead (background transmission). For  $\epsilon_F = \epsilon_{d,\downarrow}$  the dot is opening for spin down electrons. A Fano resonance appears, and its width is determined solely by  $\Gamma = 2|V|^2/|v_F|$  where  $v_F = d\epsilon/dq|_{\epsilon_F}$  is the Fermi velocity. For  $\epsilon_{d,\downarrow} < \epsilon_F < \epsilon_{d,\uparrow} + U$  the dot level is filled with one spin down electron, and does not contribute to the conductance, leading to direct transmission from left to right leads. For  $\epsilon_F = \epsilon_{d,\uparrow} + U$  the dot is opening for spin up electrons. A Fano resonance appears, with the same width as for the previous case. Finally, for  $\epsilon_F > \epsilon_{d,\uparrow} + U$ , the dot is filled with two electrons and does not contribute to the conductance, leading to direct transmission from left to right leads.

For typical quantum dots with  $L \approx 100\text{nm}$  and  $B \approx 1T$ , the spin filter effect is expected to be active for temperatures below  $100\text{mK}$ , with a distance between the spin polarized Fano resonances of the order of  $20 - 50\text{meV}$ . To observe it, one needs to monitor experimentally the spin-resolved flow of electrons with a spatial resolution less than the dot dimension.

## G. Perspectives

Gurvitz and Levinson (1993) obtained resonant reflection and transmission within a generalized description of a conducting channel (with several transverse modes)

with a single impurity.

Extensions of the theoretical models in order to include many dot levels were performed by Stefanski *et al.* (2004) for very large ( $0.1\text{eV}$ ) charging energies. Two dots with rather small charging energies ( $1\text{meV}$ ) were discussed by Stefanski (2003). A series of authors considered the limit  $U \rightarrow \infty$  (Bulka and Stefanski, 2001; Kang *et al.*, 2001; Kang and Shin, 2000). It remains to be clarified, whether such models can be used to discuss temperature effects on transport properties through quantum dots.

Lee and Bruder (2006) extended the spin filter model by including spin-orbit interactions and extending the side dot into a side ring with many levels. Estimates of Kondo temperatures, and general temperature effects, have been discussed by Aligia and Salguero (2004). Lobos and Aligia (2008) included Rashba spin-orbit coupling into the consideration of AB interferometers (see also Chi *et al.* (2007); Gong *et al.* (2008); Sanchez and Serra (2006); Serra and Sánchez (2007)). Spin inversion devices in a quasi-two-dimensional semiconductor wave guide under sectionally constant magnetic fields and spin-orbit interactions were discussed by Cardoso and Pereyra (2008).

Experimental progress was reported by Neel *et al.* (2007) through contacting the tip of a low-temperature scanning tunneling microscope with individual cobalt atoms adsorbed on Cu(100), where Fano resonances have been observed.

Single-molecule devices attracted attention recently. There one sandwiches various molecules between gold electrodes and studies their conductance properties. Impressive Fano resonances (with the background transmission dropping by several orders of magnitude) were reported recently by Finch *et al.* (2009). The additional influence of Andreev reflection at low temperatures, when the metallic contacts turn superconducting, was studied by Kormányos *et al.* (2009).

Since Fano resonances rely on phase coherence of electrons traversing the structure along different paths, several authors investigated the influence of phonons on decoherence in quantum dots (Pastawski *et al.*, 2002; Torres *et al.*, 2006). Clerk *et al.* (2001) studied the possibility to extract phase decoherence properties from measurements on the  $q$ -factor of the Fano resonance.

During the last decades, carbon nanotubes have been studied extensively because of their unconventional properties (Saito *et al.*, 1998). For applications to nanoscale electronic devices, researchers have fabricated various forms of carbon nanotubes to engineer their physical properties, including new morphologies such as X- and T-shaped junctions (Terrones *et al.*, 2000). These developments offer interesting opportunities to study phase coherent transport in novel geometries. Carbon nanotubes are excellent objects for observing phase coherence phenomena and Fano effects, and there are many theoretical studies and experimental signatures of the Fano effect in different types of carbon nanotubes (Babic and Schonenberger, 2004;

Hu *et al.*, 2006; Kim *et al.*, 2005, 2003; Yi *et al.*, 2003; Zhang and Chandrasekhar, 2006; Zhang *et al.*, 2004). In particular, Fano resonances are very pronounced in the transport properties of multiply connected carbon nanotubes where a single tube is branched off into two smaller arms and then they merge into one. Both  $\pi$ -bonding and  $\pi^*$  ( $\pi$  anti)-bonding electron transport channels show resonant Fano tunneling through discrete energy levels in the finite arms (Kim *et al.*, 2005).

There are many other systems where Fano resonances was observed and studied in details, e.g. for the resonant phonon transport between two crystalline media in the presence of a weakly bounded intermediate layer due to nonlocal interaction (Kosevich, 1997, 2008; Kosevich *et al.*, 2008).

## VII. CONCLUSIONS

This Review offers a bird-eye view on the Fano resonances in various physical systems. All examples presented here share the same basic feature - coexistence of resonant and nonresonant paths for scattering wave to propagate. It results in constructive and destructive interference phenomena and asymmetric lineshapes, first quantitatively described by Ugo Fano. It turns out to be a very common situation in any complex system describing wave propagation, either on a classical footing, or on a quantum mechanical one. This makes the Fano resonance a very generic phenomenon. The characteristic fingerprints of the Fano resonance are usually assumed to be related to an asymmetric profile of a cross-section or transmission as a function of some relevant control parameters. A detailed study of the problem shows, that symmetric profiles are allowed as well, and therefore a Fano resonance is indicating its presence whenever a resonant suppression of forward scattering (transmission) is observed. It is intimately related to the presence of a quasi-bound state resonantly interacting with a continuum of scattering states. The pinning down of such a bound state may or may not be an obvious undertaking, depending on the given physical setting. In particular, such quasi-bound states can be generated by geometrical means, and in more complicated settings by many body interactions. We focussed here on the study of Fano resonances in light propagation through artificial nanoscale optical devices, and in charge transport through quantum dots. Several other potential applications were discussed as well, touching such areas as superconductivity, Bose-Einstein condensates in optical lattices, among others.

Despite being interference in nature the Fano resonance we should pointed out here that it is quite different to other interference phenomena, such as, for instance, double slit experiment or weak localization in disordered media (Gantmakher, 2005). The latter two share the common feature of interference between two open channels (or broad continuums) represented by similar diffraction pattern of the slits in the first case, or iden-

tical length of the two counter-propagating paths along a loop in the second. The phase of a scattering wave varies relatively slowly along a continuum. Therefore, for nearly identical continua the phase accumulation during propagation along two paths will be practically the same. The constructive/destructive interference takes place when the sum of these two phases become equal to zero or  $\pi$ , and, in general, are very well separated from each other. In the case of a Fano resonance the situation is quite different. Along the discrete level path the phase undergoes sharp variation (in comparison with the continuum) with a consequent change of its sign. It results in a very strong asymmetric profile where constructive and destructive interferences are located very close to each other. Several detailed examples considered in this Review demonstrate that systems which support Fano resonance can be mapped onto the Fano-Anderson model (3). This model is very simple and provides with a core understanding of the phenomenon. It can be considered as a guideline for explanation of the Fano resonance in a particular system.

## Acknowledgments

We thank A. Dyugaev, Yu. Ovchinnikov, M. Titov and M. Rybin for very useful discussions and careful reading of parts of the manuscript. The work has been supported by the Australian Research Council through the Discovery and Centre of Excellence projects.

## References

- de Abajo, F. J. G., 2007, "Colloquium: Light scattering by particle and hole arrays," *Rev. Mod. Phys.* **79**, 1267.
- Agarwal, G. S., and P. A. Lakshmi, 1983, "Effect of spontaneous emission and recombination on the four-wave mixing profiles involving autoionizing resonances," *Phys. Rev. A* **28**, 3430–3437.
- Agrawal, G., 1995, *Nonlinear Fiber Optics* (Academic, San Diego).
- Aharony, A., O. Entin-Wohlman, B. I. Halperin, and Y. Imry, 2002, "Phase measurement in the mesoscopic Aharonov-Bohm interferometer," *Phys. Rev. B* **66**, 115311.
- Aharony, A., O. Entin-Wohlman, and Y. Imry, 2003, "Measuring the Transmission Phase of a Quantum Dot in a Closed Interferometer," *Phys. Rev. Lett.* **90**, 156802.
- Aikawa, H., K. Kobayashi, A. Sano, S. Katsumoto, and Y. Iye, 2004, "Observation of "Partial Coherence" in an Aharonov-Bohm Interferometer with a Quantum Dot," *Phys. Rev. Lett.* **92**, 176802.
- Alber, G., and P. Zoller, 1983, "Harmonic generation and multiphoton ionization near an autoionizing resonance," *Phys. Rev. A* **27**, 1373–1388.
- Aleiner, I. L., P. W. Brouwer, and L. I. Glazman, 2002, "Quantum effects in Coulomb blockade," *Phys. Rep.* **358**, 309 – 440.
- Aleshkin, V. Y., A. V. Antonov, L. V. Gavrilenko, and V. I. Gavrilenko, 2007, "Fano resonance study in impurity pho-

- to current spectra of bulk GaAs and GaAs quantum wells doped with shallow donors," *Phys. Rev. B* **75**, 125201.
- Alhassid, Y., 2000, "The statistical theory of quantum dots," *Rev. Mod. Phys.* **72**, 895–968.
- Aligia, A. A., and L. A. Salguero, 2004, "Magnetotransport through a quantum wire side coupled to a quantum dot," *Phys. Rev. B* **70**, 075307.
- Altshuler, B. L., D. Khmel'nitzkii, A. I. Larkin, and P. A. Lee, 1980, "Magnetoresistance and Hall effect in a disordered two-dimensional electron gas," *Phys. Rev. B* **22**, 5142–5153.
- Altshuler, B. L., P. A. Lee, and R. A. Webb, 1991, *Mesoscopic Phenomena in Solids* (Springer, North-Holland, Amsterdam).
- Anderson, P. W., 1961, "Localized Magnetic States in Metals," *Phys. Rev.* **124**, 41–53.
- Aoki, K., H. Yamawaki, and M. Sakashita, 1996, "Observation of Fano interference in high-pressure ice VII," *Phys. Rev. Lett.* **76**, 784–786.
- Armstrong, J. A., and J. J. Wynne, 1974, "Autoionizing States of Sr Studied by the Generation of Tunable Vacuum uv Radiation," *Phys. Rev. Lett.* **33**, 1183–1185.
- Armstrong, L., and B. L. Beers, 1975, "Comment Concerning the Study of Autoionizing States Using Parametric Generation," *Phys. Rev. Lett.* **34**, 1290–1291.
- Armstrong, L., C. E. Theodosiou, and M. J. Wall, 1978, "Interference between radiative emission and autoionization in the decay of excited states of atoms," *Phys. Rev. A* **18**, 2538–2549.
- Aubry, S., 1997, "Breathers in nonlinear lattices: Existence, linear stability and quantization," *Physica D* **103**, 201–250.
- Auger, P., 1925a, "Sur l'effet photoélectrique composé," *J. Phys. Radium* **6**, 205–208.
- Auger, P., 1925b, "Sur les rayons secondaires produit dans un gal par des rayons," *Comptes rendus* **180**, 65.
- Auger, P., 1926 *Ann. Phys. (Paris)* **6**, 183.
- Babic, B., and C. Schonenberger, 2004, "Observation of Fano resonances in single-wall carbon nanotubes," *Phys. Rev. B* **70**, 195408.
- Bachelier, G., I. Russier-Antoine, E. Benichou, C. Jonin, N. D. Fatti, F. Vallée, and P.-F. Brevet, 2008, "Fano Profiles Induced by Near-Field Coupling in Heterogeneous Dimers of Gold and Silver Nanoparticles," *Phys. Rev. Lett.* **101**, 197401.
- Bagwell, P. F., and R. K. Lake, 1992, "Resonances in transmission through an oscillating barrier," *Phys. Rev. B* **46**, 15329–15336.
- Bandopadhyay, S., B. Dutta-Roy, and H. S. Mani, 2004, "Understanding the Fano resonance through toy models," *Am. J. Phys.* **72**, 1501–1507.
- Bandrauk, A. D., and J. P. Laplante, 1976, "Fano line shapes in predissociation," *J. Chem. Phys.* **65**, 2602–2608.
- Bar-Ad, S., P. Kner, M. V. Marquezini, S. Mukamel, and D. S. Chemla, 1997, "Quantum Confined Fano Interference," *Phys. Rev. Lett.* **78**, 1363–1366.
- Barnes, W. L., A. Dereux, and T. W. Ebbesen, 2003, "Surface plasmon subwavelength optics," *Nature* **424**, 824–830.
- Bashevoy, M., V. Fedotov, and N. Zheludev, 2005, "Optical whirlpool on an absorbing metallic nanoparticle," *Opt. Express* **13**, 8372–8379.
- Bechstedt, F., and K. Peuker, 1975, "Theory of interference between electronic and phonon Raman Scattering," *Physica Status Solidi (b)* **72**, 743–752.
- Becker, U., T. Prescher, E. Schmidt, B. Sonntag, and H. E. Wetzel, 1986, "Decay channels of the discrete and continuum Xe [bold 4]d resonances," *Phys. Rev. A* **33**, 3891–3899.
- Belitsky, V. I., A. Cantarero, M. Cardona, C. Trallero-Giner, and S. T. Pavlov, 1997, "Feynman diagrams and Fano interference in light scattering from doped semiconductors," *J. Phys.: Condens. Matter* **9**, 5965–5976.
- Bell, M. I., R. N. Tyte, and M. Cardona, 1973, "Resonant Raman scattering in GaP in the E0 - E0 + [Delta]0 region," *Solid State Communications* **13**, 1833–1837.
- Beutler, H., 1935, "Über Absorptionsserien von Argon, Krypton und Xenon zu Termen zwischen den beiden Ionisierungsgrenzen  $^2P_{3/2}^{2/0}$  und  $^2P_{1/2}^{2/0}$ ," *Z. Phys. A* **93**, 177–196.
- Bhatia, A. K., and A. Temkin, 1984, "Line-shape parameters for  $^1P$  Feshbach resonances in He and  $Li^+$ ," *Phys. Rev. A* **29**, 1895–1900.
- Bianconi, A., 2003 (AIP Conf. Proc.), volume 652, 13–18.
- Billaudeau, C., S. Collin, F. Pardo, N. Bardou, and J.-L. Pelouard, 2009, "Tailoring radiative and non-radiative losses of thin nanostructured plasmonic waveguides," *Opt. Express* **17**, 3490–3499.
- Binder, P., D. Abraimov, A. V. Ustinov, S. Flach, and Y. Zolotaryuk, 2000, "Observation of Breathers in Josephson Ladders," *Phys. Rev. Lett.* **84**, 745–748.
- Bloch, I., J. Dalibard, and W. Zwerger, 2008, "Many-body physics with ultracold gases," *Rev. Mod. Phys.* **80**, 885.
- Boese, D., M. Lischka, and L. E. Reichl, 2000, "Resonances in a two-dimensional electron waveguide with a single  $\delta$ -function scatterer," *Phys. Rev. B* **61**, 5632–5636.
- Bohm, D., and D. Pines, 1951, "A Collective Description of Electron Interactions. I. Magnetic Interactions," *Phys. Rev.* **82**, 625–634.
- Bohren, C. F., and D. R. Huffman, 1998, *Absorption and Scattering of Light by Small Particles* (Wiley).
- Born, M., and E. Wolf, 1999, *Principles of Optics* (Cambridge University Press, UK, 1999).
- Bortchagovsky, E. G., and U. C. Fischer, 2003 (SPIE), volume 5064, 47–61.
- Boyd, R. W., and D. J. Gauthier, 2006, "Photonics: Transparency on an optical chip," *Nature* **441**, 701–702.
- Bravo-Abad, J., A. Rodriguez, P. Bermel, S. G. Johnson, J. D. Joannopoulos, and M. Soljacic, 2007, "Enhanced nonlinear optics in photonic-crystal microcavities," *Opt. Express* **15**, 16161–16176.
- Breit, G., and E. Wigner, 1936, "Capture of Slow Neutrons," *Phys. Rev.* **49**, 519–531.
- Bulka, B. R., and P. Stefanski, 2001, "Fano and Kondo Resonance in Electronic Current through Nanodevices," *Phys. Rev. Lett.* **86**, 5128–5131.
- Burioni, R., D. Cassi, P. Sodano, A. Trombettoni, and A. Vezani, 2005, "Propagation of discrete solitons in inhomogeneous networks," *Chaos* **15**, 043501.
- Burioni, R., D. Cassi, P. Sodano, A. Trombettoni, and A. Vezani, 2006, "Topological filters and high-pass/low-pass devices for solitons in inhomogeneous networks," *Phys. Rev. E* **73**, 066624.
- Cardona, M. (ed.), 1983, *Light Scattering in Solids* (Heidelberg: Springer).
- Cardona, M., F. Cerdeira, and T. A. Fjeldly, 1974, "Sign of the Raman tensor of diamond and zinc-blende-type semiconductors," *Phys. Rev. B* **10**, 3433–3435.
- Cardoso, J. L., and P. Pereyra, 2008, "Spin inversion devices operating at Fano anti-resonances," *EPL* **83**, 38001.
- Cerdeira, F., T. A. Fjeldly, and M. Cardona, 1973a, "Effect of

- Free Carriers on Zone-Center Vibrational Modes in Heavily Doped  $p$ -type Si. II. Optical Modes,” *Phys. Rev. B* **8**, 4734–4745.
- Cerdeira, F., T. A. Fjeldly, and M. Cardona, 1973b, “Interaction between electronic and vibronic Raman scattering in heavily doped silicon,” *Solid State Commun.* **13**, 325 – 328.
- Chakrabarti, A., 2006, “Electronic transmission in a model quantum wire with side-coupled quasiperiodic chains: Fano resonance and related issues,” *Phys. Rev. B* **74**, 205315.
- Chandrasekhar, M., J. B. Renucci, and M. Cardona, 1978, “Effects of interband excitations on Raman phonons in heavily doped  $n - Si$ ,” *Phys. Rev. B* **17**, 1623–1633.
- Chen, L., Z. Qiang, H. Yang, H. Pang, Z. Ma, and W. Zhou, 2009, “Polarization and angular dependent transmissions on transferred nanomembrane Fano filters,” *Opt. Express* **17**, 8396–8406.
- Chergui, M., N. Schwentner, and V. Chandrasekharan, 1991, “Fano profiles on multiphonon continua in electronic transitions of matrix-isolated NO,” *Phys. Rev. Lett.* **66**, 2499–2502.
- Chi, F., J.-L. Liu, and L.-L. Sun, 2007, “Fano-Rashba effect in a double quantum dot Aharonov-Bohm interferometer,” *J. Appl. Phys.* **101**, 093704.
- Clark, C. W., 2001, “Obituary: Ugo Fano (1912-2001),” *Nature* **410**, 164–164.
- Clerk, A. A., X. Waintal, and P. W. Brouwer, 2001, “Fano Resonances as a Probe of Phase Coherence in Quantum Dots,” *Phys. Rev. Lett.* **86**, 4636–4639.
- Connerade, J. P., 1998, *Highly Excited Atoms* (Cambridge University Press, UK).
- Cotting, R., J. R. Huber, and V. Engel, 1994, “Interference effects in the photodissociation of FNO,” *J. Chem. Phys.* **100**, 1040–1048.
- Cowan, A. R., and J. F. Young, 2003, “Optical bistability involving photonic crystal microcavities and Fano line shapes,” *Phys. Rev. E* **68**, 046606.
- Crance, M., and L. Armstrong, 1982a, “Fluorescence induced by resonant multiphoton ionisation near an autoionising state,” *J. Phys. B* **15**, 3199–3210.
- Crance, M., and L. Armstrong, 1982b, “Four-wave mixing under double-resonance conditions,” *J. Phys. B* **15**, 4637–4646.
- Cronenwett, S. M., T. H. Oosterkamp, and L. P. Kouwenhoven, 1998, “A Tunable Kondo Effect in Quantum Dots,” *Science* **281**, 540–544.
- Davis, L. C., and L. A. Feldkamp, 1977, “Interaction of many discrete states with many continua,” *Phys. Rev. B* **15**, 2961–2969.
- dell’Orto, T., M. D. Ventra, J. Almeida, C. Coluzza, and G. Margaritondo, 1995, “Evidence for a photocurrent Fano resonance in an artificial nanostructure,” *Phys. Rev. B* **52**, R2265–R2268.
- Dixit, S. N., and P. Lambropoulos, 1979, “Line-profile considerations of resonant multiphoton ionization,” *Phys. Rev. A* **19**, 1576–1579.
- Druger, S. D., 1977, “Coupling-strength incoherence and the absorption line shape of an isolated resonance in a large molecule,” *J. Chem. Phys.* **67**, 3249–3255.
- Dumke, R., T. Mütther, M. Volk, W. Ertmer, and G. Birkel, 2002, “Interferometer-Type Structures for Guided Atoms,” *Phys. Rev. Lett.* **89**, 220402.
- Ebbesen, T., H. Lezec, H. Ghaemi, T. Thio, and P. Wolf, 1998, “Extraordinary optical transmission through sub-wavelength hole arrays,” *Nature* **391**, 667.
- Efimov, V. N., 1970, “Energy levels arising from resonant two-body forces in a three-body system,” *Phys. Lett. B* **33**, 563 – 564.
- Efimov, V. N., 1971, “Weakly-bound states of three resonantly-interacting particles,” *Sov. J. Nucl. Phys.* **12**, 589.
- Eichmann, U., T. F. Gallagher, and R. M. Konik, 2003, “Fano Line Shapes Reconsidered: Symmetric Photoionization Peaks from Pure Continuum Excitation,” *Phys. Rev. Lett.* **90**, 233004.
- Eiermann, B., T. Anker, M. Albiez, M. Taglieber, P. Treutlein, K.-P. Marzlin, and M. K. Oberthaler, 2004, “Bright Bose-Einstein Gap Solitons of Atoms with Repulsive Interaction,” *Phys. Rev. Lett.* **92**, 230401.
- Eisenberg, H. S., Y. Silberberg, R. Morandotti, A. R. Boyd, and J. S. Aitchison, 1998, “Discrete Spatial Optical Solitons in Waveguide Arrays,” *Phys. Rev. Lett.* **81**, 3383–3386.
- Emmanouilidou, A., and L. E. Reichl, 2002, “Floquet scattering and classical-quantum correspondence in strong time-periodic fields,” *Phys. Rev. A* **65**, 033405.
- Entin-Wohlman, O., A. Aharony, Y. Imry, and Y. Levinson, 2002a, “The Fano Effect in Aharonov-Bohm Interferometers,” *J. Low Temp. Phys.* **126**, 1251.
- Entin-Wohlman, O., A. Aharony, Y. Imry, Y. Levinson, and A. Schiller, 2002b, “Broken Unitarity and Phase Measurements in Aharonov-Bohm Interferometers,” *Phys. Rev. Lett.* **88**, 166801.
- Esry, B. D., and C. H. Greene, 2006, “Quantum physics: A menage a trois laid bare,” *Nature* **440**, 289–290.
- Fan, S., 2002, “Sharp asymmetric line shapes in side-coupled waveguide-cavity systems,” *Appl. Phys. Lett.* **80**, 908–910.
- Fan, S., and J. D. Joannopoulos, 2002, “Analysis of guided resonances in photonic crystal slabs,” *Phys. Rev. B* **65**, 235112.
- Fan, S., W. Suh, and J. D. Joannopoulos, 2003, “Temporal coupled-mode theory for the Fano resonance in optical resonators,” *J. Opt. Soc. Am. A* **20**, 569–572.
- Fan, S., P. R. Villeneuve, J. D. Joannopoulos, and H. A. Haus, 1998, “Channel Drop Tunneling through Localized States,” *Phys. Rev. Lett.* **80**, 960–963.
- Fan, S., P. R. Villeneuve, J. D. Joannopoulos, M. J. Khan, C. Manolatou, and H. A. Haus, 1999, “Theoretical analysis of channel drop tunneling processes,” *Phys. Rev. B* **59**, 15882–15892.
- Fano, U., 1935, “Sullo spettro di assorbimento dei gas nobili presso il limite dello spettro d’arco,” *Nuovo Cimento* **12**, 154–161.
- Fano, U., 1936, “Some Theoretical Considerations on Anomalous Diffraction Gratings,” *Phys. Rev.* **50**, 573–573.
- Fano, U., 1937, “On the Anomalous Diffraction Gratings. II,” *Phys. Rev.* **51**, 288–288.
- Fano, U., 1938, “Zur Theorie der Intensitätsanomalien der Beugung,” *Ann. Phys. (Leipzig)* **424**, 393–443.
- Fano, U., 1941, “The theory of anomalous diffraction gratings and of quasi-stationary waves on metallic surfaces (Sommerfeld’s waves),” *J. Opt. Soc. Am.* **31**, 213.
- Fano, U., 1961, “Effects of Configuration Interaction on Intensities and Phase Shifts,” *Phys. Rev.* **124**, 1866–1878.
- Fano, U., 1964, “Exclusion of Parity Unfavored Transitions in Forward Scattering Collisions,” *Phys. Rev.* **135**, B863–B864.
- Fano, U., 1965, “Interaction between Configurations with Several Open Shells,” *Phys. Rev.* **140**, A67–A75.

- Fano, U., 1970, "Quantum Defect Theory of  $l$  Uncoupling in  $H_2$  as an Example of Channel-Interaction Treatment," *Phys. Rev. A* **2**, 353–365.
- Fano, U., 1977, "Effects of Configuration Interaction on Intensities and Phase Shifts," *Citation Classics* **8**, 219.
- Fano, U., and J. W. Cooper, 1965, "Line Profiles in the Far-ulv Absorption Spectra of the Rare Gases," *Phys. Rev.* **137**, A1364–A1379.
- Fano, U., and J. W. Cooper, 1968, "Spectral Distribution of Atomic Oscillator Strengths," *Rev. Mod. Phys.* **40**, 441–507.
- Fano, U., and C. M. Lee, 1973, "Variational Calculation of R Matrices. Application to Ar Photoabsorption," *Phys. Rev. Lett.* **31**, 1573–1576.
- Feneuille, S., S. Liberman, J. Pinard, and A. Taleb, 1979, "Observation of Fano profiles in photoionization of rubidium in the presence of a dc field," *Phys. Rev. Lett.* **42**, 1404–1406.
- Feshbach, H., 1958, "Unified theory of nuclear reactions," *Ann. Phys. (N. Y.)* **5**, 357–390.
- Feshbach, H., 1962, "A unified theory of nuclear reactions. II," *Ann. Phys. (N. Y.)* **19**, 287.
- Finch, C. M., V. M. García-Suárez, and C. J. Lambert, 2009, "Giant thermopower and figure of merit in single-molecule devices," *Phys. Rev. B* **79**, 033405.
- Flach, S., V. Fleurov, A. Gorbach, and A. Miroshnichenko, 2006, "Resonant light-light interaction in slab waveguides: angular filters and spectral hole burning," *Proc. SPIE* **5975**, 297–306.
- Flach, S., V. Fleurov, A. V. Gorbach, and A. E. Miroshnichenko, 2005, "Resonant Light Scattering by Optical Solitons," *Phys. Rev. Lett.* **95**, 023901.
- Flach, S., and A. V. Gorbach, 2008, "Discrete breathers – Advances in theory and applications," *Phys. Rep.* **467**, 1 – 116.
- Flach, S., A. E. Miroshnichenko, and M. V. Fistul, 2003a, "Wave scattering by discrete breathers," *Chaos* **13**, 596–609.
- Flach, S., A. E. Miroshnichenko, V. Fleurov, and M. V. Fistul, 2003b, "Fano Resonances with Discrete Breathers," *Phys. Rev. Lett.* **90**, 084101.
- Flach, S., and C. R. Willis, 1998, "Discrete breathers," *Phys. Rep.* **295**, 181–264.
- Fleischhauer, M., A. Imamoglu, and J. P. Marangos, 2005, "Electromagnetically induced transparency: Optics in coherent media," *Rev. Mod. Phys.* **77**, 633.
- Franson, J. D., and S. M. Hendrickson, 2006, "Optical transparency using interference between two modes of a cavity," *Phys. Rev. A* **74**, 053817.
- Fransson, J., and A. V. Balatsky, 2007, "Exchange interaction and Fano resonances in diatomic molecular systems," *Phys. Rev. B* **75**, 153309.
- Friedl, B., C. Thomsen, and M. Cardona, 1990, "Determination of the superconducting gap in  $RBa_2Cu_3O_{7-\delta}$ ," *Phys. Rev. Lett.* **65**, 915–918.
- Friedrich, H., and D. Wintgen, 1985a, "Interfering resonances and bound states in the continuum," *Phys. Rev. A* **32**, 3231–3242.
- Friedrich, H., and D. Wintgen, 1985b, "Physical realization of bound states in the continuum," *Phys. Rev. A* **31**, 3964–3966.
- Galli, M., S. L. Portalupi, M. Belotti, L. C. Andreani, L. O'Faolain, and T. F. Krauss, 2009, "Light scattering and Fano resonances in high-Q photonic crystal nanocavities," *Appl. Phys. Lett.* **94**, 071101.
- Gantmakher, V. F., 2005, *Electrons and Disorder in Solids* (Clarendon Press Oxford).
- Ganz, J., M. Raab, H. Hotop, and J. Geiger, 1984, "Changing the Beutler-Fano profile of the Ne  $ns'$  autoionizing resonances," *Phys. Rev. Lett.* **53**, 1547–1550.
- Gersen, H., T. J. Karle, R. J. P. Engelen, W. Bogaerts, J. P. Korterik, N. F. van Hulst, T. F. Krauss, and L. Kuipers, 2005, "Real-Space Observation of Ultraslow Light in Photonic Crystal Waveguides," *Phys. Rev. Lett.* **94**, 073903.
- Ghaemi, H. F., T. Thio, D. E. Grupp, T. W. Ebbesen, and H. J. Lezec, 1998, "Surface plasmons enhance optical transmission through subwavelength holes," *Phys. Rev. B* **58**, 6779–6782.
- Glazman, L. I., and M. E. Raikh, 1988, "Resonant Kondo transparency of a barrier with quasilocal impurity states," *JETP Lett.* **47**, 452–455.
- Glutsch, S., 2002, "Optical absorption of the Fano model: General case of many resonances and many continua," *Phys. Rev. B* **66**, 075310.
- Goldhaber-Gordon, D., J. Göres, M. A. Kastner, H. Shtrikman, D. Mahalu, and U. Meirav, 1998a, "From the Kondo Regime to the Mixed-Valence Regime in a Single-Electron Transistor," *Phys. Rev. Lett.* **81**, 5225–5228.
- Goldhaber-Gordon, D., J. Göres, H. Shtrikman, D. Mahalu, U. Meirav, and M. A. Kastner, 2001, "The Kondo effect in a single-electron transistor," *J. Mater. Sci. Eng. B* **84**, 17 – 21.
- Goldhaber-Gordon, D., H. Shtrikman, D. Mahalu, D. Abusch-Magder, U. Meirav, and M. A. Kastner, 1998b, "Kondo effect in a single-electron transistor," *Nature* **391**, 156–159.
- Gong, W., Y. Zheng, Y. Liu, F. N. Kariuki, and T. Lü, 2008, "Fano effect in a T-shaped double quantum dot structure in the presence of Rashba spin-orbit coupling," *Phys. Lett. A* **372**, 2934 – 2940.
- Göres, J., D. Goldhaber-Gordon, S. Heemeyer, M. A. Kastner, H. Shtrikman, D. Mahalu, and U. Meirav, 2000, "Fano resonances in electronic transport through a single-electron transistor," *Phys. Rev. B* **62**, 2188–2194.
- Grillet, C., D. Freeman, B. Luther-Davies, S. Madden, R. McPhedran, D. J. Moss, M. J. Steel, and B. J. Eggleton, 2006, "Characterization and modeling of Fano resonances in chalcogenide photonic crystal membranes," *Opt. Express* **14**, 369.
- Grupp, M., R. Walser, W. P. Schleich, A. Muramatsu, and M. Weitz, 2007, "Resonant Feshbach scattering of fermions in one-dimensional optical lattices," *J. Phys. B* **40**, 2703–2718.
- Gurvitz, S. A., and Y. B. Levinson, 1993, "Resonant reflection and transmission in a conducting channel with a single impurity," *Phys. Rev. B* **47**, 10578–10587.
- Haan, S. L., and G. S. Agarwal, 1987, "Stability of dressed states against radiative decay in strongly coupled bound-continuum transitions," *Phys. Rev. A* **35**, 4592–4604.
- Hänsel, W., P. Hommelhoff, T. W. Hänsch, and J. Reichel, 2001, "Bose-Einstein condensation on a microelectronic chip," *Nature* **413**, 498–501.
- Hanson, R., L. P. Kouwenhoven, J. R. Petta, S. Tarucha, and L. M. K. Vandersypen, 2007, "Spins in few-electron quantum dots," *Rev. Mod. Phys.* **79**, 1217.
- Hao, F., P. Nordlander, M. T. Burnett, and S. A. Maier, 2007, "Enhanced tunability and linewidth sharpening of plasmon resonances in hybridized metallic ring/disk nanocavities," *Phys. Rev. B* **76**, 245417.

- Hao, F., Y. Sonnefraud, P. van Dorpe, S. A. Maier, N. J. Halas, and P. Nordlander, 2008, "Symmetry Breaking in Plasmonic Nanocavities: Subradiant LSPR Sensing and a Tunable Fano Resonance," *Nano Lett.* **8**, 3983–3988.
- Harbers, R., S. Jochim, N. Moli, R. F. Mahrt, D. Erni, J. A. Hoffnagle, and W. D. Hinsberg, 2007, "Control of Fano line shapes by means of photonic crystal structures in a dye-doped polymer," *Appl. Phys. Lett.* **90**, 201105.
- Harmin, D. A., 1985, "Asymmetry of field-induced shape resonances in hydrogen," *Phys. Rev. A* **31**, 2984–2990.
- Hase, M., J. Demsar, and M. Kitajima, 2006a, "Photoinduced Fano resonance of coherent phonons in zinc," *Phys. Rev. B* **74**, 212301.
- Hase, M., J. Demsar, and M. Kitajima, 2006b, "Photoinduced Fano resonance of coherent phonons in zinc," *Physical Review B (Condensed Matter and Materials Physics)* **74**, 212301.
- Haus, H. A., and Y. Lai, 1991, "Narrow-band distributed feedback reflector. design," *J. Lightwave Technol.* **9**, 754.
- Heinzmann, U., J. Kessler, and J. Lorenz, 1970, "Wavelength Dependence of the Fano Effect," *Phys. Rev. Lett.* **25**, 1325–1325.
- Heller, D. F., and S. Mukamel, 1979, "Theory of vibrational overtone line shapes of polyatomic molecules," *J. Chem. Phys.* **70**, 463–472.
- Hessel, A., and A. A. Oliner, 1965, "A New Theory of Wood's Anomalies on Optical Gratings," *Applied Optics* **4**, 1275.
- Hewson, A. C., 1993, *The Kondo Problem to Heavy Fermions* (Cambridge University Press, UK).
- Hino, K.-i., 2001, "Overlap structure of Fano-resonance profiles of excitons in a semiconductor quantum well," *Phys. Rev. B* **64**, 075318.
- Hino, K.-i., and N. Tushima, 2005, "Spectral modulation of exciton Fano resonance due to Zener breakdown in strongly biased superlattices," *Phys. Rev. B* **71**, 205326.
- Hofstetter, W., J. König, and H. Schoeller, 2001, "Kondo Correlations and the Fano Effect in Closed Aharonov-Bohm Interferometers," *Phys. Rev. Lett.* **87**, 156803.
- Holfeld, C. P., F. Loser, M. Sudzius, K. Leo, D. M. Whittaker, and K. Kohler, 1998, "Fano Resonances in Semiconductor Superlattices," *Phys. Rev. Lett.* **81**, 874–877.
- Hopfield, J. J., P. J. Dean, and D. G. Thomas, 1967, "Interference between Intermediate States in the Optical Properties of Nitrogen-Doped Gallium Phosphide," *Phys. Rev.* **158**, 748–755.
- Hu, F., H. Yang, X. Yang, and J. Dong, 2006, "Electronic transport and Fano resonance in carbon nanotube ring systems," *Phys. Rev. B* **73**, 235437.
- van der Hulst, H. C., 1981, *Light Scattering by Small Particles* (Dover, New York).
- Iwanow, R., R. Schiek, G. I. Stegeman, T. Pertsch, F. Lederer, Y. Min, and W. Sohler, 2004, "Observation of Discrete Quadratic Solitons," *Phys. Rev. Lett.* **93**, 113902.
- Jacobsen, R., A. Lavrinenko, L. Frandsen, C. Peucheret, B. Zsigri, G. Moulin, J. Fage-Pedersen, and P. Borel, 2005, "Direct experimental and numerical determination of extremely high group indices in photonic crystal waveguides," *Opt. Express* **13**, 7861–7871.
- Janzen, E., G. Grossmann, R. Stedman, and H. G. Grimmeiss, 1985, "Fano resonances in chalcogen-doped silicon," *Phys. Rev. B* **31**, 8000–8012.
- Ji, Y., M. Heiblum, D. Sprinza, D. Mahalu, and H. Shtrikman, 2000, "Phase Evolution in a Kondo-Correlated System," *Science* **290**, 779–783.
- Jin, K.-j., and S. J. Xu, 2007, "Fano resonance in the luminescence spectra of donor bound excitons in polar semiconductors," *Appl. Phys. Lett.* **90**, 032107.
- Jin, K.-j., J. Zhang, Z.-h. Chen, G.-z. Yang, Z. H. Chen, X. H. Shi, and S. C. Shen, 2001, "Phonon-induced photoconductive response in doped semiconductors," *Phys. Rev. B* **64**, 205203.
- Joe, Y. S., A. M. Satanin, and C. S. Kim, 2006, "Classical analogy of Fano resonances," *Phys. Scr.* **74**, 259.
- Johnson, A. C., C. M. Marcus, M. P. Hanson, and A. C. Gossard, 2004, "Coulomb-Modified Fano Resonance in a One-Lead Quantum Dot," *Phys. Rev. Lett.* **93**, 106803.
- Kang, K., S. Y. Cho, J.-J. Kim, and S.-C. Shin, 2001, "Anti-Kondo resonance in transport through a quantum wire with a side-coupled quantum dot," *Phys. Rev. B* **63**, 113304.
- Kang, K., and S.-C. Shin, 2000, "Mesoscopic Kondo Effect in an Aharonov-Bohm Ring," *Phys. Rev. Lett.* **85**, 5619–5622.
- Kastner, M. A., 1992, "The single-electron transistor," *Rev. Mod. Phys.* **64**, 849–858.
- Kessler, J., and J. Lorenz, 1970, "Experimental Verification of the Fano Effect," *Phys. Rev. Lett.* **24**, 87–88.
- Khelif, A., B. Djafari-Rouhani, J. O. Vasseur, and P. A. Deymier, 2003, "Transmission and dispersion relations of perfect and defect-containing waveguide structures in phononic band gap materials," *Phys. Rev. B* **68**, 024302.
- Kim, B., and K. Yoshihara, 1993, "Multichannel quantum interference in the predissociation of  $\text{Cs}_2$ : Observation of q-reversal in a complex resonance," *J. Chem. Phys.* **99**, 1433–1435.
- Kim, G., S. B. Lee, T.-S. Kim, and J. Ihm, 2005, "Fano resonance and orbital filtering in multiply connected carbon nanotubes," *Phys. Rev. B* **71**, 205415.
- Kim, J., J.-R. Kim, J.-O. Lee, J. W. Park, H. M. So, N. Kim, K. Kang, K.-H. Yoo, and J.-J. Kim, 2003, "Fano Resonance in Crossed Carbon Nanotubes," *Phys. Rev. Lett.* **90**, 166403.
- Kim, S. W., 2002, "Floquet scattering in parametric electron pumps," *Phys. Rev. B* **66**, 235304.
- Kim, S. W., and S. Kim, 2000, "The structure of eigenmodes and phonon scattering by discrete breathers in the discrete nonlinear Schrödinger chain," *Physica D* **141**, 91–103.
- Kim, S. W., and S. Kim, 2001, "Fano resonances in translationally invariant nonlinear chains," *Phys. Rev. B* **63**, 212301.
- Kleinpöppen, H., and M. McDowell (eds.), 1976, *Electron and photo interaction with atoms (Festschrift for Professor Ugo Fano)* (Plenum Press, New York).
- Kobayashi, K., H. Aikawa, S. Katsumoto, and Y. Iye, 2002, "Tuning of the Fano Effect through a Quantum Dot in an Aharonov-Bohm Interferometer," *Phys. Rev. Lett.* **88**, 256806.
- Kobyakov, A., A. R. Zakharian, K. M. Gundu, and S. A. Darmanyan, 2009, "Giant optical resonances due to gain-assisted Bloch surface plasmons," *Appl. Phys. Lett.* **94**, 151111.
- Koch, H., and H. Lübbig (eds.), 1992, *Single Electron Tunneling and Mesoscopic Devices*, volume 31 of *Springer Series in Electronics and Photonics* (Springer, Berlin).
- Kokoouline, V., C. Drag, P. Pillet, and F. Masnou-Seeuws, 2002, "Lu-Fano plot for interpretation of the photoassociation spectra," *Phys. Rev. A* **65**, 062710.
- Kolorenc, P., V. Brems, and J. Horacek, 2005, "Computing resonance positions, widths, and cross sections via the Feshbach-Fano R-matrix method: Application to potential

- scattering,” *Phys. Rev. A* **72**, 012708.
- Kormányos, A., I. Grace, and C. J. Lambert, 2009, “Andreev reflection through Fano resonances in molecular wires,” *Phys. Rev. B* **79**(7), 075119.
- Kosevich, Y. A., 1997, “Capillary phenomena and macroscopic dynamics of complex two-dimensional defects in crystals,” *Prog. Surf. Sci.* **55**(1), 1 – 57.
- Kosevich, Y. A., 2008, “Multichannel propagation and scattering of phonons and photons in low-dimension nanostructures,” *Physics-Uspekhi* **51**(8), 839–859.
- Kosevich, Y. A., A. Feher, and E. S. Syrkina, 2008, “Resonance absorption, reflection, transmission of phonons and heat transfer through interface between two solids,” *Low Temp. Phys.* **34**(7), 575–582.
- Koshino, K., 2003, “Analytic approach to the optical response of one-dimensional photonic crystal slabs,” *Phys. Rev. B* **67**, 165213.
- Kraemer, T., M. Mark, P. Waldburger, J. G. Danzl, C. Chin, B. Engeser, A. D. Lange, K. Pilch, A. Jaakkola, H.-C. Nägerl, and R. Grimm, 2006, “Evidence for Efimov quantum states in an ultracold gas of caesium atoms,” *Nature* **440**, 315–318.
- Kroner, M., A. O. Govorov, S. Remi, B. Biedermann, S. Seidl, A. Badolato, P. M. Petroff, W. Zhang, R. Barbour, B. D. Gerardot, R. J. Warburton, and K. Karrai, 2008, “The nonlinear Fano effect,” *Nature* **451**, 311–314.
- Landobasa Y. Mario, S. D., and M. K. Chin, 2006, “Asymmetric Fano resonance and bistability for high extinction ratio, large modulation depth, and low power switching,” *Opt. Express* **14**, 12770–12781.
- Langreth, D. C., 1966, “Friedel Sum Rule for Anderson’s Model of Localized Impurity States,” *Phys. Rev.* **150**, 516–518.
- Le, F., N. Z. Lwin, N. J. Halas, and P. Nordlander, 2007, “Plasmonic interactions between a metallic nanoshell and a thin metallic film,” *Phys. Rev. B* **76**, 165410.
- Lebeck, M., J. C. Houver, D. Doweck, and R. R. Lucchese, 2006, “Molecular Frame Photoelectron Emission in the Presence of Autoionizing Resonances,” *Phys. Rev. Lett.* **96**, 073001.
- Lee, C.-W., 1998, “Identification of the Beutler-Fano formula in eigenphase shifts and eigentime delays near a resonance,” *Phys. Rev. A* **58**, 4581–4592.
- Lee, J. D., J. Inoue, and M. Hase, 2006, “Ultrafast Fano Resonance between Optical Phonons and Electron-Hole Pairs at the Onset of Quasiparticle Generation in a Semiconductor,” *Phys. Rev. Lett.* **97**, 157405.
- Lee, M., and C. Bruder, 2006, “Spin filter using a semiconductor quantum ring side coupled to a quantum wire,” *Phys. Rev. B* **73**, 085315.
- Lee, S., and B. Kim, 2000a, “Direct evaluation of the asymmetry parameters for isolated resonances,” *J. Phys. B* **33**, 3441–3448.
- Lee, S.-S., and S. Kim, 2000b, “Phonon scattering by breathers in the discrete nonlinear Schrödinger chain,” *Int. J. Mod. Phys. B* **14**, 1903.
- Lewis, B. R., S. T. Gibson, P. O’Keeffe, T. Ridley, K. P. Lawley, and R. J. Donovan, 2001, “Observation of Completely Destructive Quantum Interference between Interacting Resonances in Molecular Predissociation,” *Phys. Rev. Lett.* **86**, 1478–1481.
- Ley, L., R. Karcher, and R. L. Johnson, 1984, “Localized states at the conduction-band edge of amorphous silicon nitride detected by resonance photoemission,” *Phys. Rev. Lett.* **53**, 710–713.
- Li, W., and L. E. Reichl, 1999, “Floquet scattering through a time-periodic potential,” *Phys. Rev. B* **60**, 15732–15741.
- Limonov, M. F., A. I. Rykov, S. Tajima, and A. Yamanaka, 1998, “Raman Scattering Study on Fully Oxygenated  $YBa_2Cu_3O_7$  Single Crystals:  $x - y$  Anisotropy in the Superconductivity-Induced Effects,” *Phys. Rev. Lett.* **80**, 825–828.
- Limonov, M. F., S. Tajima, and A. Yamanaka, 2000, “Phononic and electronic Raman spectroscopy of the pseudogap state in underdoped  $YBa_2Cu_3O_7 - x$ ,” *Phys. Rev. B* **62**, 11859–11863.
- Lin, S. Y., E. Chow, V. Hietala, P. R. Villeneuve, and J. D. Joannopoulos, 1998, “Experimental Demonstration of Guiding and Bending of Electromagnetic Waves in a Photonic Crystal,” *Science* **282**, 274–276.
- Lobos, A. M., and A. A. Aligia, 2008, “Effects of Interactions in Transport through Aharonov-Bohm-Casher Interferometers,” *Phys. Rev. Lett.* **100**, 016803.
- Longhi, S., 2006, “Transmission and localization control by ac fields in tight-binding lattices with an impurity,” *Phys. Rev. B* **73**, 193305.
- Lousse, V., and J. P. Vigneron, 2004, “Use of Fano resonances for bistable optical transfer through photonic crystal films,” *Phys. Rev. B* **69**, 155106.
- Luk’yanchuk, B. S., T. C. Chong, L. P. Shi, M. I. Tribelsky, Z. B. Wang, L. Li, C.-W. Qiu, C. J. R. Sheppard, and J. H. Wu, 2008, in *IEEE Photonics and Global*.
- Luo, H. G., T. Xiang, X. Q. Wang, Z. B. Su, and L. Yu, 2004, “Fano Resonance for Anderson Impurity Systems,” *Phys. Rev. Lett.* **92**, 256602.
- MacKay, R. S., and S. Aubry, 1994, “Proof of existence of breathers for time-reversible or Hamiltonian networks of weakly coupled oscillators,” *Nonlinearity* **7**, 1623.
- Maeda, K., K. Ueda, T. Namioka, and K. Ito, 1992, “High-resolution measurement of Beutler-Fano profiles for autoionizing Rydberg series of Xe,” *Phys. Rev. A* **45**, 527–530.
- Maes, B., P. Bienstman, and R. Baets, 2005, “Switching in coupled nonlinear photonic-crystal resonators,” *J. Opt. Soc. Am. B* **22**, 1778–1784.
- Maes, B., P. Bienstman, and R. Baets, 2008, “Symmetry breaking with coupled Fano resonances,” *Opt. Express* **16**(5), 3069–3076.
- Magidson, V., and R. Beserman, 2002, “Fano-type interference in the Raman spectrum of photoexcited Si,” *Phys. Rev. B* **66**, 195206.
- Magnusson, R., and S. S. Wang, 1992, “New principle for optical filters,” *Appl. Phys. Lett.* **61**, 1022–1024.
- Magunov, A. I., I. Rotter, and S. I. Strakhova, 2003, “Fano resonances in the overlapping regime,” *Phys. Rev. B* **68**, 245305.
- Mahan, G., 1993, *Many-Particle Physics* (New York, Plenum Press).
- Maleki, L., A. B. Matsko, A. A. Savchenkov, and V. S. Ilchenko, 2004, “Tunable delay line with interacting whispering-gallery-moderesonators,” *Opt. Lett.* **29**, 626–628.
- Margulis, V. A., and M. A. Pyataev, 2004, “Fano resonances in a three-terminal nanodevice,” *J. Phys. Condens. Matter* **16**, 4315.
- Marin Soljačić, S. G. J. Y. F., Mihai Ibanescu, and J. D. Joannopoulos, 2002, “Optimal bistable switching in nonlinear photonic crystals,” *Phys. Rev. E* **66**, 055601.

- Marinho, R. R. T., O. Bjorneholm, S. L. Sorensen, I. Hjelte, S. Sundin, M. Bassler, S. Svensson, and A. N. de Brito, 2001, "Interference between direct and resonant channels in near-resonance photoemission in argon," *Phys. Rev. A* **63**, 032514.
- Martinez, D. F., and L. E. Reichl, 2001, "Transmission properties of the oscillating delta-function potential," *Phys. Rev. B* **64**, 245315.
- Mazumdar, I., A. R. P. Rau, and V. S. Bhasin, 2006, "Efimov States and their Fano Resonances in a Neutron-Rich Nucleus," *Phys. Rev. Lett.* **97**, 062503.
- McCormack, E. F., F. D. Teodoro, J. M. Grochocinski, and S. T. Pratt, 1998, "Dynamics of Rydberg states of nitric oxide probed by two-color resonant four-wave mixing spectroscopy," *J. Chem. Phys.* **109**, 63–71.
- Mehlhorn, W., 1998, "70 years of Auger spectroscopy, a historical perspective," *J. Electron. Spectrosc. Relat. Phenom.* **93**, 1–15.
- Meier, T., A. Schulze, P. Thomas, H. Vaupel, and K. Maschke, 1995, "Signatures of Fano resonances in four-wave-mixing experiments," *Phys. Rev. B* **51**, 13977–13986.
- Meijerink, A., and G. Blasse, 1989, "Fano antiresonance in the excitation spectra of the luminescence of divalent europium," *Phys. Rev. B* **40**, 7288–7291.
- Mekis, A., J. C. Chen, I. Kurland, S. Fan, P. R. Villeneuve, and J. D. Joannopoulos, 1996, "High Transmission through Sharp Bends in Photonic Crystal Waveguides," *Phys. Rev. Lett.* **77**, 3787–3790.
- Menéndez, J., and M. Cardona, 1985, "Interference effects: A key to understanding forbidden Raman scattering by LO phonons in GaAs," *Phys. Rev. B* **31**, 3696–3704.
- Mie, G., 1908, "Beiträge zur Optik trüber Medien, speziell kolloidaler Metallösungen," *Ann. Phys. (Leipzig)* **330**, 337–445.
- Mies, F. H., 1968, "Configuration Interaction Theory. Effects of Overlapping Resonances," *Phys. Rev.* **175**, 164–175.
- Mingaleev, S. F., and Y. S. Kivshar, 2001, "Self-Trapping and Stable Localized Modes in Nonlinear Photonic Crystals," *Phys. Rev. Lett.* **86**, 5474–5477.
- Mingaleev, S. F., and Y. S. Kivshar, 2002a, "Effective equations for photonic-crystal waveguides and circuits," *Opt. Lett.* **27**, 231–233.
- Mingaleev, S. F., and Y. S. Kivshar, 2002b, "Nonlinear transmission and light localization in photonic-crystal waveguides," *J. Opt. Soc. Am. B* **19**, 2241–2249.
- Mingaleev, S. F., Y. S. Kivshar, and R. A. Sammut, 2000, "Long-range interaction and nonlinear localized modes in photonic crystal waveguides," *Phys. Rev. E* **62**, 5777–5782.
- Mingaleev, S. F., A. E. Miroshnichenko, and Y. S. Kivshar, 2007, "Low-threshold bistability of slow light in photonic-crystal waveguides," *Opt. Express* **15**, 12380–12385.
- Mingaleev, S. F., A. E. Miroshnichenko, and Y. S. Kivshar, 2008, "Coupled-resonator-induced reflection in photonic-crystal waveguide structures," *Opt. Express* **16**, 11647–11659.
- Mingaleev, S. F., A. E. Miroshnichenko, Y. S. Kivshar, and K. Busch, 2006, "All-optical switching, bistability, and slow-light transmission in photonic crystal waveguide-resonator structures," *Phys. Rev. E* **74**, 046603.
- Miroshnichenko, A. E., 2009, "Nonlinear Fano-Feshbach resonances," *Phys. Rev. E* **79**(2), 026611.
- Miroshnichenko, A. E., S. Flach, A. V. Gorbach, B. S. Luk'yanchuk, Y. S. Kivshar, and M. I. Tribelsky, 2008, "Fano resonances: A discovery that did not happen 100 years ago," *Opt. Phon. News* **19**, 48.
- Miroshnichenko, A. E., S. Flach, and B. Malomed, 2003, "Resonant scattering of solitons," *Chaos* **13**, 874–879.
- Miroshnichenko, A. E., Y. Kivshar, C. Etrich, T. Pertsch, R. Iliew, and F. Lederer, 2009, "Dynamics and instability of nonlinear Fano resonances in photonic crystals," *Phys. Rev. A* **79**, 013809.
- Miroshnichenko, A. E., and Y. S. Kivshar, 2005a, "Engineering Fano resonances in discrete arrays," *Phys. Rev. E* **72**, 056611.
- Miroshnichenko, A. E., and Y. S. Kivshar, 2005b, "Sharp bends in photonic crystal waveguides as nonlinear Fano resonators," *Opt. Express* **13**, 3969–3976.
- Miroshnichenko, A. E., Y. S. Kivshar, R. A. Vicencio, and M. I. Molina, 2005a, "Fano resonance in quadratic waveguide arrays," *Opt. Lett.* **30**, 872–874.
- Miroshnichenko, A. E., S. F. Mingaleev, S. Flach, and Y. S. Kivshar, 2005b, "Nonlinear Fano resonance and bistable wave transmission," *Phys. Rev. E* **71**, 036626.
- Miroshnichenko, A. E., M. Schuster, S. Flach, M. V. Fistul, and A. V. Ustinov, 2005c, "Resonant plasmon scattering by discrete breathers in Josephson junction ladders," *Phys. Rev. B* **71**, 174306.
- Misochko, O., M. Hase, K. Ishioka, and M. Kitajima, 2005, "Fano interference with the alternating asymmetry parameter in time-domain experiments," *JETP Letters* **82**, 426–430.
- Misochko, O. V., K. Kisoda, K. Sakai, and S. Nakashima, 2000, "Dynamics of low-frequency phonons in the  $YBa_2Cu_3O_7 - x$  superconductor studied by time- and frequency-domain spectroscopies," *Phys. Rev. B* **61**, 4305–4313.
- van der Molen, K. L., K. J. K. Koerkamp, S. Enoch, F. B. Segerink, N. F. van Hulst, and L. Kuipers, 2005, "Role of shape and localized resonances in extraordinary transmission through periodic arrays of subwavelength holes: Experiment and theory," *Phys. Rev. B* **72**, 045421.
- Morsch, O., and M. Oberthaler, 2006, "Dynamics of Bose-Einstein condensates in optical lattices," *Rev. Mod. Phys.* **78**, 179.
- Moskovits, M., 1985, "Surface-enhanced spectroscopy," *Rev. Mod. Phys.* **57**, 783–826.
- Naweed, A., G. Farca, S. I. Shopova, and A. T. Rosenberger, 2005, "Induced transparency and absorption in coupled whispering-gallery microresonators," *Phys. Rev. A* **71**, 043804.
- Neel, N., J. Kroger, L. Limot, K. Palotas, W. A. Hofer, and R. Berndt, 2007, "Conductance and Kondo Effect in a Controlled Single-Atom Contact," *Phys. Rev. Lett.* **98**, 016801.
- von Neumann, J., and E. Wigner, 1929, "Über merkwürdige diskrete Eigenwerte / On unusual discrete eigenvalues," *Z. Phys.* **30**, 465–467.
- Ng, T. K., and P. A. Lee, 1988, "On-Site Coulomb Repulsion and Resonant Tunneling," *Phys. Rev. Lett.* **61**, 1768–1771.
- Nockel, J. U., and A. D. Stone, 1994, "Resonance line shapes in quasi-one-dimensional scattering," *Phys. Rev. B* **50**, 17415–17432.
- Notomi, M., K. Yamada, A. Shinya, J. Takahashi, C. Takahashi, and I. Yokohama, 2001, "Extremely Large Group-Velocity Dispersion of Line-Defect Waveguides in Photonic Crystal Slabs," *Phys. Rev. Lett.* **87**, 253902.
- Nussenzweig, A., E. E. Eyler, T. Bergeman, and E. Pollack, 1990, "Line shapes of ionizing Stark resonances in helium," *Phys. Rev. A* **41**, 4944–4957.

- Nygaard, N., R. Piil, and K. M. Imer, 2008a, “Two-channel Feshbach physics in a structured continuum,” *Phys. Rev. A* **78**, 023617.
- Nygaard, N., R. Piil, and K. Mø Imer, 2008b, “Feshbach molecules in a one-dimensional optical lattice,” *Phys. Rev. A* **77**, 021601.
- Oliveira, L. N., and J. W. Wilkins, 1985, “Fano antiresonances in x-ray-absorption spectroscopy,” *Phys. Rev. B* **32**, 696–707.
- Opatrný, T., and D.-G. Welsch, 2001, “Coupled cavities for enhancing the cross-phase-modulation in electromagnetically induced transparency,” *Phys. Rev. A* **64**, 023805.
- Ott, H., J. Fortagh, G. Schlotterbeck, A. Grossmann, and C. Zimmermann, 2001, “Bose-Einstein Condensation in a Surface Microtrap,” *Phys. Rev. Lett.* **87**, 230401.
- Ozbay, E., 2006, “Plasmonics: Merging Photonics and Electronics at Nanoscale Dimensions,” *Science* **311**, 189–193.
- Palfy, A., Z. Harman, and W. Scheid, 2007, “Quantum interference between nuclear excitation by electron capture and radiative recombination,” *Phys. Rev. A* **75**, 012709.
- Pastawski, H. M., L. E. F. F. Torres, and E. Medina, 2002, “Electron-phonon interaction and electronic decoherence in molecular conductors,” *Chem. Phys.* **281**, 257 – 278.
- Patthey, F., M.-H. Schaffner, W.-D. Schneider, and B. Delley, 1999, “Observation of a Fano Resonance in Photoemission,” *Phys. Rev. Lett.* **82**, 2971–2974.
- Piao, G., R. A. Lewis, and P. Fisher, 1990, “Fano resonances in the absorption spectrum of singly ionised zinc in germanium,” *Solid State Commun.* **75**, 835 – 838.
- Pichl, L., H. Nakamura, and J. Horacek, 2000, “Complete reflection in two-state crossing and noncrossing potential systems,” *J. Chem. Phys.* **113**, 906–918.
- Qiang, Z., H. Yang, L. Chen, H. Pang, Z. Ma, and W. Zhou, 2008, “Fano filters based on transferred silicon nanomembranes on plastic substrates,” *Appl. Phys. Lett.* **93**, 061106.
- Ramaker, D. E., and D. M. Schrader, 1974, “Multichannel configuration-interaction theory: Application to some resonances in helium,” *Phys. Rev. A* **9**, 1980–1991.
- Raoult, M., and F. H. Mies, 2004, “Feshbach resonance in atomic binary collisions in the Wigner threshold law regime,” *Phys. Rev. A* **70**, 012710.
- Rau, A. R. P., 2004, “Perspectives on the Fano Resonance Formula,” *Phys. Scr.* **69**, C10–C13.
- Rayleigh, L., 1871a, “On the Light from the Sky, Its Polarization and Color,” *Phil. Mag.* **41**, 107.
- Rayleigh, L., 1871b, “On the Light from the Sky, Its Polarization and Color,” *Phil. Mag.* **41**, 274.
- Rayleigh, L., 1871c, “On the scattering of light by small particles,” *Phil. Mag.* **41**, 447.
- Rayleigh, L., 1907, “On the dynamical theory of gratings,” *Proc. R. Soc. London, Ser. A* **79**, 399.
- Redner, S., 2004, “Citation Statistics From More Than a Century of Physical Review,” *arxiv:physics/0407137*.
- Reimann, S. M., and M. Manninen, 2002, “Electronic structure of quantum dots,” *Rev. Mod. Phys.* **74**, 1283–1342.
- Rice, O. K., 1933, “Predissociation and the Crossing of Molecular Potential Energy Curves,” *J. Chem. Phys.* **1**, 375–389.
- Roney, P. L., 1994a, “Theory of spectral line shape. I. Formulation and line coupling,” *J. Chem. Phys.* **101**, 1037–1049.
- Roney, P. L., 1994b, “Theory of spectral line shape. II. Collision time theory and the line wing,” *J. Chem. Phys.* **101**, 1050–1060.
- Roney, P. L., 1995, “Theory of spectral line shape. III. The Fano operator from near to far wing,” *J. Chem. Phys.* **102**, 4757–4771.
- S. J. Xu, J. L., S.-J. Xiong, and H. Z. Zheng, 2006, “New type of Fano resonant tunneling via Anderson impurities in superlattice,” *Europhys. Lett.* **74**, 875–881.
- Saito, R., G. Dresselhaus, and M. S. Dresselhaus, 1998, *Physical Properties of Carbon Nanotubes* (Imperial College Press, London).
- Sanchez, D., and L. Serra, 2006, “Fano-Rashba effect in a quantum wire,” *Phys. Rev. B* **74**, 153313.
- Sanchez, I., and F. Martin, 1994, “Hidden Fano interferences in the resonant photoionization of He-like ions,” *Phys. Rev. A* **49**, 5116–5119.
- Sarrazin, M., J.-P. Vigner, and J.-M. Vigoureux, 2003, “Role of Wood anomalies in optical properties of thin metallic films with a bidimensional array of subwavelength holes,” *Phys. Rev. B* **67**, 085415.
- Sasada, K., and N. Hatano, 2005, “Quantum interference effect of resonant transport in nano-scale systems,” *Physica E* **29**, 609 – 613.
- Sato, M., B. E. Hubbard, A. J. Sievers, B. Ilic, D. A. Czaplewski, and H. G. Craighead, 2003, “Observation of Locked Intrinsic Localized Vibrational Modes in a Micromechanical Oscillator Array,” *Phys. Rev. Lett.* **90**, 044102.
- Schmid, J., J. Weis, K. Eberl, and K. v. Klitzing, 1998, “A quantum dot in the limit of strong coupling to reservoirs,” *Physica B* **256-258**, 182 – 185.
- Schwarz, U. T., L. Q. English, and A. J. Sievers, 1999, “Experimental Generation and Observation of Intrinsic Localized Spin Wave Modes in an Antiferromagnet,” *Phys. Rev. Lett.* **83**, 223–226.
- Seaton, M. J., 1966, “Quantum defect theory I. General formulation,” *Proc. Phys. Soc. London* **88**, 801–814.
- Serra, L., and D. Sánchez, 2007, “The Fano-Rashba effect,” *J. Phys.: Conf. Ser.* **61**, 1037.
- Shenstone, A. G., 1938, “Spectroscopy: I. atomic spectra,” *Rep. Prog. Phys.* **5**, 210–227.
- Siegner, U., M.-A. Mycek, S. Glutsch, and D. S. Chemla, 1995, “Quantum interference in the system of Lorentzian and Fano magnetoexciton resonances in GaAs,” *Phys. Rev. B* **51**, 4953–4961.
- Simonian, A. W., A. B. Sproul, Z. Shi, and E. Gauja, 1995, “Observation of Fano resonance in heavily doped p-type silicon at room temperature,” *Phys. Rev. B* **52**, 5672–5674.
- Simpson, J. A., and U. Fano, 1963, “Classification of Resonances in the Electron Scattering Cross Section of Ne and He,” *Phys. Rev. Lett.* **11**, 158–159.
- Smirnov, B. M., 2003, *Physics of Atoms And Ions* (Springer, New York).
- Smith, D. D., H. Chang, K. A. Fuller, A. T. Rosenberger, and R. W. Boyd, 2004, “Coupled-resonator-induced transparency,” *Phys. Rev. A* **69**, 063804.
- Smith, K., D. E. Golden, S. Ormonde, B. W. Torres, and A. R. Davies, 1973, “Theoretical Model for Resonances in e-He Scattering near 60 eV,” *Phys. Rev. A* **8**, 3001–3011.
- Soljacic, M., and J. D. Joannopoulos, 2004, “Enhancement of nonlinear effects using photonic crystals,” *Nat. Mater.* **3**, 211–219.
- Soljačić, M., C. Luo, J. D. Joannopoulos, and S. Fan, 2003, “Nonlinear photonic crystal microdevices for optical integration,” *Opt. Lett.* **28**, 637–639.
- Spevak, I. S., A. Y. Nikitin, E. V. Bezuglyi, A. Levchenko, and A. V. Kats, 2009, “Resonantly suppressed transmission and anomalously enhanced light absorption in periodically

- modulated ultrathin metal films,” *Phys. Rev. B* **79**, 161406.
- Stefanski, P., 2003, “Quantum dots as scatterers in electronic transport: interference and correlations,” *Solid State Comm.* **128**, 29 – 34.
- Stefanski, P., A. Tagliacozzo, and B. R. Bulka, 2004, “Fano versus Kondo Resonances in a Multilevel “Semiopen” Quantum Dot,” *Phys. Rev. Lett.* **93**, 186805.
- Stillinger, F. H., and D. R. Herrick, 1975, “Bound states in the continuum,” *Phys. Rev. A* **11**, 446–454.
- Sturm, K., W. Schulke, and J. R. Schmitz, 1992, “Plasmon-Fano resonance inside the particle-hole excitation spectrum of simple metals and semiconductors,” *Phys. Rev. Lett.* **68**, 228–231.
- Suh, W., Z. Wang, and S. Fan, 2004, “Temporal coupled-mode theory and the presence of non-orthogonal modes in lossless multi-mode cavities,” *IEEE J. Quant. Electron.* **40**, 1511.
- Swanson, B. I., J. A. Brozik, S. P. Love, G. F. Strouse, A. P. Shreve, A. R. Bishop, W.-Z. Wang, and M. I. Salkola, 1999, “Observation of Intrinsically Localized Modes in a Discrete Low-Dimensional Material,” *Phys. Rev. Lett.* **82**, 3288–3291.
- Syage, J. A., and J. E. Wessel, 1987, “Antiresonance in autoionizing Rydberg series of naphthalene,” *J. Chem. Phys.* **87**, 6207–6209.
- Taylor, D. P., and P. M. Johnson, 1993, “Resonance enhanced multiphoton ionization photoelectron spectra of CO[sub 2]. III. Autoionization dominates direct ionization,” *J. Chem. Phys.* **98**, 1810–1816.
- Teodoro, F. D., and E. F. McCormack, 1998, “Theoretical treatment of quasibound resonances in two-color resonant four-wave mixing spectroscopy,” *Phys. Rev. A* **57**, 162–173.
- Teodoro, F. D., and E. F. McCormack, 1999, “State-selective quantum beat spectroscopy via coherent control of Liouville-pathway interference in two-colour resonant four-wave mixing,” *J. Phys. B* **32**, 4389–4404.
- Terrones, M., H. Terrones, F. Banhart, J.-C. Charlier, and P. M. Ajayan, 2000, “Coalescence of Single-Walled Carbon Nanotubes,” *Science* **288**, 1226–1229.
- Tomita, M., K. Totsuka, R. Hanamura, and T. Matsumoto, 2009, “Tunable Fano interference effect in coupled-microsphere resonator-induced transparency,” *J. Opt. Soc. Am. B* **26**, 813–818.
- Tong, P., B. Li, and B. Hu, 1999, “Wave transmission, phonon localization, and heat conduction of a one-dimensional Frenkel-Kontorova chain,” *Phys. Rev. B* **59**, 8639–8645.
- Torio, M. E., K. Hallberg, S. F. A. E. Miroshnichenko, and M. Titov, 2004, “Spin filters with Fano dots,” *Eur. Phys. J. B* **37**, 399.
- Torres, L. E. F. F., H. M. Pastawski, and E. Medina, 2006, “Antiresonances as precursors of decoherence,” *EPL* **73**, 164–170.
- Trias, E., J. J. Mazo, and T. P. Orlando, 2000, “Discrete Breathers in Nonlinear Lattices: Experimental Detection in a Josephson Array,” *Phys. Rev. Lett.* **84**, 741–744.
- Tribelsky, M. I., S. Flach, A. E. Miroshnichenko, A. V. Gorbach, and Y. S. Kivshar, 2008, “Light Scattering by a Finite Obstacle and Fano Resonances,” *Phys. Rev. Lett.* **100**, 043903.
- Tribelsky, M. I., and B. S. Luk’yanchuk, 2006, “Anomalous Light Scattering by Small Particles,” *Phys. Rev. Lett.* **97**, 263902.
- Ueda, K., 1987, “Spectral line shapes of autoionizing Rydberg series,” *Phys. Rev. A* **35**, 2484–2492.
- Valiente, M., and D. Petrosyan, 2009, “Scattering resonances and two-particle bound states of the extended Hubbard model,” *J. Phys. B* **42**, 121001 (4pp).
- Vicencio, R. A., J. Brand, and S. Flach, 2007, “Fano Blockade by a Bose-Einstein Condensate in an Optical Lattice,” *Phys. Rev. Lett.* **98**, 184102.
- Vittorini-Orgeas, A., and A. Bianconi, 2009, “From Majorana theory of atomic autoionization to Feshbach resonances in high temperature superconductors,” *J. Supercond. Novel Magn.* **22**, 215–221.
- Vlasov, Y. A., M. O’Boyle, H. F. Hamann, and S. J. McNab, 2005, “Active control of slow light on a chip with photonic crystal waveguides,” *Nature* **438**, 65.
- Waligorski, G., L. Zhou, and W. E. Cooke, 1997, “Technique for measuring the linewidth of autoionizing Rydberg states,” *Phys. Rev. A* **55**, 1544–1547.
- Ward, A. J., and J. B. Pendry, 1998, “Calculating photonic Green’s functions using a nonorthogonal finite-difference time-domain method,” *Phys. Rev. B* **58**, 7252–7259.
- Weidner, E., S. Combrié, A. de Rossi, N.-V.-Q. Tran, and S. Cassette, 2007, “Nonlinear and bistable behavior of an ultrahigh-Q GaAs photonic crystal nanocavity,” *Appl. Phys. Lett.* **90**, 101118.
- Wickenhauser, M., J. Burgdorfer, F. Krausz, and M. Drescher, 2005, “Time Resolved Fano Resonances,” *Phys. Rev. Lett.* **94**, 023002.
- Wiegmann, P. B., and A. M. Tsvelick, 1983, “Exact solution of the Anderson model: I,” *J. Phys. C* **16**, 2281–2319.
- Winstead, C., and P. W. Langhoff, 1991, “Feshbach-Fano formalism in Hilbert space: Application to shape resonances in molecular photoionization,” *J. Chem. Phys.* **95**, 3107–3118.
- Wood, R., 1902, “On the remarkable case of uneven distribution of light in a diffraction grating spectrum,” *Proc. R. Soc. London, Ser. A* **18**, 269.
- Wood, R. W., 1935, “Anomalous Diffraction Gratings,” *Phys. Rev.* **48**, 928–936.
- Wulf, U., and V. V. Skalozub, 2005, “Pulse propagation in resonant tunneling,” *Phys. Rev. B* **72**, 165331.
- Xu, Q., S. Sandhu, M. L. Povinelli, J. Shakya, S. Fan, and M. Lipson, 2006, “Experimental Realization of an On-Chip All-Optical Analogue to Electromagnetically Induced Transparency,” *Phys. Rev. Lett.* **96**, 123901.
- Xu, Y., Y. Li, R. K. Lee, and A. Yariv, 2000, “Scattering-theory analysis of waveguide-resonator coupling,” *Phys. Rev. E* **62**, 7389–7404.
- Yafet, Y., 1981, “Effect of shake-up transitions on the spectrum of Auger electrons in Fano resonances,” *Phys. Rev. B* **23**, 3558–3559.
- Yang, H., H. Pang, Z. Qiang, Z. Ma, and W. Zhou, 2008, “Surface-normal Fano filters based on transferred silicon nanomembranes on glass substrates,” *Electronics Letters* **44**, 858–860.
- Yang, X., C. Husko, C. W. Wong, M. Yu, and D.-L. Kwong, 2007, “Observation of femtojoule optical bistability involving Fano resonances in high-Q/V<sub>m</sub> silicon photonic crystal nanocavities,” *Appl. Phys. Lett.* **91**, 051113.
- Yanik, M. F., and S. Fan, 2004, “Stopping Light All Optically,” *Phys. Rev. Lett.* **92**, 083901.
- Yanik, M. F., S. Fan, and M. Soljačić, 2003a, “High-contrast all-optical bistable switching in photonic crystal microcavities,” *Appl. Phys. Lett.* **83**, 2739–2741.
- Yanik, M. F., S. Fan, M. Soljačić, and J. D. Joannopoulos, 2003b, “All-optical transistor action with bistable switch-

- ing in a photonic crystal cross-waveguide geometry,” *Opt. Lett.* **28**, 2506–2508.
- Yanik, M. F., W. Suh, Z. Wang, and S. Fan, 2004, “Stopping Light in a Waveguide with an All-Optical Analog of Electromagnetically Induced Transparency,” *Phys. Rev. Lett.* **93**, 233903.
- Yi, W., L. Lu, H. Hu, Z. W. Pan, and S. S. Xie, 2003, “Tunneling into Multiwalled Carbon Nanotubes: Coulomb Blockade and the Fano Resonance,” *Phys. Rev. Lett.* **91**, 076801.
- Zhang, W., A. O. Govorov, and G. W. Bryant, 2006, “Semiconductor-Metal Nanoparticle Molecules: Hybrid Excitons and the Nonlinear Fano Effect,” *Phys. Rev. Lett.* **97**, 146804.
- Zhang, Z., and V. Chandrasekhar, 2006, “Signatures of phase coherence in the low-temperature transport properties of multiwall carbon nanotubes,” *Phys. Rev. B* **73**, 075421.
- Zhang, Z., D. A. Dikin, R. S. Ruoff, and V. Chandrasekhar, 2004, “Conduction in carbon nanotubes through metastable resonant states,” *Europhys. Lett.* **68**, 713–719.